

BHI-00145
Rev. 00

Physical Stability of Long-Term Surface Barriers - Assessment of Potentially Disruptive Natural Events

Authors

N. R. Wing
IT Hanford, Inc.

F. M. Corpuz
Bechtel Hanford, Inc.

K. L. Petersen
Pacific Northwest Laboratory

A. M. Tallman
Westinghouse Hanford Company

Date Published
May 1995



Prepared for the U.S. Department of Energy
Office of Environmental Restoration and
Waste Management

Bechtel Hanford, Inc.
Richland, Washington

Approved for Public Release

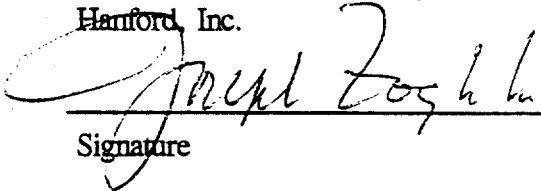
BHI-00145
REV: 00
OU: N/A
TSD: N/A
ERA: N/A

APPROVAL PAGE

Title of Document: PHYSICAL STABILITY OF LONG-TERM SURFACE BARRIERS -
ASSESSMENT OF POTENTIALLY DISRUPTIVE NATURAL
EVENTS

Author(s): N. R. Wing, IT Hanford, Inc.
K. L. Petersen, Pacific Northwest Laboratory
F. M. Corpuz, Bechtel Hanford, Inc.
A. M. Tallman, Westinghouse Hanford Company

Approval: J. G. Zoghbi, Acting Manager, Technology Demonstration Project, Bechtel
Hanford, Inc.


Signature

5/4/95
Date

The approval signature on this page indicates that this document
has been authorized for information release to the public through
appropriate channels. No other forms or signatures are required
to document this information release.

CONTENTS

1.0	INTRODUCTION	1
2.0	BACKGROUND	1
3.0	DETAILED DISCUSSION	4
3.1	SITE DESCRIPTION	4
3.2	METEOROLOGY	4
3.2.1	Regional Climatology Description and History	6
3.2.2	Wind	6
3.2.3	Precipitation	9
3.3	HYDROLOGY	18
3.3.1	Surface Hydrology	18
3.3.2	Groundwater Hydrology	18
3.4	GEOLOGY AND SEISMOLOGY	19
3.4.1	Topography and Physiography	19
3.4.2	Stratigraphy	19
3.4.3	Structural Geology and Tectonic Setting	26
3.4.4	Site Structural Geology	26
3.4.5	Seismology	29
3.4.6	Seismic Hazard	29
3.5	VOLCANIC HAZARDS	31
3.5.1	Columbia River Basalt Group Volcanism	31
3.5.2	Cascade Volcanism	33
3.6	GEOTECHNICAL STUDIES	33
3.7	ENGINEERED BARRIER CHARACTERIZATION AND STRUCTURAL ANALYSIS	33
3.7.1	Laboratory Testing	34
3.7.2	Barrier Analysis	34
3.7.3	Barrier Layer Integrity	35
4.0	REFERENCES	35

APPENDIX:

A	PRELIMINARY STABILITY ANALYSES FOR PROTOTYPE SURFACE BARRIER - 200 EAST AREA	A-1
---	---	-----

FIGURES:

1.	Cross Section of Typical Long-Term Surface Isolation Barrier	3
2.	Topographic Map of the Hanford Site	5
3.	Location of Hanford Meteorology Station and 12 Supplementary Wind Stations	7
4.	Wind Roses for the Wind Stations Shown in Figure 3	8

CONTENTS (cont.)

FIGURES (cont.):

5.	Wind Hazard at the Hanford Site	10
6.	Total Annual Precipitation at the Hanford Site, 1913 to 1980, and the Probability (%) that the Total Annual Precipitation will not Exceed a Given Amount	11
7.	Greatest Depth of Snow on the Ground During the Winters of 1946-1947 to 1980-1981 and the Probability (%) that the Greatest Depth of Snow will not Exceed a Given Amount	14
8.	Major Drainage Divides on the Hanford Site and Vicinity	16
9.	Geologic Structure of the Pasco Basin and the Hanford Site	20
10.	Divisions of the Columbia Intermontane Province and Adjacent Provinces	21
11.	Landforms of the Pasco Basin and the Hanford Site	22
12.	Generalized Stratigraphy of the Hanford Site	23
13.	Generalized Stratigraphy of the Suprabasalt Sediments Beneath the Hanford Site	25
14.	Index Map of the Geologic Provinces	27
15.	Structural Subprovinces and Extent of Columbia River Basalt Group	28
16.	Contribution of Sources to the Mean Seismic Hazard at the 200 East Area	30
17.	Computed Mean and 5th to 95th Percentile Seismic Hazard Curves for the 200 East Area	32

TABLES:

1.	Average Return Period for Various Precipitation Amounts Based on Extreme Analysis of 1947 Through 1969 Records at the Hanford Meteorological Station	13
2.	Average Precipitation Intensity During Specified Time Periods Based on Extreme Analysis of 1947 Through 1969 Records at the Hanford Meteorological Station	13
3.	Probable Maximum Precipitation from Thunderstorms of Various Durations	17

1.0 INTRODUCTION

The purpose of this task is to assess those extreme natural events (phenomena) likely to affect a long-term protective barrier at the Hanford Site (Wing 1994). Probabilistically based natural phenomena assessments are used where available. The level or intensity of disruptive natural events determined to have a reasonable probability of occurring during the design life of the Hanford Barrier will be assessed and/or tested to determine their consequences on the performance of the Hanford Barrier. This assessment covers tornados and other high-wind conditions, high-intensity precipitation, stream flooding, earthquakes, and volcanic ash deposition.

2.0 BACKGROUND

Long-term surface barriers have been proposed for use at the U.S. Department of Energy's (DOE) Hanford Site near Richland, Washington, to isolate and dispose of certain types of waste in place. The implementation of an in-place disposal alternative probably will require some type of protective covering that will provide long-term isolation of the wastes from the accessible environment. The Hanford Site Surface Barrier Development Program (BDP) was organized to develop the technology needed to provide a long-term surface barrier capability for the Hanford Site and elsewhere. The reader is referred to Wing (1993, 1994) for more detailed discussion of the BDP.

Wing (1993, 1994) discusses the functional requirements and the tasks required to develop the barrier. Preliminary performance objectives for the long-term surface barriers are the following:

- Function in a semiarid to subhumid climate
- Limit the recharge of water through the waste to the water table to near-zero amounts (0.05 cm of water per year [1.6×10^{-9} cm/s])
- Be maintenance free
- Minimize the likelihood of plant, animal, and human intrusion
- Limit the exhalation of noxious gases
- Minimize erosion-related problems
- Meet or exceed *Resource Conservation and Recovery Act* (RCRA) cover performance requirements
- Isolate wastes for a minimum of 1,000 years
- Be acceptable to regulatory agencies and the public.

Fifteen groups of tasks were identified by the barrier development team to resolve the technical concerns and complete the development and design of protective barriers (Wing 1994):

1. Project management
2. Biointrusion control
3. Water infiltration control
4. Erosion/deposition control
5. Physical stability testing
6. Human interference control
7. Barrier construction materials procurement
8. Prototype barrier designs and testing
9. Model applications and validation
10. Natural analog studies
11. Assessment of effects of long-term climate change
12. Interface with regulatory agencies
13. RCRA equivalency
14. Technology integration and transfer
15. Final design.

This study addresses task group number 5, physical stability testing.

The information generated within each of the above tasks provides data for barrier designs. Enough information exists to allow the design and construction of a prototype. The design of the prototype barrier was completed in 1993, and construction was completed in 1994. Figure 1 shows a typical long-term surface barrier. Evidence of barrier performance will be obtained by conducting laboratory experiments, field tests, computer modeling, and other studies that establish confidence in the barrier's ability to meet its 1,000-year design life. The design and construction of the prototype barrier have integrated the various components of the barrier into one system.

Because the long-term surface barrier is intended to remain functional for more than 1,000 years, it is important to understand the potential impact of natural phenomena with long recurrence times or low probability of occurrence. Participants at the Value Engineering (VE) workshop (DOE-RL 1993) recommended that the literature on potentially disruptive natural events be reviewed. Most of the studies that address natural phenomena hazards have been performed for this region in support of the design, construction, and qualification of nuclear facilities. The VE recommendations are included under task group number 5, physical stability testing. The specific task is "Assessment of Potentially Disruptive Natural Events (PHYS-1)." Wing (1994) specifically notes that the assessment covers tornados and other high-wind conditions; high-intensity precipitation; earthquakes; the deposition of volcanic ash; and any other possible disruptive events that could act on the barrier, and indicates that the task comprises the following activities:

- Reviewing/assessing literature on potentially disruptive natural events
- Preparing a laboratory/field test plan, as required
- Performing the required laboratory/field tests
- Preparing design recommendations based on the results of this task.

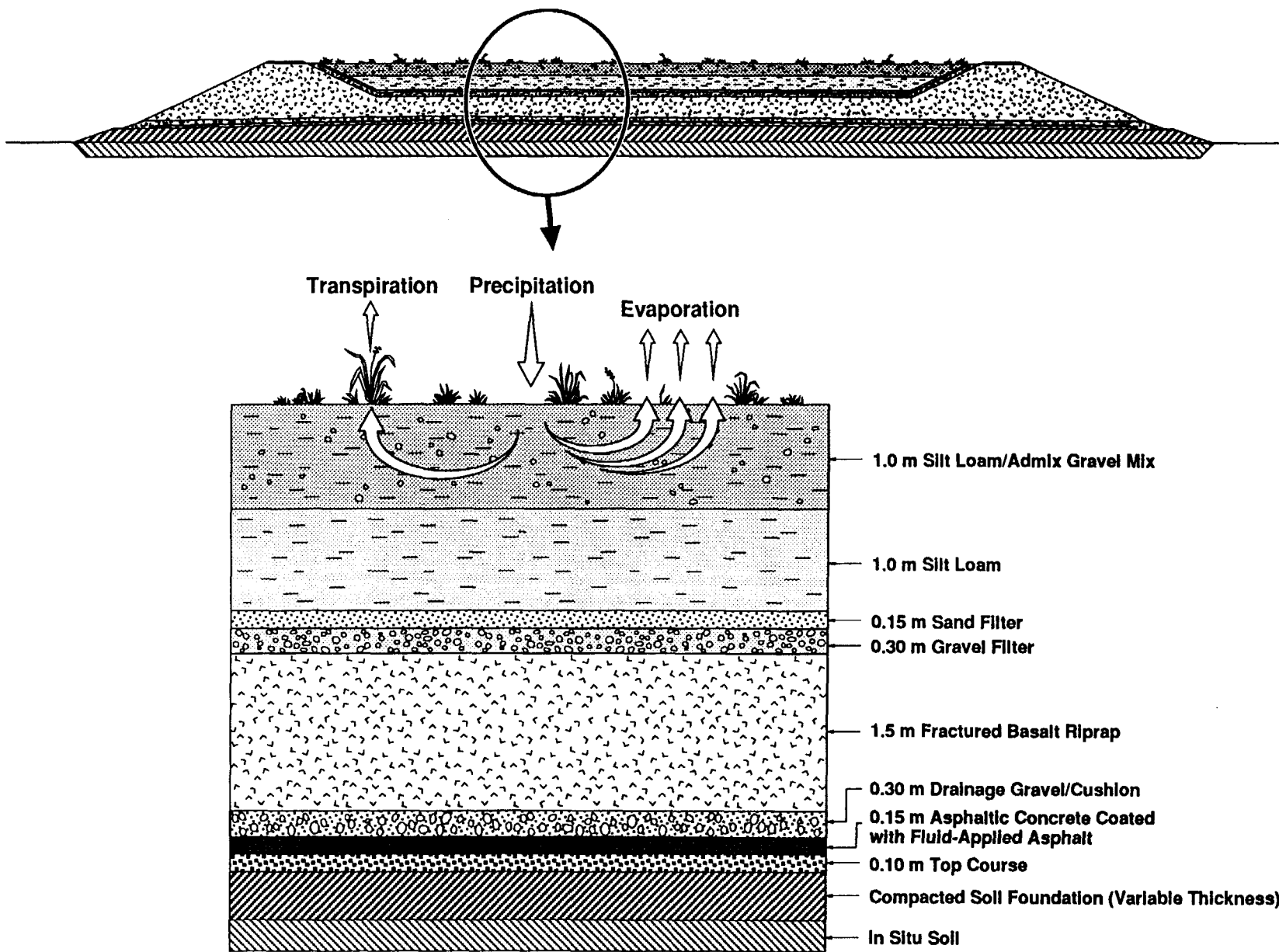


Figure 1. Cross Section of Typical Long-Term Surface Isolation Barrier.

BH1-00145
Rev. 00

H9304018.10

This document addressed the first activity in the above list for the following events: tornados and other high-wind conditions; high-intensity precipitation; earthquakes; and the deposition of volcanic ash, and provides the basis for some testing of extremes of the prototype barrier.

One natural event not treated is range fires. The subject of fire damage is addressed both in the water and wind erosion task and in the water balance task groups. However, the frequency of such events is not addressed. Prehistoric fire frequency has been studied in the surrounding forested areas but not in the steppe vegetation of eastern Washington (Mehring 1985). Prediction of fire frequency has been complicated by the arrival of modern man, who is capable both of starting and stopping fires.

Testing and monitoring of the prototype barrier is planned for a minimum of 3 years, commencing immediately following construction (Gee et al. 1993). Data provided below on extremes for wind and precipitation will provide bounding ranges for the testing and monitoring. The information on earthquakes helps provide confidence in the stability of the barrier to perform as planned for its 1,000-year design life.

The extreme events are discussed below under the topics of Meteorology, Hydrology, Geology and Seismology, and Geotechnical Studies.

3.0 DETAILED DISCUSSION

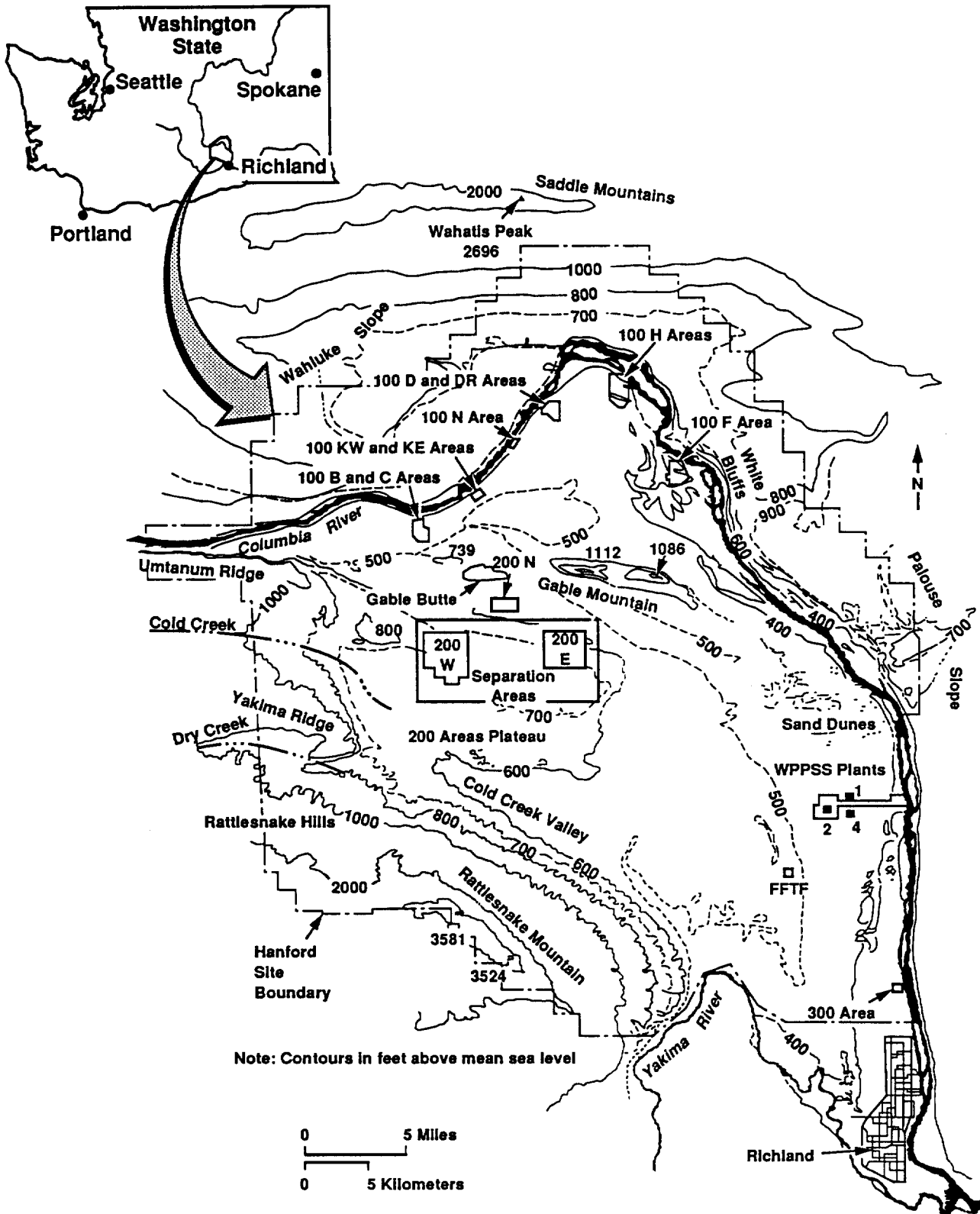
3.1 SITE DESCRIPTION

The Hanford Site is a 1,500-km² area located in the state of Washington (Figure 2). The Columbia River enters the Site at the northwest corner and crosses over to form the eastern boundary as it flows southward. The Yakima River, flowing from west to east, empties into the Columbia River at the Tri-Cities (Richland-Kennewick-Pasco). The Yakima River forms the southern boundary of the Hanford Site. The Hanford Site is bordered on the north by the Saddle Mountains and on the west by the Rattlesnake Hills. Dominant natural features include the Columbia River, anticlinal ridges of basalt in and along the Hanford Site boundary, and sand dunes located near the river. The surrounding basaltic ridges rise to elevations as high as 1,100 m. The most broadly distributed vegetation on the Hanford Site is sagebrush, wheatgrass, blue bunch wheatgrass, and other shrub plant species common to central Washington (Sackschewsky et al. 1992).

3.2 METEOROLOGY

During the period from April 1912 through March 1943, cooperative observers for the U.S. Weather Bureau (now the National Weather Service) recorded daily maximum and minimum temperatures, as well as precipitation, including measurements of unmelted snow, at the Hanford Townsite, about 16 km east-northeast of the present Hanford Meteorological Station (HMS) (Hoitink and Burk 1994). From late 1943 until mid-1944, the U.S. Weather Bureau recorded some meteorological observations in Richland. Then, in 1944, as part of the Manhattan Project, the HMS was established. Hourly observations began on December 7, 1944.

Figure 2. Topographic Map of the Hanford Site.



H9111014.2a

The HMS is centrally located on the Hanford Site, on the east side of the 200 West Area (Figure 2). A range of meteorologic variables are observed and measured at the HMS and its 125-m tower: temperature, relative humidity, precipitation, atmospheric pressure, solar radiation, cloud cover, visibility, and subsurface temperatures. *The Data Collection Component of the Hanford Meteorology Monitoring Program* (Glantz and Islam 1988) describes in detail the HMS methods for meteorologic instrumentation and data collection.

3.2.1 Regional Climatology Description and History

The climate of the Pasco Basin can be classified as mid-latitude semiarid (NRC 1982). The basin can also be classified as a mid-latitude desert, depending on the climatological classification scheme used. Summers are warm and dry with abundant sunshine, and large daily temperature variations are common during this season with intense solar heating and nighttime cooling. Daytime high temperatures in June, July, and August can exceed 38 °C, with nighttime lows between 10 and 15 °C. Winters are cool with occasional precipitation. Cold air associated with modified arctic air masses that reach the area can cause temperatures to drop below -18 °C. Overcast skies and fog periodically occur in the winter.

Local topographical features have a significant effect on temperature, wind, and precipitation. All air masses that reach the Pasco Basin undergo some modification as they pass over the complex Pacific Northwest topography (DOE-RL 1982). The Cascade Range to the west and the Rocky Mountains to the east and north are an important influence on the climate of the region, as is proximity to the Pacific Ocean. The Hanford Site has a relatively low annual average rainfall, 16 cm, as a result of the rain shadow created by the Cascade Range (Stone et al. 1983). Further detail related to climate can be found in DOE (1988). Additional climate information is being developed to support task number 11, assessment of effects of long-term climate change (Wing 1994).

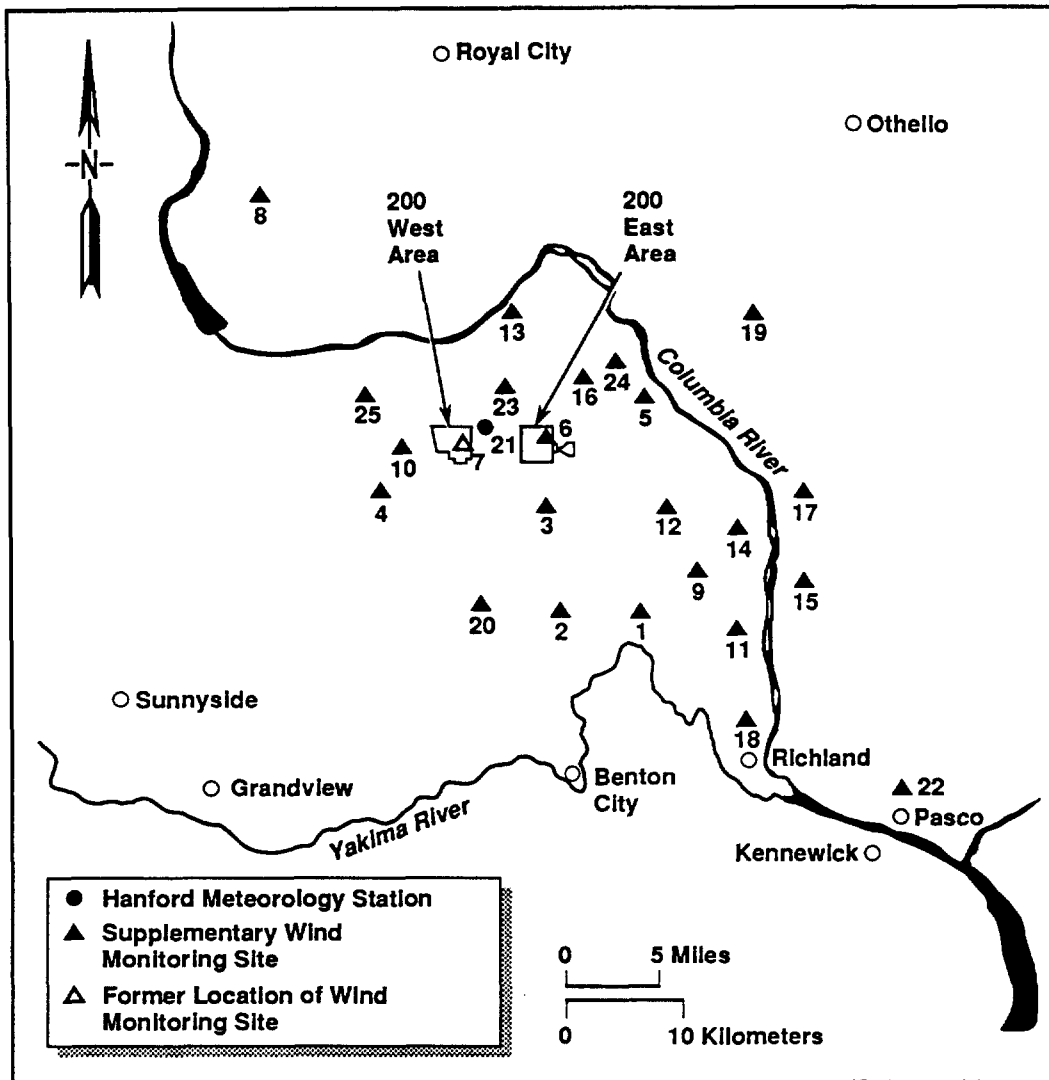
3.2.2 Wind

3.2.2.1 Data Sources. Wind data are collected at the HMS at the surface (2.1 m above ground) and at the 15.2-, 30.5-, 61.0-, 91.4-, and 121.9-m levels of a 125-m tower. Three 60-m towers, with wind-measuring instrumentation at the 10-, 25-, and 60-m levels, are located at the 300, 400, and 100-N Areas. In addition, wind instruments on twenty-one 9.1-m towers distributed around the Hanford Site (Figure 3) provide supplementary data for defining wind patterns.

Prevailing wind directions on the 200 Area Plateau are from the northwest in all months of the year (Figure 4). Secondary maxima occur for southwesterly winds. Summaries of wind directions indicate that winds from the northwest quadrant occur most often during the winter and summer. During the spring and fall, the frequency of southwesterly winds increases with a corresponding decrease in northwest flow. Winds blowing from other directions (e.g., northeast) display minimal variation from month to month.

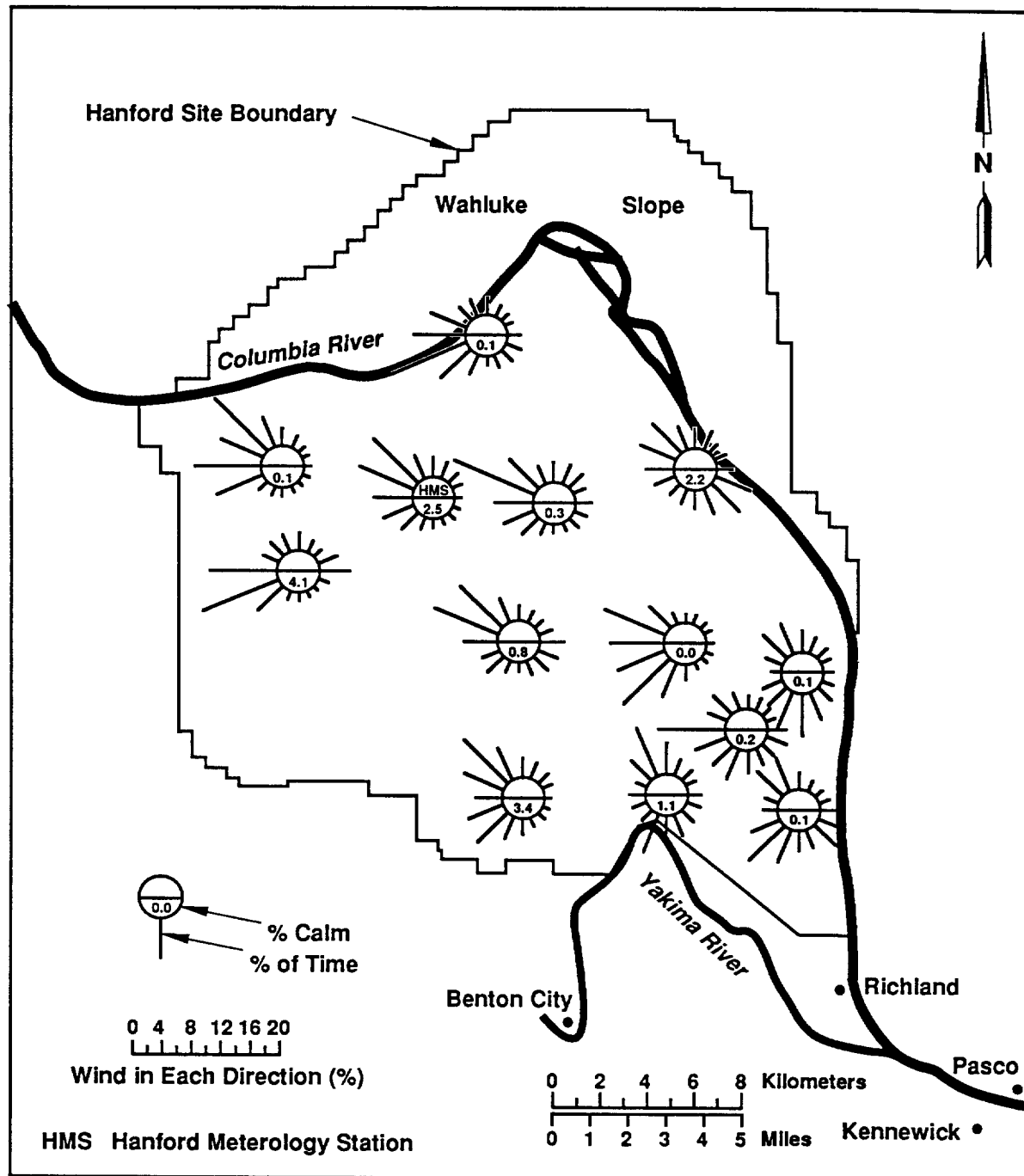
Monthly and annual joint-frequency distributions of wind direction versus wind speed for the HMS are given in Stone et al. (1983). Monthly average wind speeds are lowest during the winter months, averaging 10 to 11 km/h, and highest during the summer, averaging 14 to 16 km/h. Wind speeds

Figure 3. Location of Hanford Meteorological Station and 12 Supplementary Wind Stations.



Station Number	Station Name	Station Number	Station Name
1	Prosser Barricade	14	WPPSS
2	Emergency Operations Center	15	Franklin County
3	Army Loop Road	16	Gable Mountain
4	Rattlesnake Springs	17	Ringold
5	Edna	18	Richland Airport
6	200-East	19	Sagehill
7	200-West	20	Rattlesnake Mountain
8	Wahluke Slope	21	Hanford Meteorology Station (121.9-m)
9	FFTF (60-m)	22	Pasco Airport
10	Yakima Barricade	23	Gable West
11	300-Area (60-m)	24	100-F
12	Wye Barricade	25	Vernita
13	100-N (60-m)		

Figure 4. Wind Roses for the Wind Stations Shown in Figure 3.



well above average usually are associated with southwesterly winds. However, the summertime drainage winds are generally northwesterly and frequently reach 50 km/h. These winds are most prevalent over the northern part of the Hanford Site.

3.2.2.2 Probabilistic Wind/Tornado Hazard Assessment. The wind data collected at the Hanford Site and surrounding locations have been used to develop probabilistic straight-wind and tornado hazard assessments for the Hanford Site (Coats and Murray 1985, Ramsdell and Andrews 1986, Ramsdell et al. 1986). These independent studies have similar results. The Coats and Murray (1985) study is 5% to 7% lower than and within the uncertainty bands of Ramsdell and Andrews (1986). As Figure 5 shows, straight-wind velocities exceed tornado velocities at annual frequencies greater than 10^{-5} ($> 100,000$ years) (Coats and Murray 1985, Ramsdell and Andrews 1986). The chance that straight wind will exceed 80 mi/h (128 km/h) (measured in fastest mile [1.6 km]) during the 1,000-year design life of the barrier is approximately 10%, and the chance of a tornado with speeds less than 100 mi/h (160 km/h) is less than 1%.

3.2.2.3 Preliminary Impact Assessment. Wind and tornadoes are not considered to significantly affect the performance of the barrier. The barrier is constructed of materials not easily eroded by wind. However, task 4, erosion/deposition control tasks (Wing 1994), will address the effects of the wind hazards identified in Figure 6.

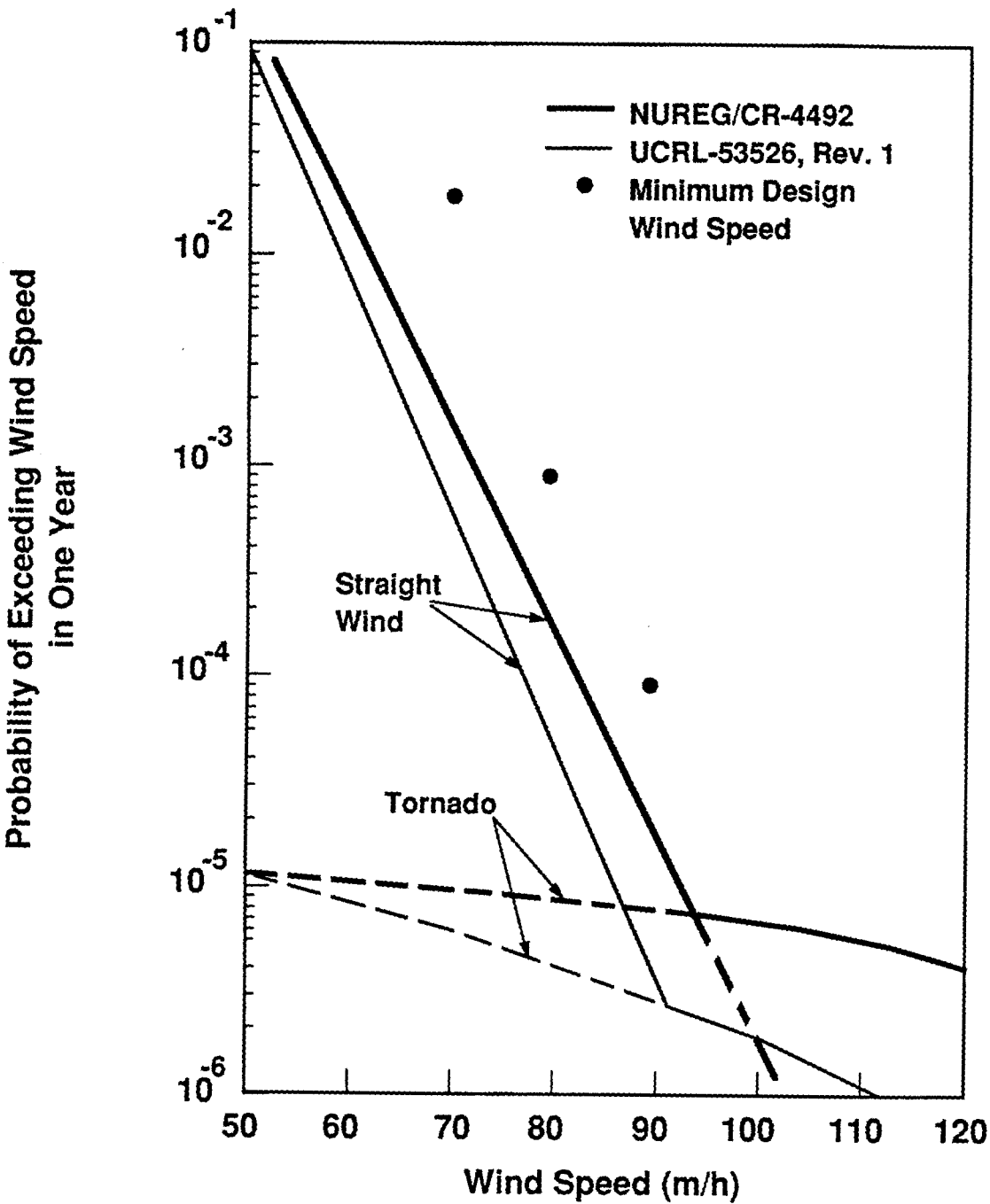
3.2.3 Precipitation

3.2.3.1 Data Sources. Precipitation measurements have been made at the HMS since 1945. During the spring of 1987, four other locations for measuring precipitation were added to the HMS measurement system. These locations are Rattlesnake Mountain, Richland Airport, Rattlesnake Springs, and Yakima Barricade. Climatological precipitation measurements also have been made on the Rattlesnake Mountain Arid Lands Ecology Reserve located on the western slope (Stone et al. 1983).

The mean annual precipitation at the HMS is 16 cm (Stone et al. 1983). Historical data indicate that over a period of roughly 80 years, the annual precipitation on the Hanford Site has varied from a low of 8 cm to a high of 30 cm. On average, 43% of the annual precipitation falls during November, December, and January. January is the wettest month, with an average of nearly 100 h of precipitation producing just over 2 cm of water. A slight secondary maximum in precipitation occurs in late spring. Only 11% of the annual precipitation falls during July, August, and September. July is the driest month, with an average of only 11 h of precipitation producing 0.4 cm of water. Summer precipitation is, on average, nearly twice as intense as winter precipitation.

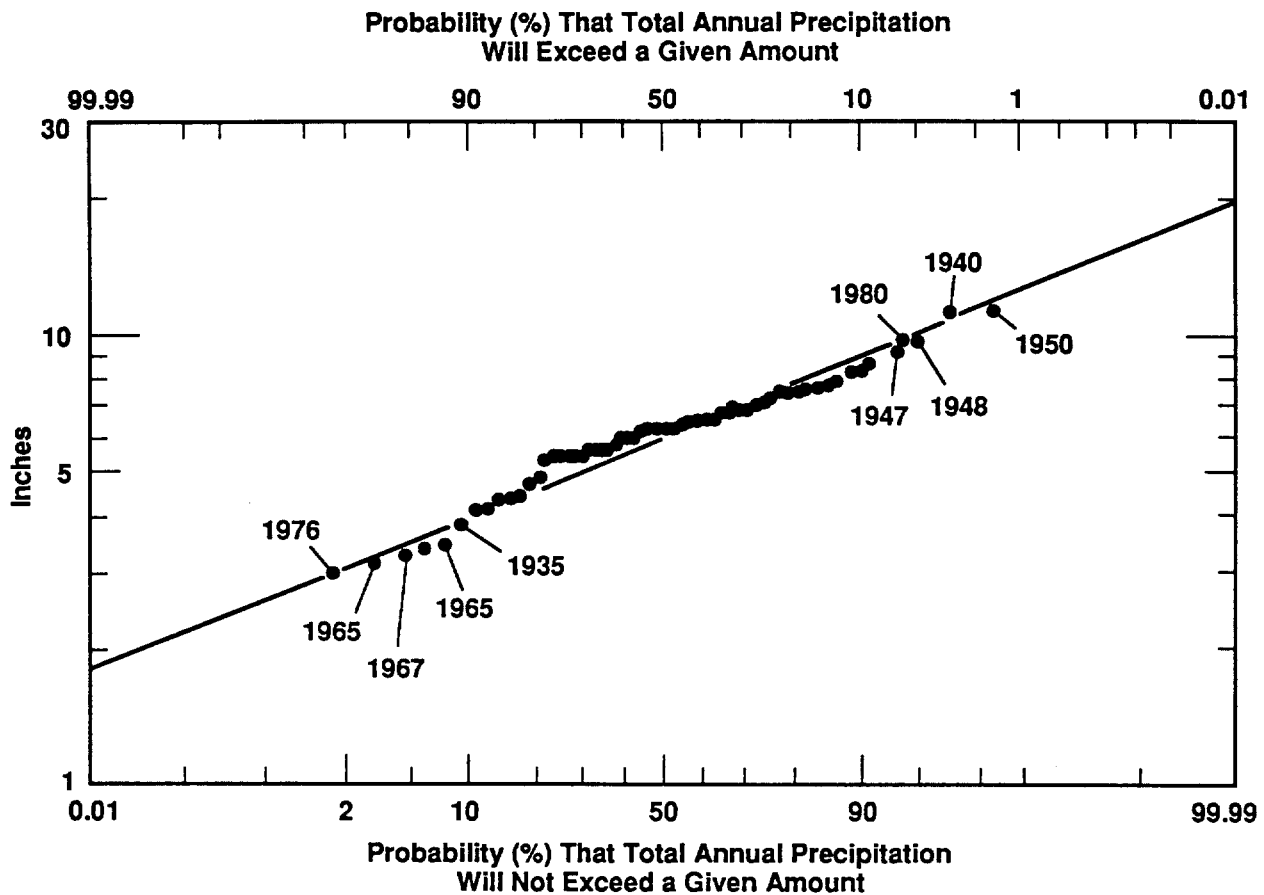
Total annual snowfall, which includes all frozen precipitation, has varied from a low of 0.8 cm to a high of more than 110 cm. The average annual snowfall is 34 cm. Snowfall accounts for 38% of all precipitation by water content from December through February. However, in only one winter in four is an accumulation of as much as 15 cm expected. The average seasonal number of days with 15 cm or more of snow on the ground is 4, although the 1992-1993 winter had 41 (Hoitink and Burk 1994). The record greatest depth of snow on the ground is 62 cm, which occurred in February 1916. However, since that date, the greatest depth has been 31 cm, occurring in December 1964 (Stone et al. 1983).

Figure 5. Wind Hazard at the Hanford Site. (To convert miles per hour to kilometers per hour, multiply by 1.6.)



38909066.8

Figure 6. Total Annual Precipitation at the Hanford Site, 1913 to 1980, and the Probability (%) that the Total Annual Precipitation will not Exceed a Given Amount.
(To convert inches to centimeters, multiply by 2.54.)



NOTE: Data for 1943 through 1946 are not available.

Hail has been recorded at the HMS; however, two days is usually the most that hail occurs during a year (Stone et al. 1983). The hailstones have been small with a maximum diameter in the range of 5 to 8 mm. The largest hailstone measured at the HMS was 10 mm in diameter. Glazed ice occurs an average of six times a year, usually between November and March. Rime ice (i.e., supercooled droplets that freeze on contact with solid objects) is generally associated with the supercooled fog either at higher elevations in the nearby hills or along the banks of the Columbia River.

Only 10 thunderstorm days per year are recorded at the HMS on average, although this number has varied from a low of 3 to a high of 23 (Stone et al. 1983). Although theoretically thunderstorms can occur during any month of the year, none have been observed in November or January. They occur most frequently from April through September. Stone et al. (1983) offers data on the number of monthly and annual thunderstorm days. The largest number of thunderstorm days recorded in a single month is eight, a number that has occurred in both June and August three times since 1948. Severe thunderstorms are exceedingly rare at the Hanford Site.

3.2.3.2 Probabilistic Precipitation Assessment. Precipitation in excess of 1 cm during a 24-h period occurs an average of twice a year. Precipitation of 4 cm in a 24-h period can be expected to occur at the Hanford Site once every 25 years (Stone et al. 1983). Four centimeters of precipitation in a 24-h period constitutes the Site design-basis storm. Tables 1 and 2 present the precipitation amounts and intensities for the average return periods of 100, 500, and 1,000 years, along with existing records. These estimates and existing records are based on extreme value analysis of HMS records for the period 1947 through 1969 (Stone et al. 1983).

For prototype barrier testing, according to Table 1, the 1,000-year storm at the Hanford Site is calculated to accumulate 5.59 cm of precipitation in 6 h (compared to a maximum record of 4.27 cm) and to have accumulated 6.81 cm of precipitation in 24 h (compared to the maximum recorded of 4.85 cm). The 1,000-year 6.81 cm amount is 42% of the annual mean precipitation of 16 cm, all delivered in a 24-h period.

Total annual precipitation at the Hanford Site and the probability that the total annual precipitation will not exceed a given amount is shown in Figure 6 for the period 1913 to 1980. The maximum annual precipitation received at the Site through 1993 is 29 cm in 1950 (the next highest is 28.1 cm in 1983) (Hoitink and Burk 1994). Thus the record high range is 180% of, or nearly double, the 16-cm annual average.

The slope of the intercept in Figure 6 shows that the probability that the annual precipitation amount will not exceed 31 cm is 1 in 100 years; that it will not exceed 41 cm is 1 in 1,000 years; and that it will not exceed 51 cm is 1 in 10,000 years. For prototype barrier testing, the annual amount to be placed on the prototype barrier as a stress-test equivalent to the 1,000-year return period is 41 cm, or 256% of the normal 16-cm annual average. As noted above, the recorded high is 180% of normal.

Figure 7 shows the greatest depth of snow on the ground during the winters of 1946-1947 to 1980-1981 and the probability that the greatest depth will not exceed a given amount. The average snowfall is 34 cm (Stone et al. 1983). The greatest depth of snow recorded on the ground is 62 cm (February 1916); this amount is nearly double the average amount. The slope of the intercept in

Table 1. Average Return Period for Various Precipitation Amounts Based on Extreme Analysis of 1947 Through 1969 Records at the Hanford Meteorological Station.

Return (yr)	Amount (cm) per time period						
	20 min	60 min	2 h	3 h	6 h	12 h	24 h
100	1.52	2.06	2.44	2.77	4.04	4.75	5.05
500	1.85	2.59	3.10	3.38	5.08	5.94	6.27
1,000	2.03	2.82	3.38	3.68	5.59	6.48	6.81
Record	1.40 ^a	1.50	2.24	2.74	4.27	4.78	4.85

^aEstimated.
Stone et al. (1983)

Table 2. Average Precipitation Intensity During Specified Time Periods Based on Extreme Analysis of 1947 Through 1969 Records at the Hanford Meteorological Station.

Return (yr)	Intensity (cm/h) per time period						
	20 min	60 min	2 h	3 h	6 h	12 h	24 h
100	4.57	2.06	1.22	0.91	0.69	0.40	0.21
500	5.59	2.59	1.55	1.12	0.83	0.50	0.26
1,000	6.10	2.82	1.70	1.22	0.94	0.54	0.28
Record	4.19 ^a	1.50	1.18	0.91	0.71	0.40	0.20

^aEstimated.
Stone et al. (1983).

Figure 7. Greatest Depth of Snow on the Ground During the Winters of 1946-1947 to 1980-1981 and the Probability (%) that the Greatest Depth of Snow will not Exceed a Given Amount.
(To convert inches to centimeters, multiply by 2.54.)

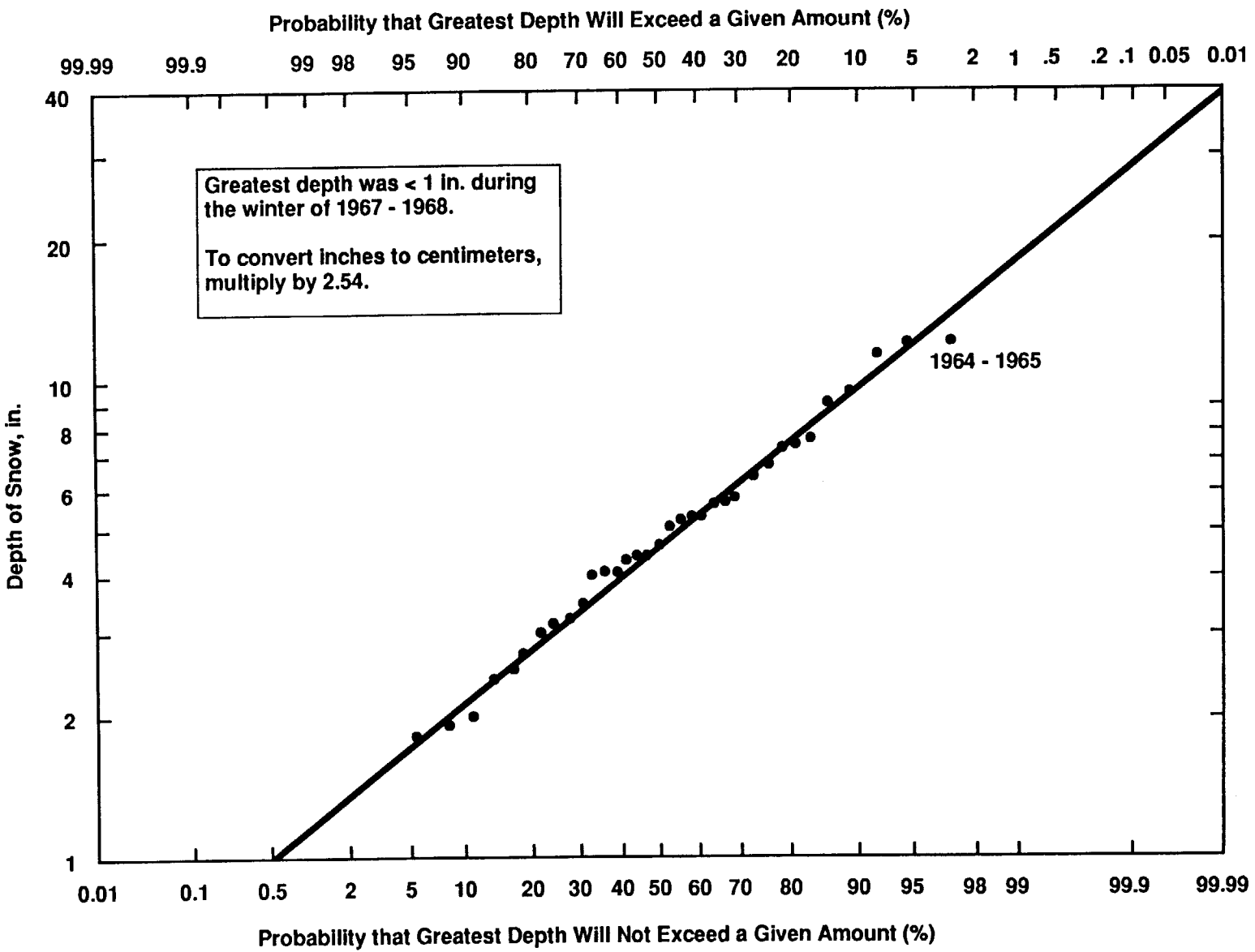


Figure 7 indicates that the probability that the greatest snow depth will not exceed 43 cm is 1 in 100 years; that it will not exceed 67 cm is 1 in 1,000 years; and that it will not exceed 100 cm is 1 in 10,000 years. These figures may prove useful because a snow-making machine will be used to stress test the barrier (Gee et al. 1993).

3.2.3.3 Probable Maximum Precipitation. The probable maximum precipitation (PMP) is theoretically the greatest depth of precipitation for a given duration that is physically possible over a storm area of a given size at a particular geographical location at a certain time of year. During the 48-year period of record at the HMS (1945-1993), only 2 days have had more than 2.5 cm of precipitation: October 10, 1957, with 4 cm; and June 17, 1950, with 2.77 cm (Hoitink and Burk 1994).

The maximum amount of precipitation ever recorded on the Hanford Site in any 24-h period was 4.85 cm (October 10-11, 1957) (Stone et al. 1983; see also Table 1). As noted above, the accumulation of precipitation over 24 h and with a 1,000-year return period is 6.81 cm or 125% of the record. Several attempts have been made to determine the PMP in the region of the prototype barrier.

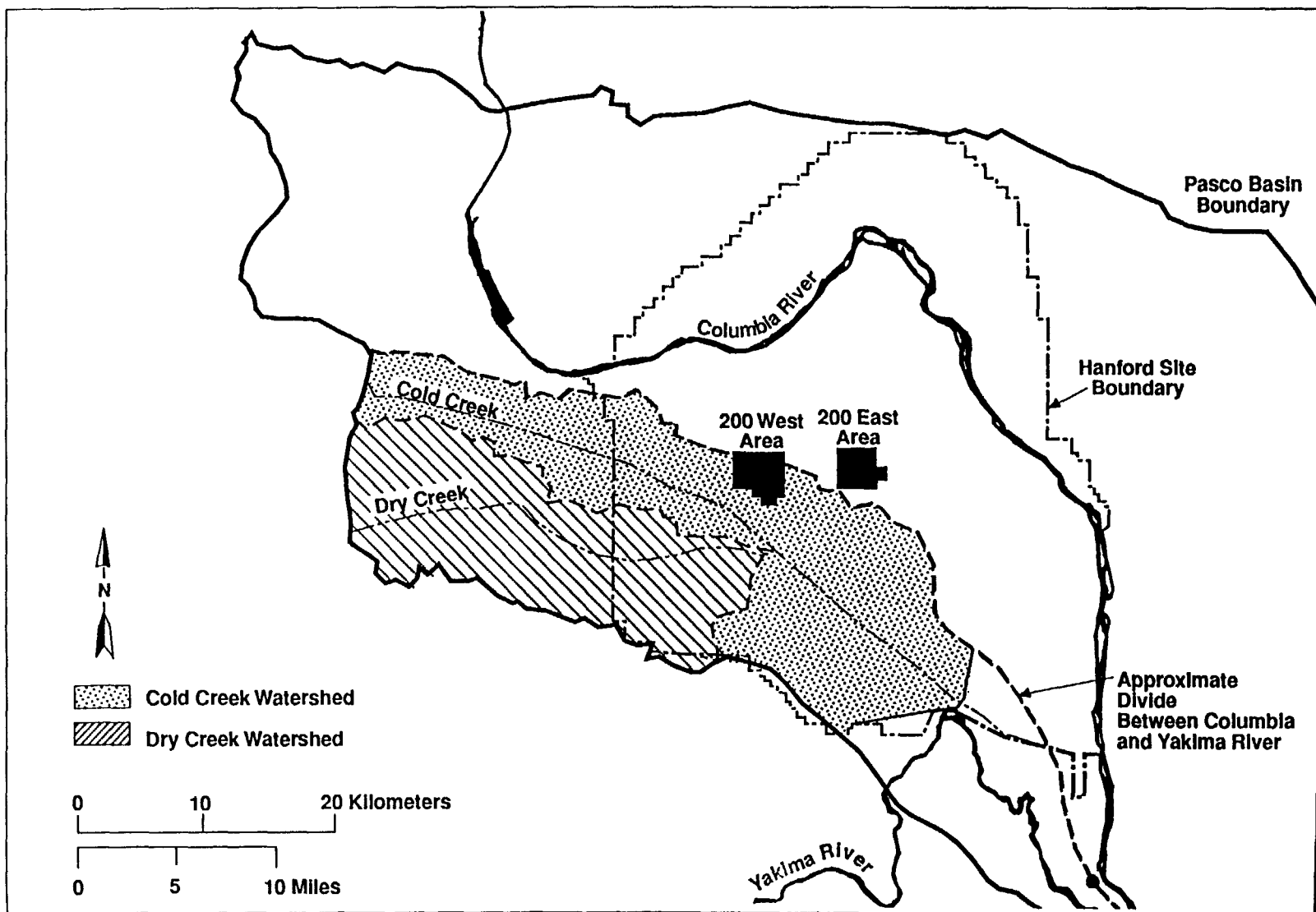
The maximum credible amount of precipitation that could fall on the Hanford Site within a 24-h period (or PMP) has been calculated to be 28 cm (or 175% of the average annual precipitation of 16 cm) (DOE 1987). The probability for exceeding this amount has been estimated to be 1 in 1,000,000 years (DOE 1987).

The Skaggs and Walters (1981) flood risk analysis of Cold Creek near the Hanford Site includes an analysis of the PMP for two sections of that drainage. Their analysis uses as a dividing point between the Upper Cold Creek drainage and the lower Cold Creek drainage the confluence of Dry Creek and Cold Creek (Figure 8). They use procedures developed by the U.S. Weather Bureau (1966) for calculating the PMP and note that, as discussed in the U.S. Weather Bureau report, PMP east of the Cascade Range can occur as general storms of durations up to 72 h throughout the months of October through June or for smaller basins as thunderstorms of shorter durations.

Using U.S. Weather Bureau (1966) data for the general storm PMP for the Cold Creek Basin above the confluence with Dry Creek, Skaggs and Walters concluded that the maximum precipitation can be expected to occur in a storm during the month of June, producing a 3-day total of 31.57 cm (or a 24-h average of 10.52 cm). The maximum 6-h rainfall, however, was computed to be 11.48 cm, or 205% of the 6-h accumulation of 6.48 cm during a storm with a return period of 1,000 years, as shown in Table 1 and discussed above.

Skaggs and Walters (1981) note that the U.S. Weather Bureau (1966) did not include thunderstorms in developing its data, but provided separate procedures. Based on these procedures, the 6-h PMP thunderstorms for both Upper and Lower Cold Creek drainage were computed (Table 3). For Upper Cold Creek, the 6-h PMP thunderstorm was computed to be 18.53 cm. During the general-storm PMP, the maximum 6-h PMP, as indicated above, was only 11.48 cm. There is marked reduction of precipitation depths for the larger drainage area (see Table 3). And it can also be noted that the HMS falls just on the border of the Lower Cold Creek drainage (Figure 8); thus, its records are more likely to reflect the Lower Cold Creek data.

Figure 8. Major Drainage Divides on the Hanford Site and Vicinity.



39110013.48

Table 3. Probable Maximum Precipitation from Thunderstorms of Various Durations.

Location	Drainage area (km ²)	Incremental rainfall amounts (cm) per specified duration of time (h)						
		1	2	3	4	5	6	Sum
Upper Cold Creek (above Dry Creek)	223	1.0	3.6	9.9	1.8	1.3	1.0	18.5
Lower Cold Creek (at the Yakima River)	940	0.5	2.8	5.8	1.3	0.8	0.5	11.7

Skaggs and Walters (1981).

In short, the following values can provide the basis for prototype stress testing. The maximum precipitation recorded for the Hanford Site in 24 h is 4.85 cm; the estimated maximum with a 1,000-year return period is 6.81 cm; and the estimated maximum with a 24-h PMP is 28 cm. The maximum precipitation recorded for the Hanford Site in 6 h is 4.27 cm; the estimated 6-h PMP with a 1,000-year return period is 5.59 cm. There are three different values for the 6-h PMP based on drainage area and storm type. For Upper Cold Creek with general-storm precipitation, the 6-h PMP is 11.48 cm. For Lower Cold Creek with thunderstorm precipitation, the 6-h PMP is 11.7 cm. For Upper Cold Creek with thunderstorm precipitation, the 6-h PMP is 18.5 cm.

3.2.3.4 Paleoclimatic Evidence for Extreme Precipitation. To put the discussion of storms with a 1,000-year return period or PMP into an historical perspective, it is useful to look at paleoclimatic evidence for past extremes. The longer the record, the more confidence that can be placed in the bounding conditions derived from these calculations.

Although there is some evidence for the occurrence of extreme precipitation events during the past 2,000 years as evinced by Columbia River floods (e.g., Chatters and Hoover 1986), there is a lot more paleoclimatic data on long-term precipitation averages. Whitlock (1994) uses a 75,000-year pollen record from Carp Lake near Goldendale, Washington, to reconstruct the climate of the Columbia Basin over that time period. Whitlock estimates that mean annual precipitation ranged from a low of 50% to 75% of modern levels up to a high of 128% of modern levels. She concludes that for the majority of the record (almost 65,000 of the 75,000 years), the climate in the Columbia Basin was drier than at present (i.e., precipitation averaged less than 16 cm in the region of the Hanford Site).

Chatters and Hoover (1992) examine the paleoclimatic evidence for the last 10,000 years and reconstruct the wettest extreme mean climate thus far indicated for the Hanford region as that which occurred during the period from 4,400 to 3,900 years ago. At that time, precipitation averaged approximately 125% to 130% of modern levels (i.e., approximately 20 cm), temperatures were cooler, and most precipitation fell in winter, probably as snow.

3.2.3.5 Preliminary Impact Assessment - Precipitation. These studies, and others, present no evidence that the long-term precipitation average ever reached 300% of modern levels (i.e., 48 cm annually), which has been taken as the upper bounding annual amount to test the prototype barrier (Gee et al. 1993). However, the maximum annual precipitation received at Hanford through 1993 is 29.0 cm (181% of normal), which occurred in 1950 (the next highest being 28.1 cm [176% of normal, in 1983]). Thus, it would seem that for prototype testing, 200% of normal probably is not conservative enough on scales of 1,000 years. Nevertheless, 300% of normal is believed to be conservative for the following reasons: calculations indicate that the probability that annual precipitation will not exceed 31.0 cm/yr (198% of normal) is 1 in 100 years, that it will not exceed 41.0 cm/yr (256% of normal) is 1 in 1,000 years, and that it will not exceed 51.0 cm/yr (319% of normal) is 1 in 10,000 years. Decisions to use precipitation amounts equivalent to the 1,000-year return periods or PMP should prove to be valid extreme tests of barrier performance because for most of the last 75,000 years, annual precipitation was lower than it is now.

3.3 HYDROLOGY

3.3.1 Surface Hydrology

The Columbia River, the Yakima River, and the Cold Creek watershed are the principal surface water bodies in the Hanford Site vicinity. Their flooding histories and potential are addressed in DOE (1988), which concludes that river or stream flooding is not a credible event for the 200 Area Plateau. A catastrophic flood similar to those that inundated the area during Pleistocene is not considered a credible event over the next 1,000 years.

The stream closest to the 200 Area Plateau is Cold Creek. Historical flood flow information for this stream is not available. The estimated 100-year flood peak discharge is 180 m³/s upstream of its confluence with Dry Creek and 560 m³/s at the Yakima River (Skaggs and Walters 1981). A probable maximum flood, with no return period given, was also estimated. In this scenario, the southwest part of the 200 West extension is flooded.

Flooding related to streams or rivers will have no effect on the barrier if it is located on the 200 Area Plateau. Part of the 200 West Area, the western extension, is located on the flank of the 200 Area Plateau. The Skaggs and Walters study (1981) indicates that the southwestern portion of the 200 West Area extension could be flooded by the Cold Creek probable maximum flood.

3.3.2 Groundwater Hydrology

On the 200 Area Plateau, the water table ranges from about 60 to greater than 90 m below ground surface. No credible natural phenomena could raise the water table to a level that would affect the performance of the barrier during its design life.

3.4 GEOLOGY AND SEISMOLOGY

The physical setting of the Hanford Site and the 200 Areas has been characterized extensively as a result of past site activities. A more detailed discussion of the Hanford Site and its geology appears in DOE (1988), Meyers and Price (1981), Reidel and Hooper (1989), and Lindsey (1992a, 1992b).

3.4.1 Topography and Physiography

The Hanford Site (Figure 9) is situated within the Pasco Basin of south-central Washington. The Pasco Basin is one of a number of topographic depressions located within the Columbia Intermontane Physiographic Province (Figure 10), a broad basin located between the Cascade Range and the Rocky Mountains. The Columbia Intermontane Province is the product of Miocene continental flood basalt volcanism and regional deformation that occurred over the past 17 million years. The Pasco Basin is bounded on the north by the Saddle Mountains; on the west by Umtanum Ridge, Yakima Ridge, and the Rattlesnake Mountain and the Rattlesnake Hills; and on the east by the Palouse slope (Figure 9).

Surface topography at the Hanford Site is the result of (1) uplift of anticlinal ridges, (2) Pleistocene cataclysmic flooding, (3) Holocene eolian activity, and (4) landsliding along the ridges and the Columbia River. Uplift of the ridges began in the Miocene Epoch and continues to the present. Cataclysmic flooding occurred when ice dams in western Montana and northern Idaho were breached, allowing large volumes of water to spill across eastern and central Washington. The last major flood occurred approximately 13,000 years ago, during the late Pleistocene Epoch. Since the end of the Pleistocene Epoch, local winds have reworked the flood sediments, depositing dune sands in the lower elevations and loess (windblown silt) around the margins of the Pasco Basin. Generally, sand dunes have been stabilized by vegetation (Figure 11).

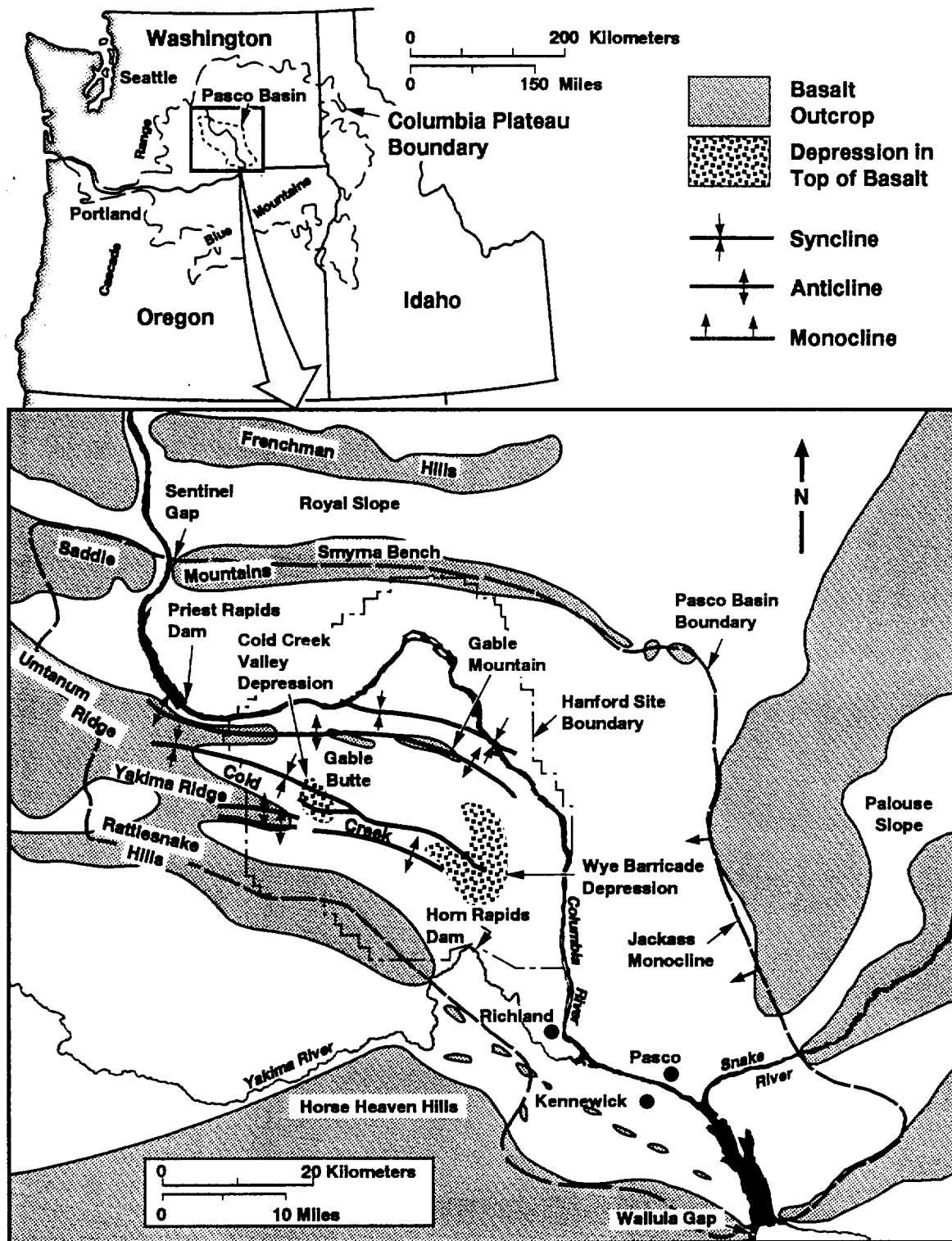
The 200 Areas are situated on a broad flat area called the 200 Area Plateau near the center of the Hanford Site at an elevation of approximately 198 to 229 m above mean sea level.

3.4.2 Stratigraphy

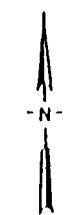
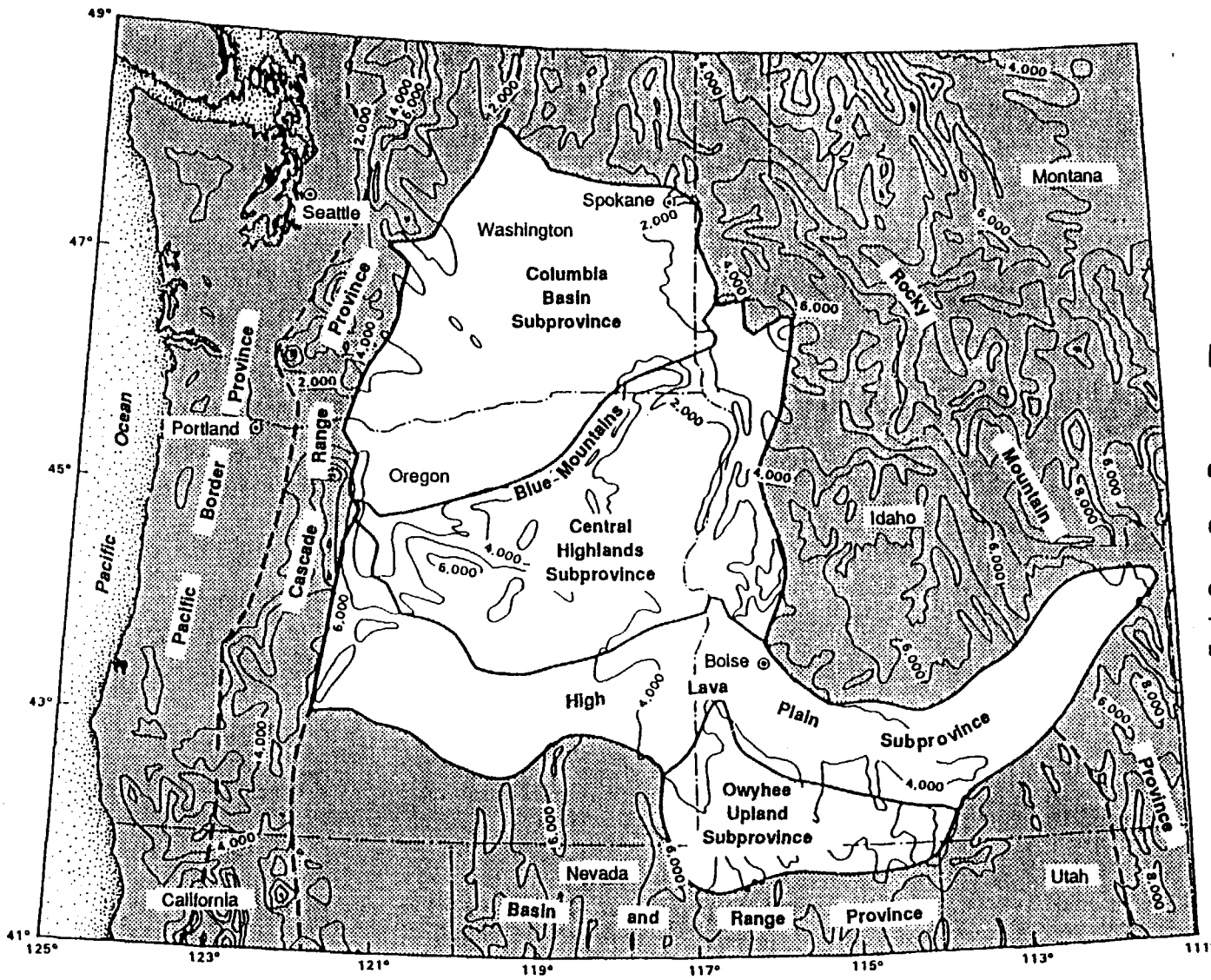
The Hanford Site is underlain by Miocene-aged basalt of the Columbia River Basalt Group and late Miocene to Pleistocene suprabasalt sediments. The basalts and sediments thicken into the Pasco Basin and generally reach maximum thicknesses in the Cold Creek syncline. Older Cenozoic sedimentary and volcanoclastic rocks underlying the basalts are not exposed at the surface near the Hanford Site. Site stratigraphy is summarized in Figure 12 and described in the following sections.

3.4.2.1 Columbia River Basalt Group. The Columbia River Basalt Group (CRBG) comprises an assemblage of tholeiitic, continental flood basalts of Miocene age. These flows cover an area of more than 163,157 km² in Washington, Oregon, and Idaho and have an estimated volume of about 174,356 km³ (Tolan et al. 1989). Isotopic age determinations indicate that basalt flows were erupted approximately 17 to 6 million years before the present, with more than 98% by volume being erupted in a 2.5-million year period 17 to 14.5 million years ago (Reidel et al. 1989). The most current information on the CRBG is presented by Reidel and Hooper (1989).

Figure 9. Geologic Structure of the Pasco Basin and the Hanford Site.



H8111014.1



□ Columbia Intermontane Province

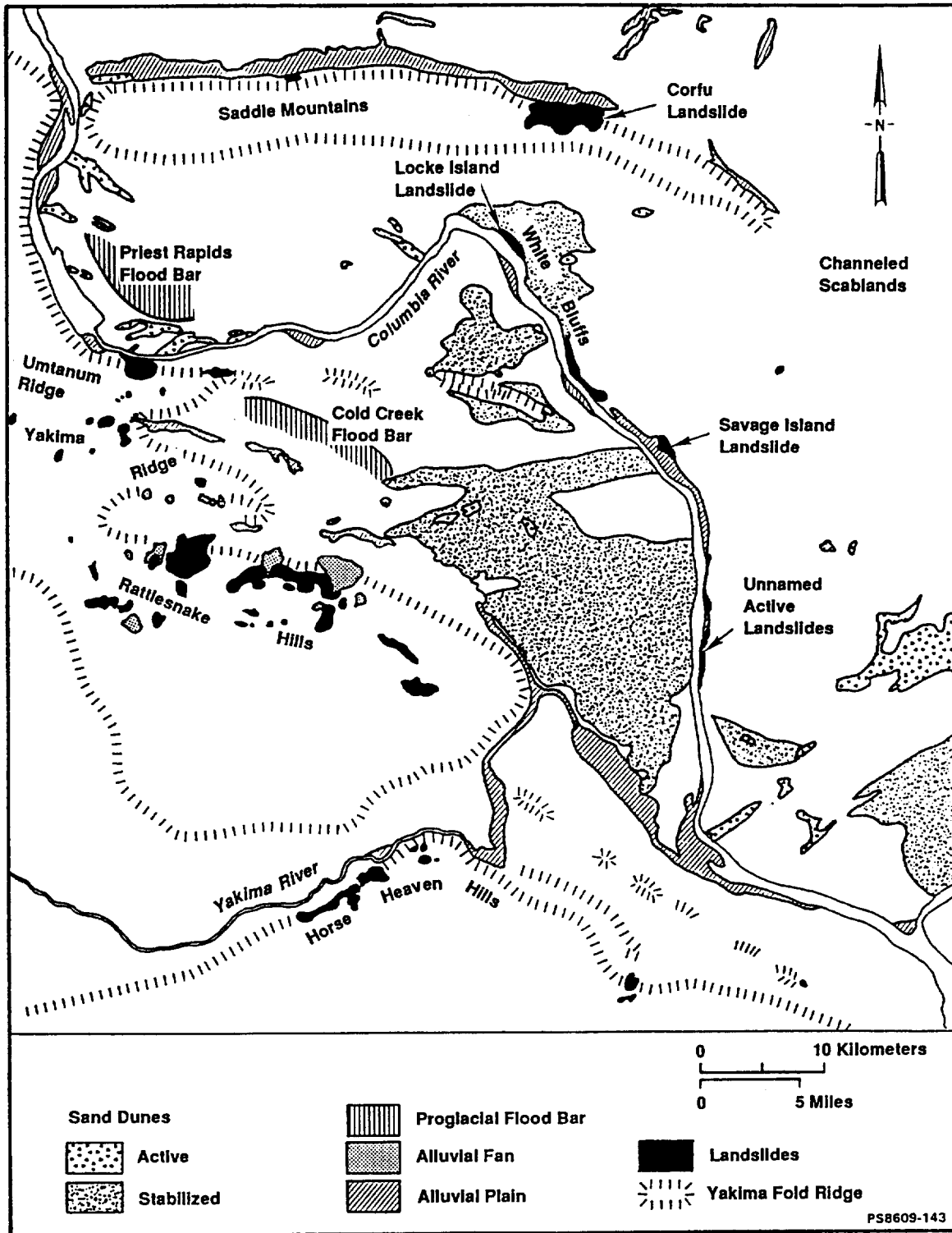
0 100 Kilometers
0 50 Miles

Contour Interval = 2000 ft
To convert feet to meters, multiply by 0.3048

PS8609-137
PS-90-249

Figure 10. Divisions of the Columbia Intermontane Province and Adjacent Provinces.

Figure 11. Landforms of the Pasco Basin and the Hanford Site.



PS-90-246

Figure 12. Generalized Stratigraphy of the Hanford Site.

[illegible]

*The Grande Ronde Basalt consists of at least 120 major basalt flows comprising 17 members. N₂, R₂, N₁, and R₁ are magnetostratigraphic units.

3.4.2.2 Ellensburg Formation. The Ellensburg Formation consists of all sedimentary units that occur between the basalt flows of the CRBG in the central Columbia Basin. The Ellensburg Formation generally displays two main lithologies, volcanoclastics and siliciclastics. The volcanoclastics consist mainly of primary pyroclastic air-fall deposits and reworked epiclastics derived from volcanic terrains west of the Columbia Plateau. Siliciclastic strata in the Ellensburg Formation consist of clastic, plutonic, and metamorphic detritus derived from the Rocky Mountain terrain. These two lithologies occur as both distinct and mixed in the Pasco Basin. A detailed discussion of the Ellensburg Formation in the Hanford Site is given by Reidel and Fecht (1981).

3.2.4.3 Ringold Formation. The Ringold Formation at the Hanford Site is up to 185 m thick in the deepest part of the Cold Creek syncline south of the 200 West Area and 170 m thick in the western Wahluke syncline near the 100-B Area. It is largely absent in the northern and northeastern parts of the 200 East Area and adjacent to areas to the north in the vicinity of West Pond.

The Ringold Formation is divided on the basis of sediment facies associations and their distribution, Figure 13 (Lindsey 1991). Facies associations in the Ringold Formation are summarized as follows:

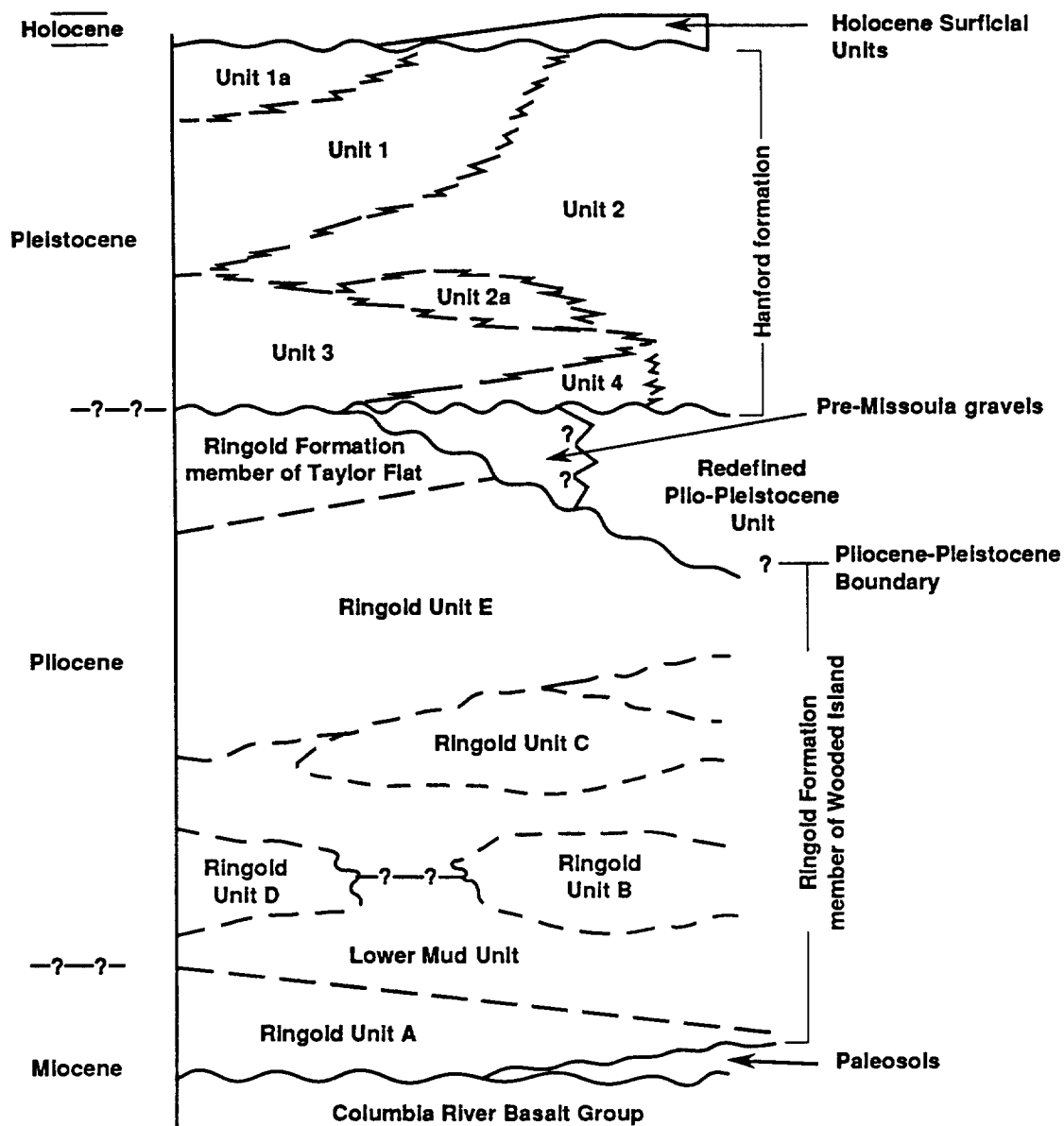
- Clast-supported granule to cobble gravel with a sandy matrix
- Quartzo-feldspathic sands that display cross-bedding and cross-lamination in outcrop
- Overbank facies association consisting of laminated to massive silt, silty fine-grained sand, and paleosols containing variable amounts of CaCO_3
- Plane-laminated to massive clay with thin silt and silty sand interbeds
- A gravel facies that was deposited largely by debris flows in alluvial fan settings.

3.4.2.3 Post-Ringold Pre-Hanford Deposits. Thin alluvial deposits situated stratigraphically between the Ringold Formation and the Hanford formation are found throughout the Pasco Basin. These deposits are referred to informally as (1) Plio-Pleistocene unit, (2) pre-Missoula gravels, and (3) early "Palouse" soil.

3.4.2.4 Hanford Formation. The Hanford formation consists of pebble to boulder gravel, fine- to coarse-grained sand, and silt. It consists of gravel-dominated deposits and deposits dominated by sand and silt. The gravel deposits range from well sorted to poorly sorted. The fine-grained deposits, which make up the most extensive and voluminous part of the Hanford formation, are divided into two facies: (1) plane-laminated sand and (2) normally graded rhythmites, also referred to as "Touchet Beds." The Hanford formation is commonly divided into two informal members: the Pasco gravels and the Touchet Beds (Tallman et al. 1981, Fecht et al. 1987, DOE 1988). The Pasco gravels generally correspond to the gravelly facies, and the Touchet Beds to the sandy to silty facies. The Hanford formation is thickest in the Cold Creek bar in the vicinity of the 200 Areas, where it is up to 65 m thick (Figure 13). Hanford Site deposits are absent on ridges higher than approximately 360 m above mean sea level.

3.4.2.5 Holocene Surficial Deposits. Holocene surficial deposits consist of silt, sand, and gravel that form a thin (<4.9 m) veneer across much of the Hanford Site. These sediments were deposited by a mix of eolian and alluvial processes.

Figure 13. Generalized Stratigraphy of the Suprabasalt Sediments Beneath the Hanford Site.



H9409017.1

3.4.3 Structural Geology and Tectonic Setting

3.4.3.1 Tectonic Framework. The Columbia Plateau (Figure 14) is a part of the North American continental plate and lies in a back-arc setting east of the Cascade Range. It is bounded on the north by the Okanogan Highlands, on the east by the Northern Rocky Mountains and Idaho Batholith, and on the south by the High Lava Plains and Snake River Plain.

3.4.3.2 Regional Structural Geology. The Columbia Plateau can be divided into three informal structural subprovinces (Figure 15): Blue Mountains, Palouse, and Yakima Fold Belt (Tolan and Reidel 1989). These structural subprovinces are delineated on the basis of their structural fabric, unlike the physiographic provinces that are defined on the basis of landforms. The Hanford Site is located near the junction of the Yakima Fold Belt and the Palouse subprovinces.

The principal characteristics of the Yakima Fold Belt are a series of segmented, narrow, asymmetric anticlines that have wavelengths between 5 and 31 km and amplitudes commonly less than 1 km (Reidel et al. 1989). These anticlinal ridges are separated by broad synclines or basins that, in many cases, contain thick accumulations of Neogene- to Quaternary-age sediments. The Pasco Basin is one of the larger structural basins in the Columbia Plateau.

The northern limbs of the generally east-west trending asymmetric anticlines of the Yakima Fold Belt dip steeply to the north or are vertical. The southern limbs generally dip at relatively shallow angles to the south. Thrust or high-angle reverse faults with fault planes that strike parallel or subparallel to the axial trends are found principally on the north sides of these anticlines. The amount of vertical stratigraphic offset associated with these faults varies, but commonly exceeds hundreds of meters.

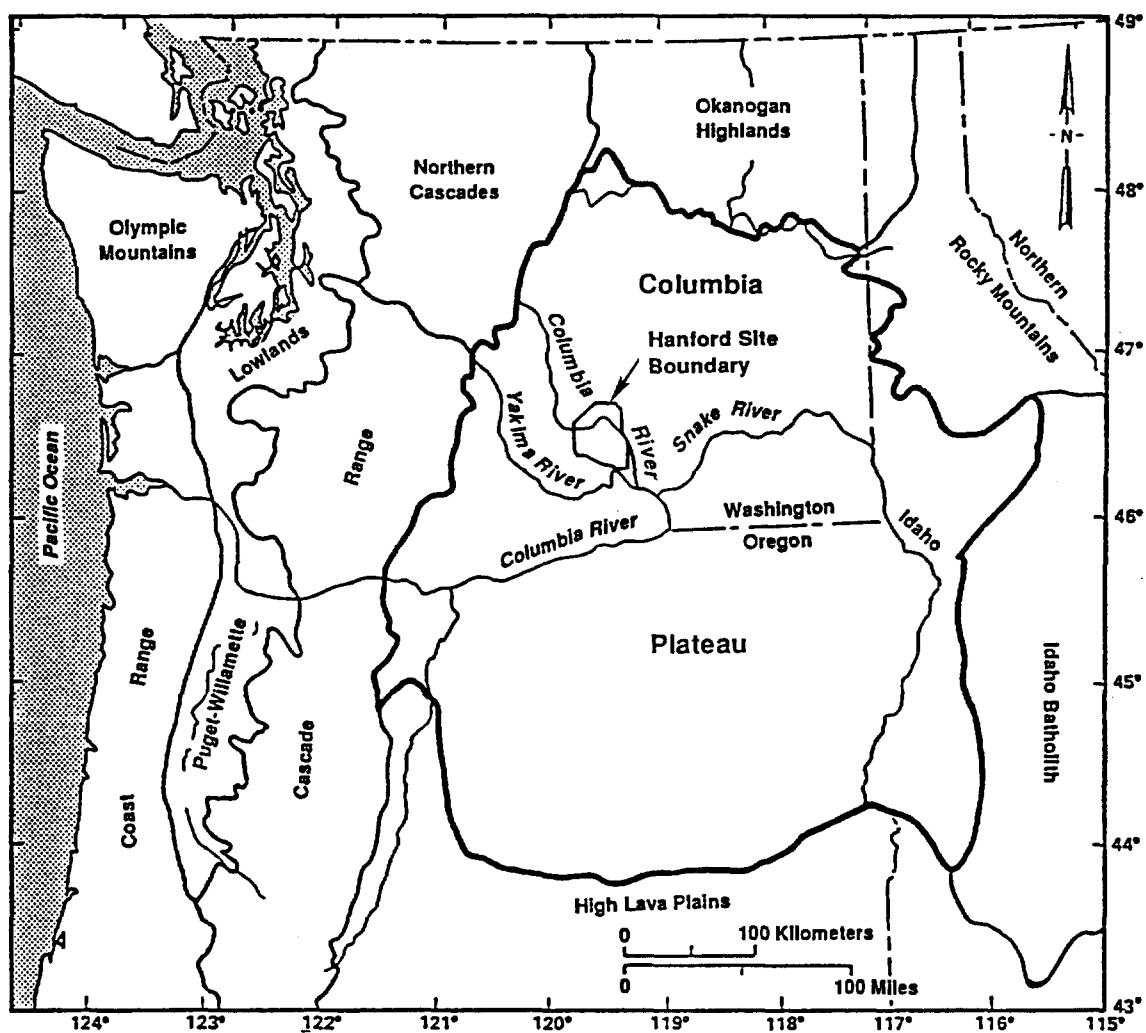
Deformation of the Yakima Folds occurred under north-south compression and was contemporaneous with the eruption of the basalt flows (Reidel 1984, Reidel et al. 1989). The fold belt was enlarging during the eruption of the CRBG and continued to enlarge through the Pliocene Epoch, into the Pleistocene Epoch, and perhaps to the present.

3.4.4 Site Structural Geology

The Hanford Site is situated in the Pasco Basin, one of the largest structural basins on the Columbia Plateau. The Pasco Basin is bounded on the north by the Saddle Mountains anticline; on the west by the Umtanum Ridge, Yakima Ridge, and Rattlesnake Hills anticlines; and on the south by the Rattlesnake Mountain anticline (Figure 12). The Palouse slope, a west-dipping monocline, bounds the Pasco Basin on the east.

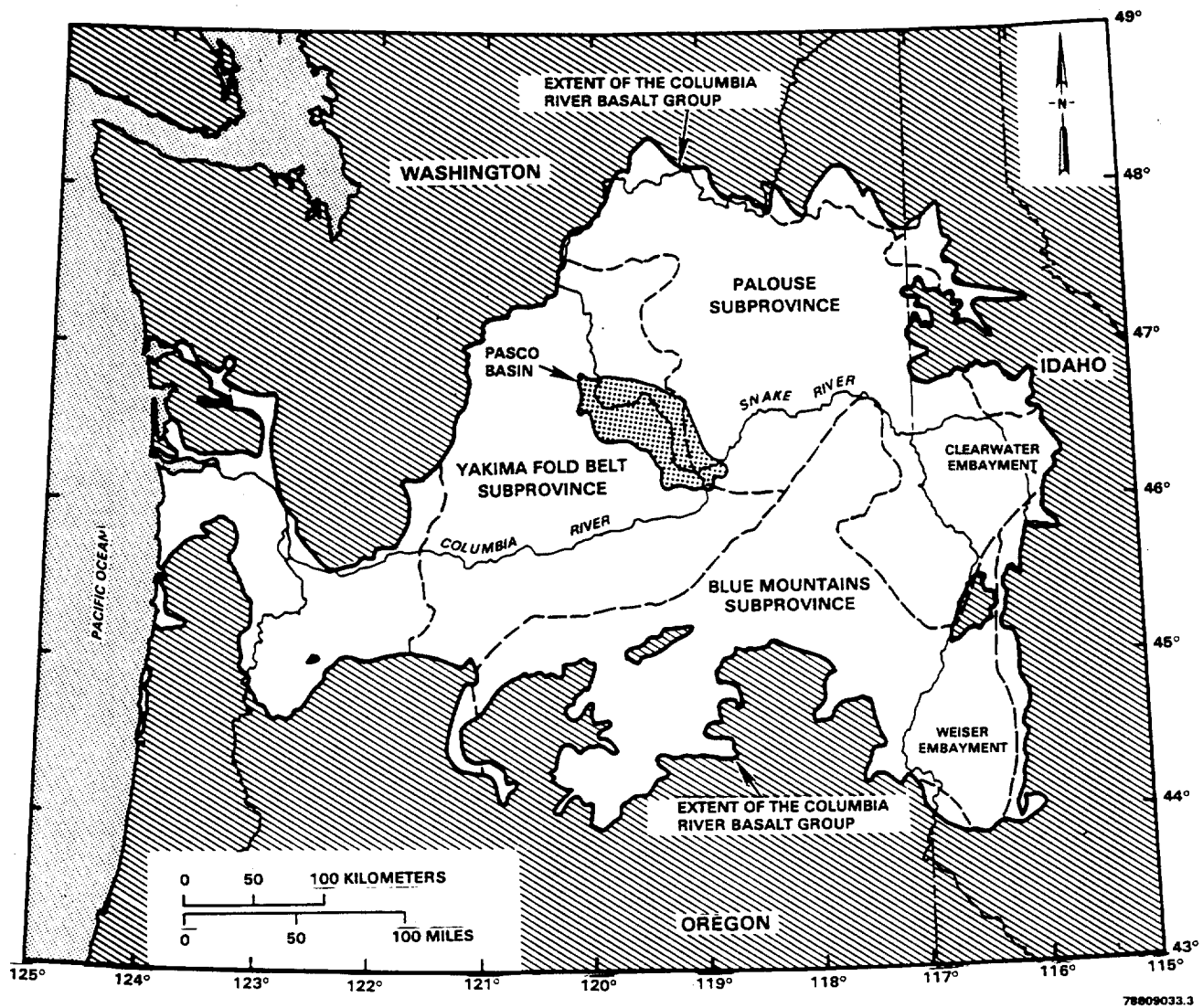
The 200 and 300 Areas are situated on the south flank of the Umtanum-Gable Mountain anticline where the Miocene-age basalt bedrock dips to the southwest into the Cold Creek syncline. The 100 Areas lie north of the Umtanum-Gable Mountain anticline in the Wahluke syncline. The deepest parts of the Cold Creek syncline, the Wye Barricade depression and the Cold Creek depression, are approximately 12 km southeast of the 200 Areas and under the 200 West Area, respectively.

Figure 14. Index Map of the Geologic Provinces.



PS8609-193
PS-90-248

Figure 15. Structural Subprovinces and Extent of Columbia River Basalt Group.



3.4.5 Seismology

Westinghouse Hanford Company (WHC) operates a 20-station seismic network in and around the Hanford Site for the DOE. Earthquakes with a magnitude of 1.5 or greater can be located accurately with this array. A catalog of earthquakes recorded in and around the Hanford Site appears in DOE (1988).

Eastern Washington, especially the Columbia Plateau region, is a seismically inactive area when compared to the rest of the western United States (DOE 1988). The closest regions of historic moderate-to-large earthquake generation are in western Washington and Oregon and western Montana and eastern Idaho. The most significant event relative to the Hanford Site is the 1936 Milton-Freewater, Oregon, earthquake, with a magnitude of 5.75, that occurred more than 90 km away. The largest Modified Mercalli Intensity was felt at Walla Walla, Washington, and was VI. This event was approximately 105 km from the Hanford Site.

Since mid-1969 there has been a Hanford seismic network capable of locating all earthquakes of Richter magnitude 1.5 and larger at or near the Hanford Site, and magnitude 2.0 and larger throughout the rest of southeastern Washington. The historic seismic record for eastern Washington began in approximately 1850; no earthquakes large enough to be felt had epicenters on the Hanford Site. The only evidence of past moderate or possibly large earthquake activity is geologic evidence. This evidence is shown by the anticlinal folds and faulting associated with Rattlesnake Mountain, Saddle Mountain, and Gable Mountain.

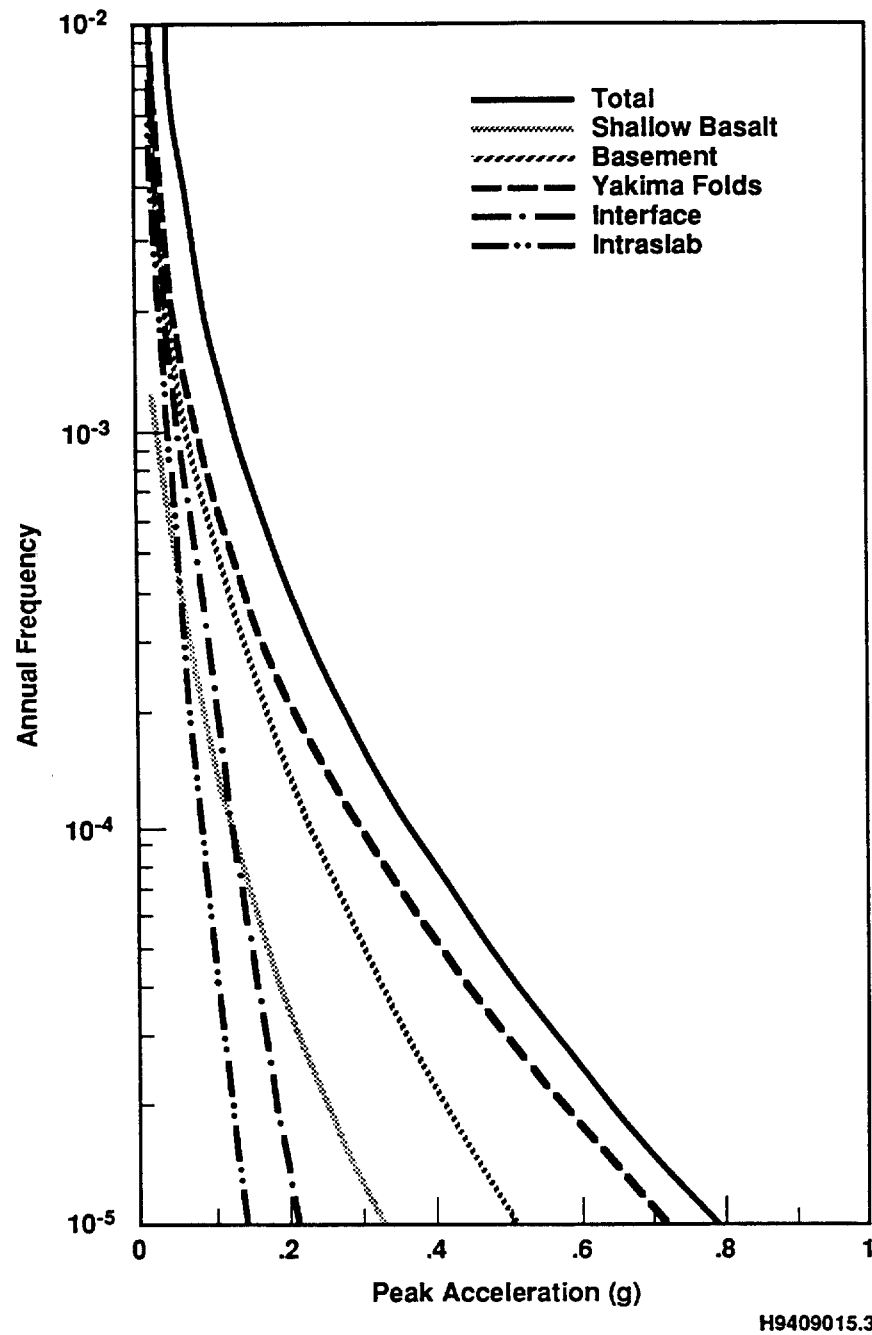
3.4.6 Seismic Hazard

3.4.6.1 Source Model. Earthquake activity in the Columbia Basin, central Washington, is attributed to three separate source regions of the seismogenic crust: fault sources expressed at the surface as the Yakima Folds and related thrust/reverse faults; a shallow basalt source that accounts for the observed seismicity within the CRBG that is not spatially associated with the Yakima Folds; and a crystalline basement source region that extends from the top of the crystalline basement to the base of the seismogenic crust. Another source for ground motion from earthquakes outside the Columbia Basin is the Cascadia Subduction Zone. These source regions are assumed to account for all observed seismicity and are developed within the framework of a regional crustal model based on available surface and subsurface geologic data, geophysical data, and seismicity data. A more detailed discussion of the modeling of these sources appears in Geomatrix (1993). The seismic sources are discussed below.

Yakima Folds. The location and characteristics of the Yakima Fold faults or inferred faults were used to estimate the probability of activity, maximum magnitude, and recurrence rates for each Yakima Fold source. The results were used as data in the determination of the contribution of Yakima Folds to the seismic hazard of the Hanford Site. As Figure 16 illustrates, the Yakima Fold source is the predominant contributor in the 200 Areas.

Shallow Basalt. Small- to moderate-magnitude earthquakes have been recorded instrumentally in the Columbia River basalts. These events are not associated spatially with the Yakima Fold axes or orientation nor are they associated with other known structures. This source is explicitly separate from the Yakima Fold sources in the seismic hazard assessment. Spatial distribution, maximum

Figure 16. Contribution of Sources to the Mean Seismic Hazard at the 200 East Area.



magnitude, earthquake recurrence, magnitude distribution, and a probability of activity of 1.0 are included in the assessment of contribution from this source.

Basement Sources. The basement seismic sources in the Hanford Site vicinity are those that exist within the crystalline crust beneath the relatively low-velocity sub-basalt sediments. The occurrence of seismicity within this zone confirms that it is seismogenic, and alternative models are used to explain the basement source. The basement source is the second largest contributor (Figure 16).

Cascadia Subduction Zone. The Cascadia subduction zone lies along the west coast of North America from northern California to mid-Vancouver Island. Subduction zones are related to two separate and distinct processes: stresses within the subduction slab and compressional stresses at the interface between the two plates. Both processes are characterized and modeled on the basis of both Cascadia-specific and world-wide subduction zone data and are included in the hazard assessment. This interface source significantly contributes to the longer period ground motion.

3.4.6.2 Probabilistic Seismic Hazard Assessment. The probabilistic seismic hazard assessment completed for the Hanford Site (Geomatrix 1993) is the basis for the following discussion and provides additional detail. The computed mean to 5th- to 95th-percentile hazard curves for the 200 East Area appear in Figure 17. The 200 West Area hazard curves are essentially the same as those for the 200 East Area. Also shown are the results for 5%-damped spectral acceleration at 0.3 and 2.0 seconds.

The mean peak acceleration with an annual frequency of 10^{-3} or a return period of 1,000 years is about 0.14 g for both the 200 East and 200 West Areas. Or, there is about a 63% chance that 0.14 g will be exceeded during the 1,000-year design life. The 10^{-4} or the 10,000-year return ground motion is about 0.38 g. The probability of exceeding this ground motion in 1,000 years is about 10%. The barrier was analyzed to the 1,000- and 10,000-year return period ground motion and is discussed in Section 3.7.2.

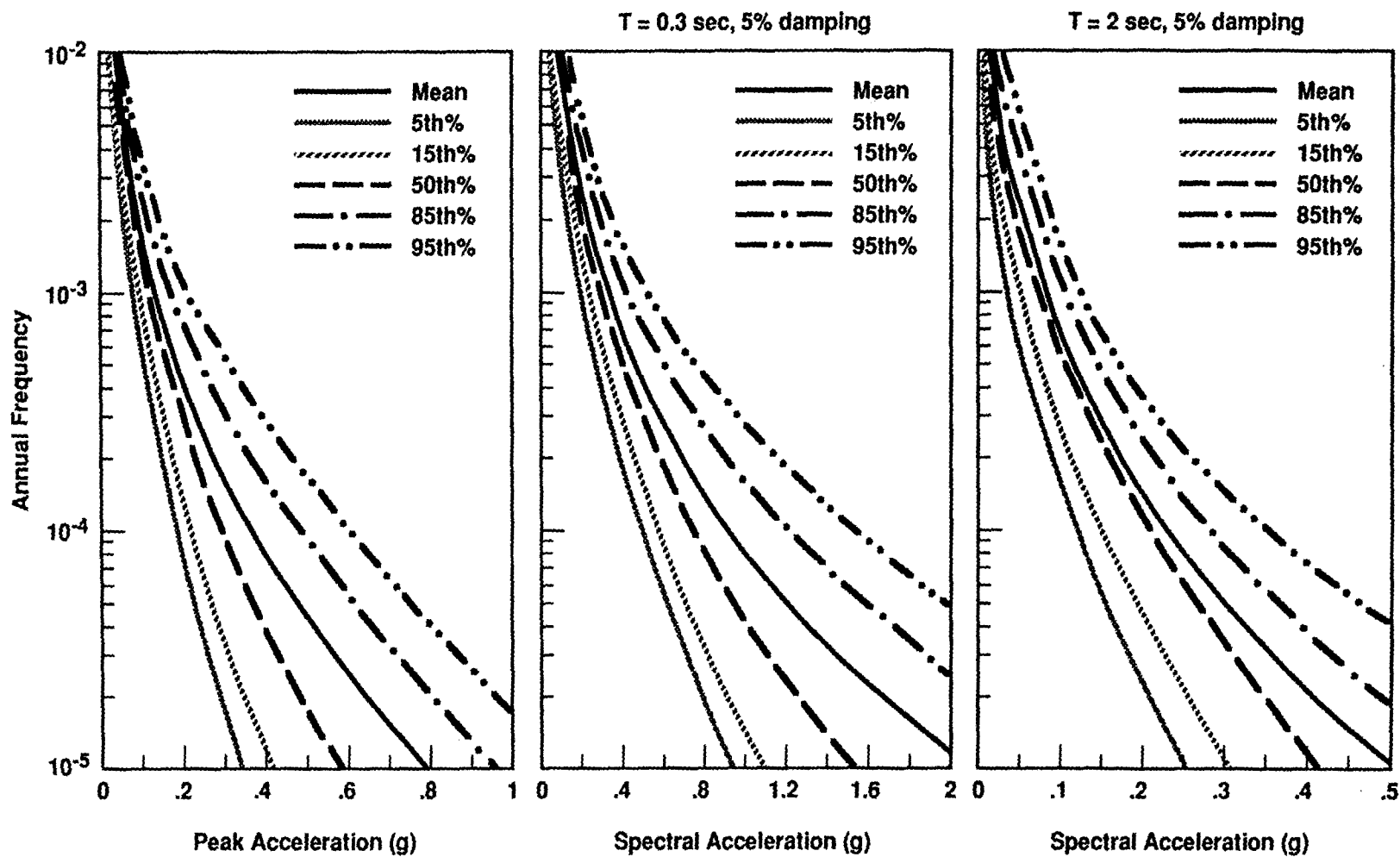
3.5 VOLCANIC HAZARDS

The Pacific Northwest has a long history of igneous activity that has produced both intrusive and extrusive volcanic rocks. The history of volcanism during the last 60 million years (Cenozoic Era) is well preserved and provides the basis for assessing the volcanic hazard of the Hanford Site and surrounding area.

3.5.1 Columbia River Basalt Group Volcanism

The Columbia River basalt was erupted from fissures, chiefly in the tri-state area of Idaho, Oregon, and Washington, from about 17 m.y.B.P. to about 6 m.y.B.P. The only known CRBG dikes and vents near the Pasco Basin occur along the eastern margin of the basin. These fissures and dikes are the source of the Ice Harbor Basalt (8.5 m.y.B.P.), the youngest CRBG in the Pasco Basin. CRBG volcanism is dismissed as a hazard because the most recent CRBG eruption was about 6 million years ago after 10 million years of decreasing flow volume and frequency of occurrence. Further, there are no indications such as high-heat flow that would suggest renewed CRBG volcanism.

Figure 17. Computed Mean and 5th to 95th Percentile Seismic Hazard Curves for the 200 East Area.



H9409015.1

3.5.2 Cascade Volcanism

Cascade volcanic activity is divided into two main episodes. The first period, occurring between about 38 and 5 million years ago, was located in the western part of the Cascade Range of today. Since 5 million years ago, the second episode has been occurring. Many large-strato volcanoes have been active during historical time, including Lasses Peak, Mount Shasta, Mount Rainier, Mount Hood, Mount Baker, and Mount St. Helens. Ash (tephra) and other, larger pyroclastic material; lava, mud, and debris flows; and associated mudslides and landslides are all products of Cascade volcanism.

The nearest Cascade volcano is more than 100 km from the Hanford Site. Tephra from the Cascade volcanoes has been found in the sediments in and around the Hanford Site. During the 1980 eruption of Mount St. Helens, approximately 1 cm of ash fell on the northern part of the Hanford Site. The volcanic hazard depends on the probability and type of renewed eruptive activity and the meteorological conditions that control the direction and distance of air transport. A preliminary volcanic hazard assessment (Hoblitt et al. 1987) indicates that 10 cm of uncompacted ash would have an annual frequency of 10^{-3} or a 63% chance of occurring during the 1,000-year design life. This value seems conservative in terms of the sediment record; however, Hoblitt's assessment is the only attempt to quantify the hazard.

Ashfall may affect the long-term barrier in two ways: by killing low vegetation and by covering the barrier with a more impermeable layer. These effects of ashfall are not considered significant to barrier performance at this time.

3.6 GEOTECHNICAL STUDIES

Future applications of the long-term surface barrier are anticipated to be predominantly in the 200 East and 200 West Areas. The 200 Areas of the Hanford Site are underlain by sediments of the Hanford formation and the Ringold Formation (see Figure 13). The geotechnical properties can be described as a deep, stiff soil site with competent surface sediments (100 ft/s shear wave velocity) except in locations of loess or dune sand.

3.7 ENGINEERED BARRIER CHARACTERIZATION AND STRUCTURAL ANALYSIS

A prototype for the long-term surface barrier has been constructed in the northwestern part of the 200 East Area of the Hanford Site on existing crib 216-B-57 in the 200-BP-1 Operable Unit. A description of the material and dimensions of the various layers and the functional requirements appear in Wing (1993).

For purposes of the analyses presented in this report, engineering properties of the various materials in the prototype barrier were based on literature values for similar engineered materials and on engineering judgement. Laboratory testing was done on the fluid applied asphalt (FAA) material as appropriate measurements were not available in the literature.

3.7.1 Laboratory Testing

A laboratory testing program investigated the shear strength of the FAA and its interface with the overlying drainage gravel and the underlying asphaltic concrete (AC). Results of the direct shear testing of the FAA interface appear in Appendix A.

Results of these preliminary tests give a cohesion value of approximately 100 lb/ft² and internal friction angle of approximately 10 deg. Results of the laboratory and engineering analyses indicate that slope creep of materials overlying the FAA is a potential. Hence, a recommendation has been provided that the existing prototype barrier side slopes be surveyed and monitored to evaluate any creep effects for materials overlying the FAA.

Examination of the core sample after the direct shear testing indicated that the overlying drainage gravel materials partially penetrated the underlying FAA materials at test overburden loads equivalent to static field loads. Drainage gravel penetration into the FAA is described in detail in Appendix A.

3.7.2 Barrier Analysis

An analysis of the stability of the static slope and analyses of associated earthquake deformation were performed for the prototype barrier at the 216-B-57 crib in the 200-BP-1 Operable Unit. The analyses and results appear in Appendix A. The analyses are relatively nonrigorous examinations of the potential effects of an extreme earthquake event. It is doubtful that more rigorous analyses would provide significantly better assessments of the potential effects.

In general, a range of values of engineering properties was considered for each of the various elements in the prototype surface barrier, and a parametric sensitivity analysis performed. In addition, the barrier geometry and cross section were taken as those of the prototype surface barrier, as shown on drawings H-2-817484 through H-2-817496 (Fort et al. 1993).

A summary of significant findings from the analyses of static slope stability and seismic deformation are as follows.

- The minimum static safety factor for the prototype barrier is on the order of 1.5, occurring along the two horizontal to one vertical (2:1) basalt side slopes.
- Under nonseismic static loading conditions, the potential for downhill creep of the FAA and overlying materials has been identified.
- For the 1,000-year recurrence interval (67% probability of exceedance over 1,000 years) seismic loading conditions, the permanent seismic deformations are estimated to be on the order of 0 to 0.8 mm or less. The displacement plane for the most critical surface is within the wedge of the basalt side slope, starting from the top of the slope extending vertically downward to the FAA layer, then extending horizontally, essentially along the FAA to just below the toe of the basalt side slope.
- For the 10,000-year recurrence interval (10% probability of exceedance over 10,000 years) seismic loading conditions, the permanent seismic deformations are estimated to be on the

order of 0 to 20.5 mm or less. The displacement plane for the most critical surface is within the wedge of the basalt side slope, starting from the top of the slope extending vertically downward to the FAA layer, then extending horizontally, essentially along the FAA to just below the toe of the basalt side slope.

3.7.3 Barrier Layer Integrity

The scenario of slope displacement under seismic loading conditions, described above, shows probable movement of materials over the FAA along the FAA surface. Whether or not the FAA is susceptible to permanent tears or breakage in this scenario cannot be determined without further laboratory and engineering analyses. However, as noted above, the movement plane exposure at the top of the slopes is likely well outside the underlying waste form limits.

4.0 REFERENCES

- Chatters, J. C. and K. A. Hoover, 1986, "Changing Late Holocene Flooding Frequencies on the Columbia River, Washington," *Quaternary Research*, 26:309-320.
- Chatters, J. C. and K. A. Hoover, 1992, "Response of the Columbia River Fluvial System to Holocene Climatic Change," *Quaternary Research*, 26:309-320.
- Coats, D. W. and P. C. Murray, 1985, *Natural Phenomena Hazards Modeling Project: Extreme Wind/Tornado Hazard Models for Department of Energy Sites*, UCRL-53526, Lawrence Livermore National Laboratory, Livermore, California.
- DOE, 1987, *Final Environmental Impact Statement: Disposal of Hanford Defense High-Level, Transuranic and Tank Wastes, Hanford Site, Richland, Washington*, DOE/EIS-0113, U.S. Department of Energy, Washington, D.C.
- DOE, 1988, *Consultation Draft Site Characterization Plan*, DOE/RW-0164, Vol. 1-9, Office of Civilian Radioactive Waste Management, U.S. Department of Energy, Washington, D.C.
- DOE-RL, 1982, *Site Characterization Report for the Basalt Waste Isolation Project*, 3 vol., DOE/RL 82-3, U.S. Department of Energy, Richland Operations Office, Richland, Washington.
- DOE-RL, 1993, *Report on the Value Engineering Study of Permanent Isolation Surface Barrier and Warning Marker System Development Plan at the Hanford Site*, DOE/RL/12074--8, Rev. 0, U.S. Department of Energy, Richland Operations Office, Richland, Washington.
- Fecht, K. R., S. P. Reidel, and A. M. Tallman, 1987, "Paleodrainage of the Columbia River System on the Columbia Plateau of Washington State -- A Summary," in *Selected Papers on the Geology of Washington*, edited by J. D. Schuster, Division of Geology and Earth Resources, Bulletin 77, pp. 219-248.

- Fort, D. L., S. D. Consort, B. R. Fillion, L. A. Gaddis, and R. G. Hollenbeck, 1993, *Construction Specification for Prototype Surface Barrier at 200-BP-11 Operable Unit*, W-263-C2, Rev. 0, Kaiser Engineers Hanford Company, Richland, Washington.
- Gee, G. W., L. L. Cadwell, H. D. Freeman, M. W. Ligothe, S. O. Link, R. A. Romine, and W. H. Walters, Jr., 1993, *Testing and Monitoring Plan for the Permanent Isolation Surface Barrier Prototype*, PNL-8391, Pacific Northwest Laboratory, Richland, Washington.
- Geomatrix, 1993, *Probabilistic Seismic Hazard Analysis DOE Hanford Site, Washington*, WHC-SD-W236A1-IT-002, prepared for Westinghouse Hanford Company, Richland, Washington.
- Glantz, C. S. and M. M. Islam, 1988, *The Data Collection Component of the Hanford Meteorology Monitoring Program*, PNL-6684, Pacific Northwest Laboratory, Richland, Washington.
- Glantz, C. S., M. N. Schwartz, K. W. Burk, R. B. Kasper, M. W. Ligothe, and P. J. Perrault, 1990, *Climatological Summary of Wind and Temperature Data for the Hanford Meteorology Monitoring Network*, PNL-7471, Pacific Northwest Laboratory, Richland, Washington.
- Hoblitt, R. P., C. D. Miller, and W. E. Scott, 1987, *Volcanic Hazards with Regard to Siting Nuclear-Power Plants in the Pacific Northwest*, Open-File Report 87-297, U.S. Geological Survey, Vancouver, Washington.
- Hoitink, D. J. and K. W. Burk, 1994, *Climatological Data Summary 1993 with Historical Data*, PNL-9809, Pacific Northwest Laboratory, Richland, Washington.
- Lindsey, K. A., 1991, *Revised Stratigraphy for the Ringold Formation, Hanford Site, South-Central Washington*, WHC-SD-EN-EE-004, Rev. 0, Westinghouse Hanford Company, Richland, Washington.
- Lindsey, K. A., 1992a, *Geologic Setting of the 200 West Area: An Update*, WHC-SD-EN-TI-008, Westinghouse Hanford Company, Richland, Washington.
- Lindsey, K. A., 1992b, *Geologic Setting of the 200 West Area: An Update*, WHC-SD-EN-TI-021, Westinghouse Hanford Company, Richland, Washington.
- Mehring, P. J., Jr., 1985, "Late Quaternary Pollen Records from the Interior Pacific Northwest and Northern Great Basin of the United States," in *Pollen Records of Late-Quaternary North American Sediments*, ed. V. M. Bryant, Jr., and R. G. Holloway, American Association of Stratigraphic Palynologists, Dallas, Texas, pp. 167-189.
- Meyers, C. W. and S. M. Price, 1981, "Bedrock Structure of the Cold Creek Syncline Area," in *Subsurface Geology of the Cold Creek Syncline*, RHO-BWI-ST-14, Rockwell Hanford Operations, Richland, Washington.
- NRC, 1982, *Safety Evaluation Report (Related to the Operation of WPPSS Nuclear Project No. 2)*, NUREG-0892, Supplement No. 1, U.S. Nuclear Regulatory Commission, Washington, D.C.

- Ramsdell, J. V. and G. L. Andrews, 1986, *Tornado Climatology of the Contiguous United States*, NUREG/CR-4461, U.S. Nuclear Regulatory Commission, Washington, D.C.
- Reidel, S. P., 1984, "The Saddle Mountains: The Evolution of an Anticline in the Yakima Fold Belt," *American Journal of Science*, 284:942-978.
- Reidel, S. P. and K. R. Fecht, 1981, "Wanapum and Saddle Mountains Basalt in the Cold Creek Syncline Area," in *Subsurface Geology of the Cold Creek Syncline*, RHO-BWI-ST-14, Rockwell Hanford Operations, Richland, Washington.
- Reidel, S. P. and P. R. Hooper, editors, 1989, *Volcanism and Tectonism in the Columbia River Flood-Basalt Province*, Special Paper 239, Geological Society of America, Boulder, Colorado, p. 386, plate 1.
- Reidel, S. P., T. L. Tolan, P. R. Hooper, M. H. Beeson, K. R. Fecht, R. D. Bentley, and J. L. Anderson, 1989, "The Grande Ronde Basalt, Columbia River Basalt Group: Stratigraphic Descriptions and Correlations in Washington, Oregon, and Idaho," in *Volcanism and Tectonism in the Columbia River Flood-Basalt Province*, Special Paper 239, eds. S. P. Reidel and P. R. Hooper, Geological Society of America, Boulder, Colorado, pp. 21-53.
- Sackschewsky, M. R., D. S. Landeen, J. L. Downs, W. H. Rickard, and G. I. Baird, 1992, *Vascular Plants of the Hanford Site*, WHC-EP-0554, Westinghouse Hanford Company, Richland, Washington.
- Skaggs, R. L. and W. H. Walters, 1981, *Flood Risk Analysis of Cold Creek Near the Hanford Site*, RHO-BI-C-120/PNL-4219, Pacific Northwest Laboratory for Rockwell Hanford Operations, Richland, Washington.
- Stone, W. A., D. E. Jenne, and J. M. Thorpe, 1972, *Climatography of the Hanford Area*, BNWL-1605, AEC Research and Development Reports, Pacific Northwest Laboratory, Richland, Washington.
- Stone, W. A., J. M. Thorp, O. P. Gifford, and D. J. Hoitink, 1983, *Climatological Summary for the Hanford Area*, PNL-4622, Pacific Northwest Laboratory, Richland, Washington.
- Tallman, A. M., J. T. Lillie, and K. R. Fecht, 1981, "Suprabasalt Sediments of the Cold Creek Syncline Area," in *Subsurface Geology of the Cold Creek Syncline*, RHO-BWI-ST-14, C. W. Meyers and S. M. Price, Rockwell Hanford Operations, Richland, Washington.
- Tolan, T. L. and S. P. Reidel, 1989, "Structure Map of a Portion of the Columbia River Flood-Basalt Province," in *Volcanism and Tectonism in the Columbia River Flood-Basalt Province*, Special Paper 239, ed. S. P. Reidel and P. R. Hooper, Geological Society of American, Boulder, Colorado, plate 1.

- Tolan, T. L. and S. P. Reidel, M. H. Beeson, J. L. Anderson, K. R. Fecht, and D. A. Swanson, 1989, "Revisions to the Extent and Volume of the Columbia River Basalt Group," in *Volcanism and Tectonism in the Columbia River Flood-Basalt Province*, Special Paper 239, ed. S. P. Reidel and P. R. Hooper, Geological Society of American, Boulder, Colorado, pp. 1-20.
- U.S. Weather Bureau, 1966, *Probable Maximum Precipitation, Northwest States*, Hydrometeorological Report No. 43, U.S. Department of Commerce, Environmental Science Services Administration, Weather Bureau, Washington, D.C. [reprinted with revisions, April 1981].
- Wing, N. R., 1993, *Permanent Isolation Surface Barrier: Functional Performance*, WHC-EP-0650, Westinghouse Hanford Company, Richland, Washington.
- Wing, N. R., 1994, *Permanent Isolation Surface Barrier Development Plan*, WHC-EP-0673, Westinghouse Hanford Company, Richland, Washington.
- Whitlock, C., 1994, *American Quaternary Association: Program and Abstracts of the 13th Biennial Meeting*, American Quaternary Association, University of Minnesota, Minneapolis.
- WPPSS, 1980, *Final Safety Analysis Report*, WPPSS Nuclear Project No. 2, Washington Public Power Supply System, Inc., Richland, Washington.

APPENDIX A

**PRELIMINARY STABILITY ANALYSES FOR PROTOTYPE SURFACE BARRIER -
200 EAST AREA**

Prepared by A. A. Saleh and D. E. Daniel
The University of Texas, Department of Civil Engineering,
for Bechtel Hanford, Inc.

TABLE OF CONTENTS

<u>Section</u>	<u>Title</u>	<u>Page No.</u>
1.0	Introduction	1
2.0	Site Location	1
3.0	Natural Soil and Groundwater Conditions	1
4.0	Cross Section of Barrier	2
5.0	Laboratory Testing Program	2
6.0	Stability Analyses	3
	6.1 Selection of Cross Sections	3
	6.2 Selection of Engineering Properties	4
	6.3 Selection of Design Parameters	4
	6.4 Method of Analysis and Computer Program	4
	6.5 Static Safety Factors	5
	6.6 Earthquake-Induced Deformations	5
7.0	Conclusions and Recommendations	6
8.0	Creep and Integrity of Fluid Applied Applied Asphalt	6
9.0	Limitations	7

TABLES

FIGURES

APPENDICES

TABLES

No. Title

- | | |
|---|---|
| 1 | Material Properties |
| 2 | Seismic Deformation Estimates- Section E1 |
| 3 | Seismic Deformation Estimates- Section N1 |

FIGURES

No. Title

- | | |
|----|---|
| 1 | Site Location |
| 2 | Cross Section Locations |
| 3 | Section E1 |
| 4 | Section N1 |
| 5 | Section N2 |
| 6 | Section W1 |
| 7 | Minimum Factor of Safety- Section E1 (w/ Potential Sliding Mass) |
| 8 | Minimum Factor of Safety- Section N1 (w/ Potential Sliding Mass) |
| 9 | Factor of Safety versus Seismic Coefficient- Section E1 |
| 10 | Factor of Safety versus Seismic Coefficient- Section N1 |
| 11 | Factor of Safety for Infinite Slope with Seismic Force and 2:1 Slope |
| 12 | Factor of Safety for Infinite Slope with Seismic Force and 4:1 Slope |
| 13 | Factor of Safety for Infinite Slope with Seismic Force and 5:1 Slope |
| 14 | Factor of Safety for Infinite Slope with Seismic Force and 10:1 Slope |

APPENDICES

Appendix Title

- | | |
|---|----------------------------|
| A | Laboratory Testing Results |
| B | References |

1.0 Introduction

This study was performed to analyze potential seismically-induced deformations of the prototype surface barrier at the 200 East Area of the Hanford, Washington site. It is our understanding that the barrier covers a former disposal site identified as 216-B-57 crib. The outcome of this work was intended to be an assessment of the probable effects of seismic shaking upon the performance of the surface barrier. The work included estimation of the engineering properties of the materials that comprise the barrier, measurement of the properties of the layer of fluid applied asphalt (and interfaces with underlying and overlying layers), development of cross sections for slope stability analyses, analysis of the factor of safety against static sliding of slopes, analysis of the factor of safety against pseudo-dynamic sliding of slopes, and calculation of the deformations of slopes that might be anticipated during earthquake shaking.

This work constitutes the first step in evaluating the probable effects of seismically-induced shaking upon the prototype barrier. The main objective was to identify the risk that seismic forces could cause large deformations within the prototype barrier. If the work indicates that significant deformations are very unlikely, then further analyses may not be warranted at this time. On the other hand, if the work indicates that significant, damaging deformations might occur, then we would recommend that further, more sophisticated testing and analyses be undertaken.

Although the work focused on estimating seismically-induced deformations, analysis of the static stability was an important step in the overall process. During the course of this work, concern developed regarding the static strength of the layer of fluid applied asphalt, and a significant fraction of our work was directed toward study of static stability of this layer.

2.0 Site Location

The prototype surface barrier is located at the 200 East Area of the Hanford site in Hanford, Washington (Figure 1).

3.0 Natural Soil and Groundwater Conditions

Although no specific field testing programs were conducted for this

study, a large number of geological/geotechnical boreholes have been drilled for various projects near the location of the prototype. Available data provided to the authors were reviewed to gain knowledge of the existing soils surrounding the subject site. Based on this information and site visits to some of the borrow areas by the authors, it is believed that the soils underlying the surface barrier consist chiefly of medium dense to dense sandy gravel to gravely sand.

Groundwater levels are believed to be approximately 240 feet below the ground surface, thus having no significant effect on the stability of the barrier slopes being studied in this report.

4.0 Cross Section of Barrier

The barrier consists of fine-soil layers (upper and lower silt layers) overlying other layers of coarser materials such as sands, gravels, and basalt rock. The fine soil layers provide the medium for establishing plants and storing excess water, which is recycled back to the atmosphere by evaporation and transpiration processes. The coarser materials create a capillary break that inhibits the downward percolation of water through the barrier. In addition, a low-permeability layer (asphaltic concrete coated with fluid applied asphalt) is used below the coarser materials to divert any percolating water that gets through the capillary break and to limit the upward movement of gases from the waste zone. Finally, underlying the asphaltic concrete layer are compacted layers of granular soils. The total height of the barrier varies between 4 meters at the south end to 10.25 meters at the northeast corner (these dimensions are approximate).

5.0 Laboratory Testing Program

A laboratory testing program was carried out to investigate the shear strength of the fluid applied asphalt (FAA) and its interface with the overlying drainage gravel. Core samples of the FAA and asphaltic concrete, as well as sheets of FAA, were shipped to us from the Hanford site. These samples were obtained from a test pad to the north of the existing barrier. Buckets of FAA material were also shipped, but because (a) the sheets of material covered a sufficient area to provide the necessary number of test specimens, and (b) the internal strength of the FAA was found to be less than the interface strength between the FAA and asphaltic concrete, it was not necessary to fabricate samples from buckets of FAA material.

Details of the actual testing equipment, procedures, and test results are provided in Appendix A. The following key findings are noted:

- When the FAA/asphaltic concrete interface was sheared, failure occurred in the FAA itself. Adhesion between the FAA and asphaltic concrete was strong enough to prevent failure from occurring at this interface.
- When the FAA/gravel interface was tested, gravel typically penetrated about two-thirds of the way through the FAA. Only in one test (at a compressive stress of 30 psi) did gravel penetrate fully. The actual compressive stress on the FAA in the prototype barrier is less than 15 psi. When this interface was sheared, deformation occurred in the FAA, near the maximum depth of penetration of gravel into the FAA.
- The shear strength parameters recommended for stability analyses are 0.7 psi for cohesion (c), and 10 degrees for the friction angle (ϕ).

A strain rate of 0.01 inch per minute was used for all the tests performed during this program. This rate is recommended by ASTM for large-scale direct shear tests; however, it is our opinion that due to the viscous nature of the FAA material, the strain rate plays a major role in determining the shear strength of the FAA for the purpose of long-term stability analyses. Therefore, the shear strength parameters used in this report should be considered preliminary, and further laboratory work on this material is recommended prior to use of the fluid applied asphalt on other surface barriers at Hanford.

6.0 Stability Analyses

6.1 Selection of Cross Sections

Four cross sections were selected for analysis of slope stability. These are shown on Figures 2 through 6. Section E1 was considered to be the most critical section for static stability due to the down sloping FAA layer. Section N1 was selected for its overall height (one meter higher than that of section E1), which was believed to have some effect when considering the dynamic stability of the barrier. Other sections were considered for the analysis, namely, sections N2 and W1 with section W1 being considered one of the most stable sections for both static and

dynamic loadings, thus providing an upper bound for the factor of safety. Section N2 was later believed to be less critical than N1 and was not considered further for any of the dynamic analysis.

6.2 Selection of Engineering Properties

Ranges of engineering properties were selected for most of the materials. Selection of a range in properties resulted in a parametric study. Table 1 presents the assumed ranges of engineering properties as well as the shear strength of the FAA which was obtained from a series of laboratory tests performed at the University of Texas at Austin. It should be noted that given the problem geometry, only the basalt rock and the FAA had a major effect upon the stability of the critical section. For different geometries, the properties of the other materials could be more important than they are for the prototype barrier. The friction angle of the basalt, as can be seen in Table 1, was varied from 35 to 55 degrees. In addition, a range of shear wave velocity of 800 to 2000 fps was selected for the barrier material for purposes of dynamic analyses.

6.3 Selection of Design Parameters

Two return periods were considered in this study: 1,000 years and 10,000 years. In addition, two ground accelerations were considered for each of the return periods. Both accelerations were based on information provided to us. However, one acceleration was obtained through existing seismic charts given the provided earthquake magnitude and distance to the fault, and the other obtained directly from response spectra that was supplied. It should be noted that only the 5% damping curves (which are the most conservative) were used in this study.

6.4 Method of Analysis and Computer Program

Static Stability

For static stability analyses, UTEXAS3, which is a computer program developed by Dr. Stephen G. Wright at the University of Texas at Austin, was used with Spencer Method for analysis.

Dynamic Stability

The seismic deformation analyses was carried out utilizing the approach developed by Seed and Makdisi, 1977, "A Simplified Procedure for Estimating Earthquake-Induced Deformations in Dams and Embankments. " In determining the yield acceleration, which is an integral part of Seed's Procedure, UTEXAS3 computer program was used again. In this step, the critical shear surface found during the static stability analysis was fixed and the horizontal acceleration was increased incrementally to establish the yield acceleration which corresponds to a factor of safety of 1. Generally, for slopes, vertical accelerations are ignored and horizontal accelerations are considered more critical. Therefore, only horizontal accelerations were used in this study.

6.5 Static Safety Factors

Extensive search routines were conducted to determine the minimum factor of safety for both sections E1 and N1 using UTEXAS3 and for both circular and non-circular failure surfaces. Figures 6 and 7 present the final critical shear surfaces for sections E1 and N1, respectively. The minimum factor of safety was found to be 1.384 for section E1, and 1.418 for section N1. For Section W1, the factor of safety for the infinite slope was found to control. The minimum factor of safety for section W1 is 5.774, which can also be obtained from Figure 14 for a seismic coefficient, k , of zero. Figures 11 through 14 present the results of a parametric study involving various slope ratios, friction angles, and seismic coefficients, which can be used to assess the stability of cohesionless slopes where the minimum factor of safety is that of the infinite slope.

6.6 Earthquake-Induced Deformations

Figures 9 and 10 present the results of various computer runs, using UTEXAS3, in which each of the critical shear surfaces (found in section 6.5) was subjected to different horizontal accelerations in order to establish the yield acceleration. The yield acceleration, which corresponds to a factor of safety of unity, was estimated to be 0.145g for section E1, and 0.152g for section N1.

Tables 2 and 3 present the remainder of the steps recommended by Seed's approach to estimate the earthquake-induced deformations for both sections E1 and N1 and for various friction angles for the basalt rock. As

can be seen, the deformations are negligible for both of the return periods. The computed deformations range from:

<u>Section</u>	<u>Deformation (cm)</u>	
	<u>1,000 yr</u>	<u>10,000 yr</u>
E1	0 - 0.04	0 - 1.17
N1	0 - 0.08	0 - 2.05

Section 7.2 of this report comments on the limitations of Seed's method for application to this problem and the significance of the numbers presented in Tables 2 and 3.

7.0 Conclusions and Recommendations

From the analyses presented, seismically-induced movement of the prototype barrier is expected to be very small (on the order of 2 cm or less). Seed and Bonaparte* recently summarized the current practice for seismic design of liner and cover systems for waste fills and note that seismic deformations less than 15 cm (6 in.) are viewed by designers as being acceptable levels of seismic displacement. The risk of significant damage occurring as a result of seismic shaking of the prototype barrier appears to be extremely small.

We do not recommend further analyses of possible seismic effects on the prototype barrier at this time — the cost to significantly refine the analyses presented herein would be very high, and the anticipated conclusion is the same.

8.0 Creep and Integrity of Fluid Applied Asphalt

The fluid applied asphalt (FAA) appears to be the weakest layer in the prototype barrier. Due to the viscous nature of the FAA, deformations are more probable under sustained static loading than during an earthquake.

Two issues concerning the FAA were identified and may warrant

* "Seismic Analysis and Design of Lined Waste Fills: Current Practice," by Raymond B. Seed and Rudolph Bonaparte, *Stability and Performance of Slopes and Embankments - II*, Raymond B. Seed and Ross W. Boulanger (Eds.), American Society of Civil Engineers, 1992, Vol. 2, pp. 1521-1545.

further consideration. The first is creep of the FAA. More laboratory testing work is needed to investigate the effect of deformation rates on the strength of the FAA. It is our opinion that the deformation rate used in the laboratory testing may not be appropriate for the long-term stability analysis of the barrier. The static factors of safety reported in this report may not truly reflect the potential for creep to cause deformations. Of course, for the FAA to creep, the materials undergoing movement have to have somewhere to go, and the basalt limits the potential for movement. If creep were to occur, however, then load might be shed to the basalt. We feel that creep is of sufficient concern to warrant (1) field instrumentation of deformations to determine if creep is occurring, and (2) if the data indicate that movements are taking place, further laboratory work to better characterize the creep properties of the asphalt.

A second issue of concern is the integrity of the FAA as a hydraulic barrier. The penetration of the FAA by the gravel helps to strengthen the FAA but raises questions about the hydraulic properties of the FAA. The hydraulic performance of a gravel-impregnated layer of fluid applied asphalt has not been quantified. If the fluid applied asphalt is used in other surface barriers at Hanford, we recommend that this issue be investigated for those facilities.

9.0 Limitations

The simplified method outlined by Seed and Makdisi and used here contains simplifying assumptions may not be fully appropriate for analysis of surface barriers. All of the cases analyzed by Seed and Makdisi involved high dams with heights ranging from 75 to over 150 feet. In addition, the periods in their study ranged from 0.6 to 1.0 second, while the periods for this study was significantly smaller (see Tables 2 and 3). The reader should recognize that the analyses summarized here represent estimates of field behavior that are based on an approximate method of analysis.

TABLES

Table 2- Seismic Deformation Estimates
Section E1 (1,000 yr. Design Life)

Friction Angle for Basalt, in degrees:
 Failure Surface:
 Yield Seismic Coefficient, K_y :

35
NC
0.145

45
NC
0.180

55
NC
0.220

Total Height, H , in meters:
 Shear Surface Depth, y , in meters:
 Depth to Height Ratio, y/H :
 K_{max}/U_{max} : (Makdisi & Seed)

9.30
4.97
0.53
0.60

9.30
4.97
0.53
0.60

9.30
4.97
0.53
0.60

Design Life, in years:
 Earthquake Magnitude, Richter Scale:
 Shortest Distance to Fault (in km)
 (in miles)
 Rock Acceleration (Seed & Kriass)
 Ground Acceleration (Seed & Kriass)
 Shear Wave Velocity, V_s , (in fps)
 (in mps)
 Emb. Period, T_o , in sec.: (Wiegel)
 Emb. Sp. Acc./Ground Acc. (Seed, et al.)
 Embankment Spectral Acc., U_{max} :
 Eff. Peak Horiz. Acc. of Slid. Mass, K_{max} :
 K_y/K_{max} :
 U , Normalized: (Makdisi & Seed)

1,000				1,000				1,000			
6.00		(See note 3)		6.00		(See note 3)		6.00		(See note 3)	
15.00				15.00				15.00			
9.38				9.38				9.38			
0.23				0.23				0.23			
0.20		0.14		0.20		0.14		0.20		0.14	
800	2000	800	2000	800	2000	800	2000	800	2000	800	2000
244	610	244	610	244	610	244	610	244	610	244	610
0.10	0.04	0.10	0.04	0.10	0.04	0.10	0.04	0.10	0.04	0.10	0.04
1.50	1.10	1.50	1.10	1.50	1.10	1.50	1.10	1.50	1.10	1.50	1.10
0.30	0.22	0.21	0.15	0.30	0.22	0.21	0.15	0.30	0.22	0.21	0.15
0.18	0.13	0.13	0.09	0.18	0.13	0.13	0.09	0.18	0.13	0.13	0.09
0.81	1.10	1.15	1.57	1.00	1.36	1.43	1.95	1.22	1.67	1.75	2.38
0.0020	0.0001	0.0001	0.0001	0.0001	0.0001	0.0001	0.0001	0.0001	0.0001	0.0001	0.0001
0.04	0.00	0.00	0.00	0.00	0.00	0.00	0.00	0.00	0.00	0.00	0.00

Deformation, U , in cm:

Notes:

1. Shaded cells are numbers obtained from Seed's charts
2. Deformations are obtained using available data (EQ magnitude of 6.5)
3. Ground Acceleration as given by Client
4. $T_o = 2.62H/V_s$

BHI-00145
 Rev. 00

Table 2- Seismic Deformation Estimates (cont'd)
Section E1 (10,000 yr. Design Life)

Friction Angle for Basalt, in degrees:
 Failure Surface:
 Yield Seismic Coefficient, K_y :

35
NC
0.145

45
NC
0.180

55
NC
0.220

Total Height, H , in meters:
 Shear Surface Depth, y , in meters:
 Depth to Height Ratio, y/H :
 K_{max}/U_{max} : (Makdisi & Seed)

9.30
4.97
0.53
0.60

9.30
4.97
0.53
0.60

9.30
4.97
0.53
0.60

Design Life, in years:
 Earthquake Magnitude, Richter Scale:
 Shortest Distance to Fault (in km)
 (in miles)

Rock Acceleration (Seed & Idriss)
 Ground Acceleration (Seed & Idriss)
 Shear Wave Velocity, V_s , (in fpa)
 (in mps)

Emb. Period, T_o , in sec.: (Wiegel)
 Emb. Sp. Acc./Ground Acc. (Seed, et al.)
 Embankment Spectral Acc., U_{max} :
 Eff. Peak Horiz. Acc. of Slid. Mass, K_{max} :
 K_y/K_{max} :
 U , Normalized: (Makdisi & Seed)

Deformation, U , in cm:

10,000				10,000				10,000			
6.00				6.00				6.00			
6.00				6.00				6.00			
3.75				3.75				3.75			
0.42		(See note 3)		0.42		(See note 3)		0.42		(See note 3)	
0.34		0.38		0.34		0.38		0.34		0.38	
800	2000	800	2000	800	2000	800	2000	800	2000	800	2000
244	610	244	610	244	610	244	610	244	610	244	610
0.10	0.04	0.10	0.04	0.10	0.04	0.10	0.04	0.10	0.04	0.10	0.04
1.50	1.10	1.50	1.10	1.50	1.10	1.50	1.10	1.50	1.10	1.50	1.10
0.51	0.37	0.57	0.42	0.51	0.37	0.57	0.42	0.51	0.37	0.57	0.42
0.31	0.22	0.34	0.25	0.31	0.22	0.34	0.25	0.31	0.22	0.34	0.25
0.47	0.65	0.42	0.58	0.59	0.80	0.53	0.72	0.72	0.98	0.64	0.88
0.0300	0.0070	0.0350	0.0150	0.0150	0.0020	0.0200	0.0040	0.0050	0.0001	0.0065	0.0005
0.90	0.06	1.17	0.15	0.45	0.02	0.67	0.04	0.15	0.00	0.22	0.00

Notes:

1. Shaded cells are numbers obtained from Seed's charts
2. Deformations are obtained using available data (EQ magnitude of 6.5)
3. Ground Acceleration as given by Client
4. $T_o = 2.62H/V_s$

Table 3- Seismic Deformation Estimates
Section N1 (1,000 yr. Design Life)

Friction Angle for Basalt, in degrees:
 Failure Surface:
 Yield Seismic Coefficient, Ky:

35
NC
0.152

45
NC
0.210

55
NC
0.240

Total Height, H, in meters:
 Shear Surface Depth, y, in meters:
 Depth to Height Ratio, y/H:
 Kmax/Umax: (Makdisi & Seed)

10.25
4.88
0.48
0.67

10.25
4.83
0.47
0.67

10.25
4.89
0.48
0.67

Design Life, in years:
 Earthquake Magnitude, Richter Scale:
 Shortest Distance to Fault (in km)
 (in miles)
 Rock Acceleration (Seed & Kiria)
 Ground Acceleration (Seed & Kiria)
 Shear Wave Velocity, Vs, (in fps)
 (in mps)
 Emb. Period, To, in sec.: (Wiegell)
 Emb. Sp. Acc./Ground Acc. (Seed, et al.)
 Embankment Spectral Acc., Umax:
 Eff. Peak Horiz. Acc. of Slid. Mass, Kmax:
 Ky/Kmax:
 U, Normalized: (Makdisi & Seed)

1,000				1,000				1,000			
6.00		(See note 3)		6.00		(See note 3)		6.00		(See note 3)	
15.00				15.00				15.00			
9.38				9.38				9.38			
0.23				0.23				0.23			
0.20				0.20				0.20			
800	2000	800	2000	800	2000	800	2000	800	2000	800	2000
244	610	244	610	244	610	244	610	244	610	244	610
0.11	0.04	0.11	0.04	0.11	0.04	0.11	0.04	0.11	0.04	0.11	0.04
1.50	1.10	1.50	1.10	1.50	1.10	1.50	1.10	1.50	1.10	1.50	1.10
0.30	0.22	0.21	0.15	0.30	0.22	0.21	0.15	0.30	0.22	0.21	0.15
0.20	0.15	0.14	0.10	0.20	0.15	0.14	0.10	0.20	0.15	0.14	0.10
0.76	1.04	1.09	1.48	1.04	1.42	1.49	2.04	1.20	1.64	1.72	2.34
0.0035	0.0001	0.0001	0.0001	0.0001	0.0001	0.0001	0.0001	0.0001	0.0001	0.0001	0.0001
0.08	0.00	0.00	0.00	0.00	0.00	0.00	0.00	0.00	0.00	0.00	0.00

Notes:

1. Shaded cells are numbers obtained from Seed's charts
2. Deformations are obtained using available data (EQ magnitude of 6.5)
3. Ground Acceleration as given by Client
4. $T_o = 2.62H/V_s$

BHI-00145
 Rev. 00

Table 3- Seismic Deformation Estimates (cont'd)
Section N1 (10,000 yr. Design Life)

Friction Angle for Basalt, in degrees:
 Failure Surface:
 Yield Seismic Coefficient, K_y :

35
NC
0.152

45
NC
0.210

55
NC
0.240

Total Height, H , in meters:
 Shear Surface Depth, y , in meters:
 Depth to Height Ratio, y/H :
 K_{max}/U_{max} : (Makdisi & Seed)

10.25
4.88
0.48
0.67

10.25
4.83
0.47
0.67

10.25
4.89
0.48
0.67

Design Life, in years:
 Earthquake Magnitude, Richter Scale:
 Shortest Distance to Fault (in km)
 (in miles)
 Rock Acceleration (Seed & Idriss)
 Ground Acceleration (Seed & Idriss)
 Shear Wave Velocity, V_s , (in fps)
 (in mps)
 Emb. Period, T_o , in sec.: (Wiegel)
 Emb. Sp. Acc./Ground Acc. (Seed, et al.)
 Embankment Spectral Acc., U_{max} :
 Eff. Peak Horiz. Acc. of Slid. Mass, K_{max} :
 K_y/K_{max} :
 U , Normalized: (Makdisi & Seed)

10,000				10,000				10,000			
6.00				6.00				6.00			
6.00				6.00				6.00			
3.75				3.75				3.75			
0.42				0.42				0.42			
0.34				0.34				0.34			
(See note 3)				(See note 3)				(See note 3)			
800	2000	800	2000	800	2000	800	2000	800	2000	800	2000
244	610	244	610	244	610	244	610	244	610	244	610
0.11	0.04	0.11	0.04	0.11	0.04	0.11	0.04	0.11	0.04	0.11	0.04
1.50	1.10	1.50	1.10	1.50	1.10	1.50	1.10	1.50	1.10	1.50	1.10
0.51	0.37	0.57	0.42	0.51	0.37	0.57	0.42	0.51	0.37	0.57	0.42
0.34	0.25	0.38	0.28	0.34	0.25	0.38	0.28	0.34	0.25	0.38	0.28
0.45	0.61	0.40	0.55	0.61	0.84	0.55	0.75	0.71	0.96	0.63	0.86
0.0350	0.0100	0.0500	0.0200	0.0100	0.0020	0.0200	0.0035	0.0050	0.0001	0.0080	0.0008
1.28	0.11	2.05	0.24	0.37	0.02	0.83	0.04	0.18	0.00	0.33	0.01

Notes:

1. Shaded cells are numbers obtained from Seed's charts
2. Deformations are obtained using available data (EQ magnitude of 6.5)
3. Ground Acceleration as given by Client
4. $T_o = 2.62H/V_s$

FIGURES

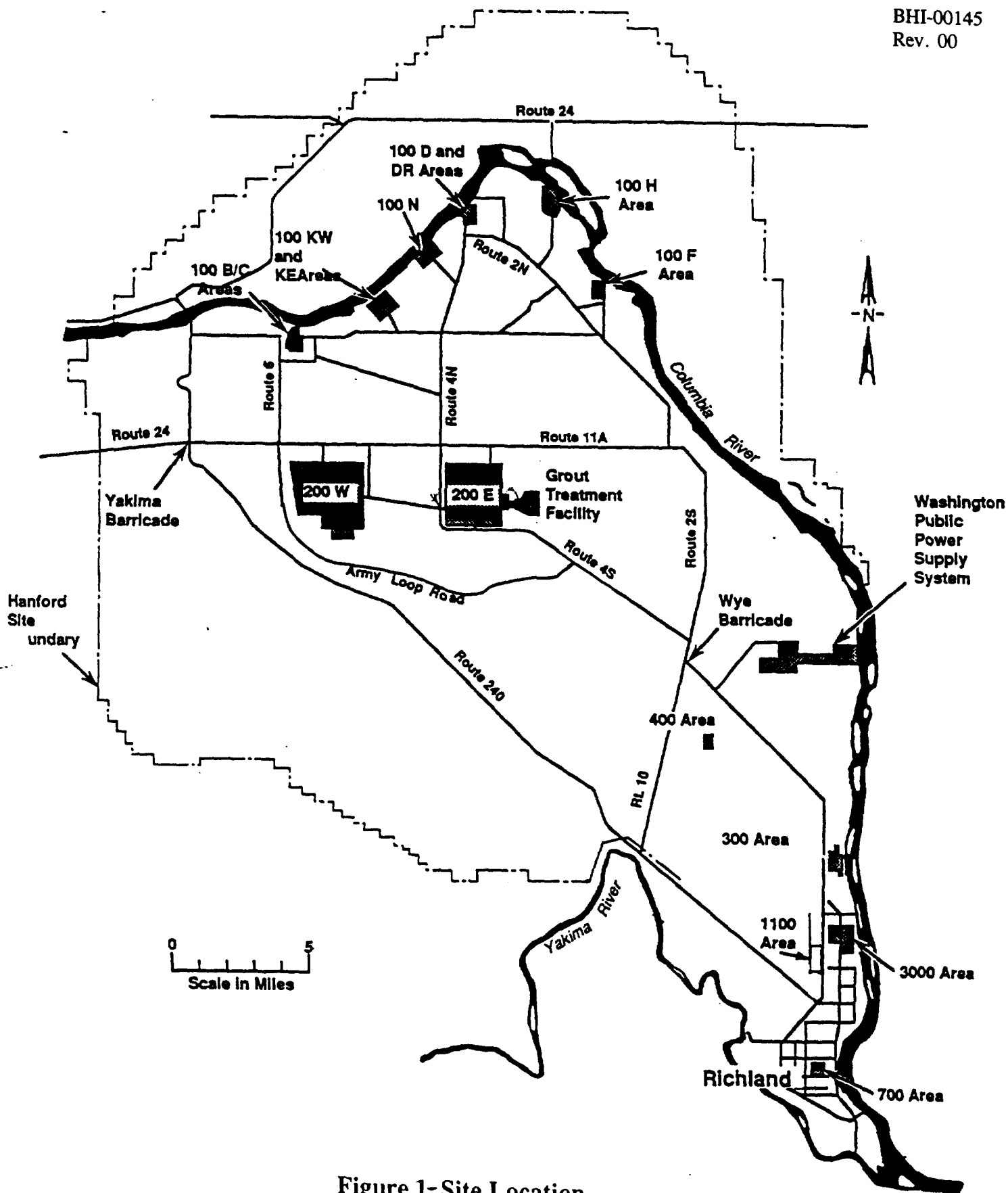


Figure 1-Site Location

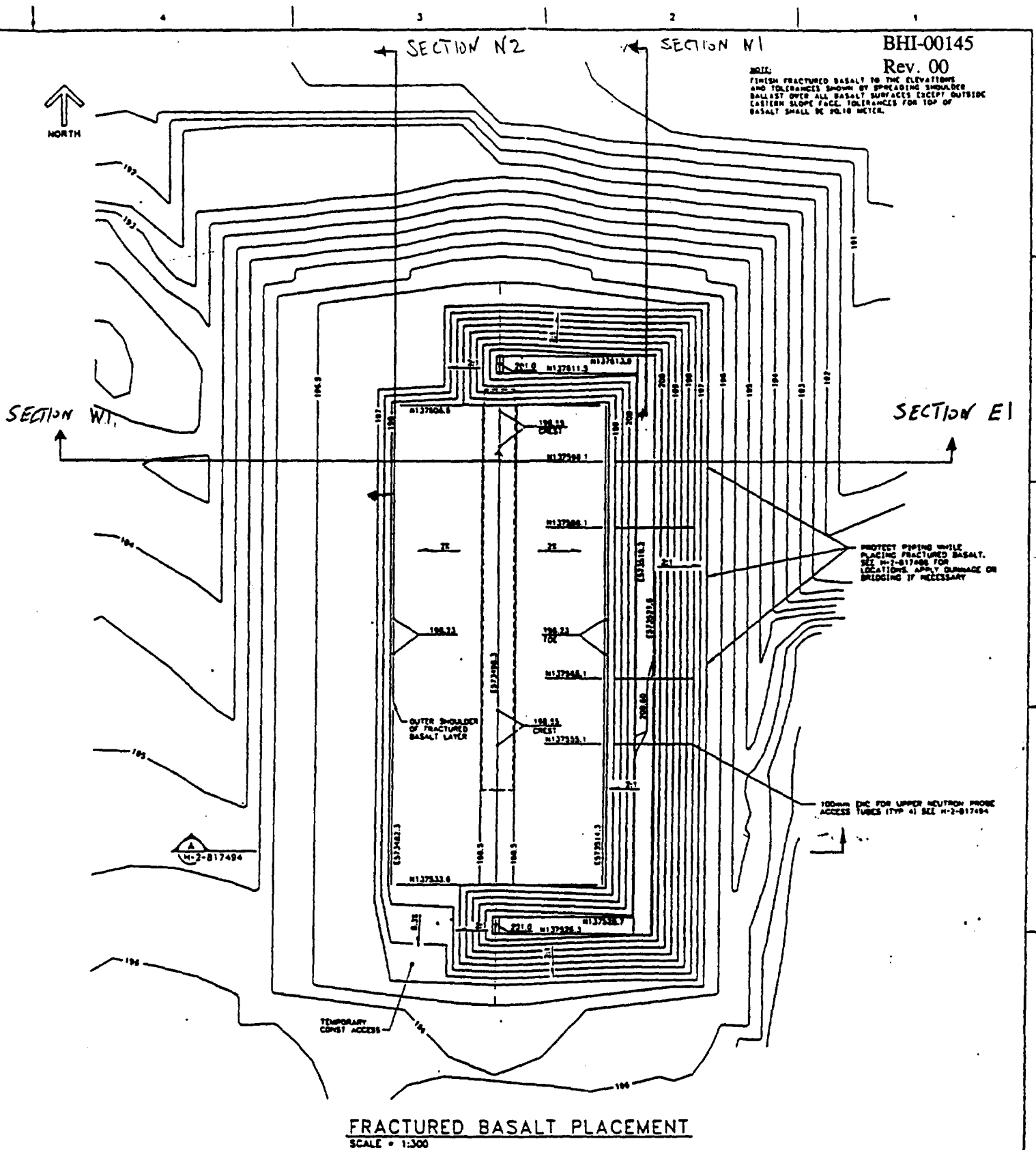


Figure 2-Cross-Section Location



APPROVAL

NOT APPROVED FOR CONSTRUCTION

A-19		BA LORENZO U.S. DEPARTMENT OF ENERGY HIGHLAND FIELD OFFICE KAISER ENGINEERS HANFORD COMPANY CIVIL PLANS DRAINAGE & BASALT LAYERS H-263 - PROTOTYPE SURFACE BARRIER F 210-0-37 0110 H-2-817490 0 SHOWN 10000 ER3412 1 of 1	
2-817494 DRAINAGE LIST 2-817494 BASALT LAYERS		2-817494 BASALT LAYERS 2-817494 BASALT LAYERS	

2-DEC-ACD2-110-NH

SECTION E1

(N137598.1)

Note: see Table 1 for
material properties

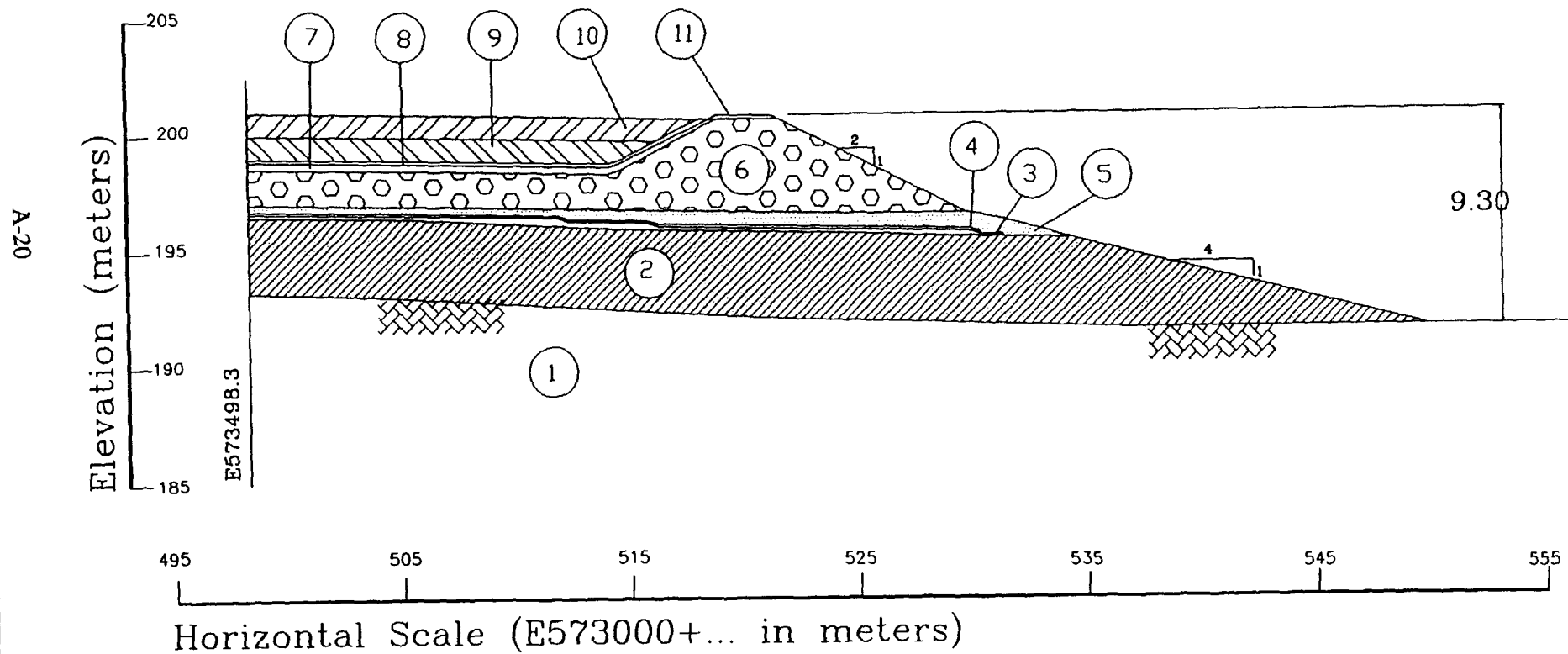


Figure 3

SECTION N1

(E 573520.4)

Note: see Table 1 for material properties

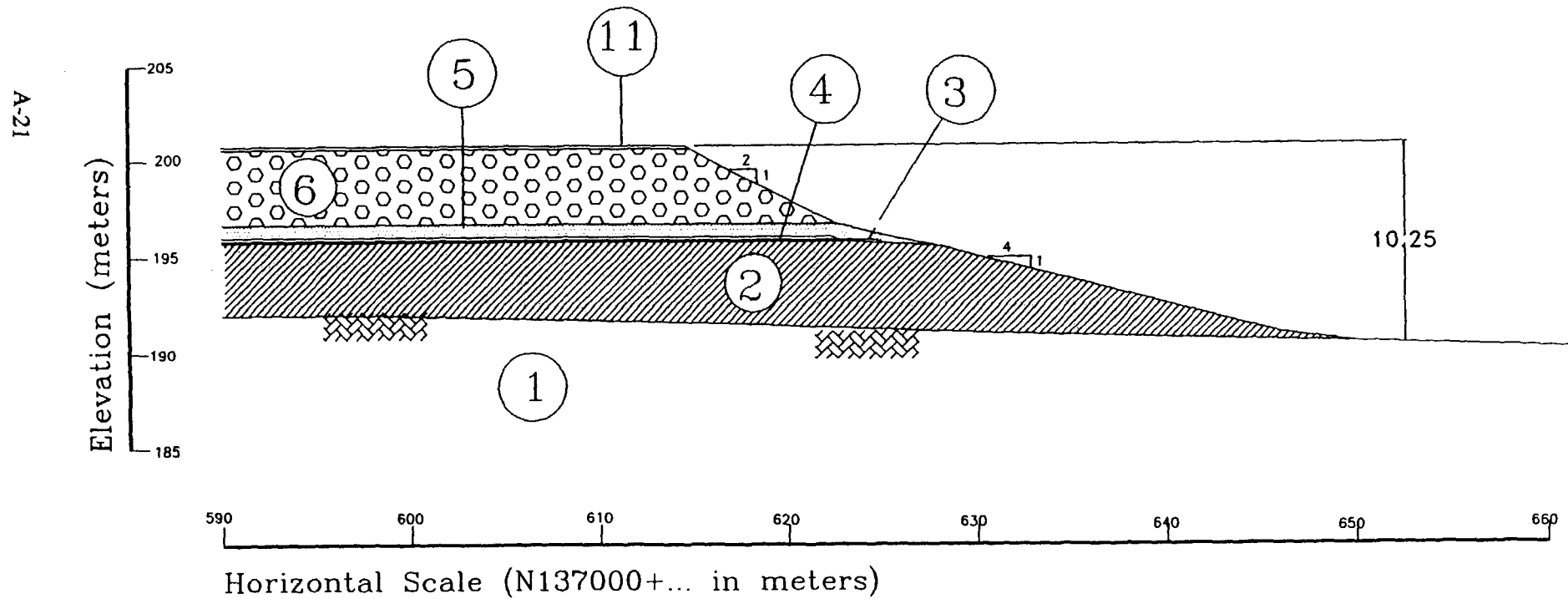


Figure 4

SECTION N2

(E 573482.3)

Material Properties

(see Table 1)

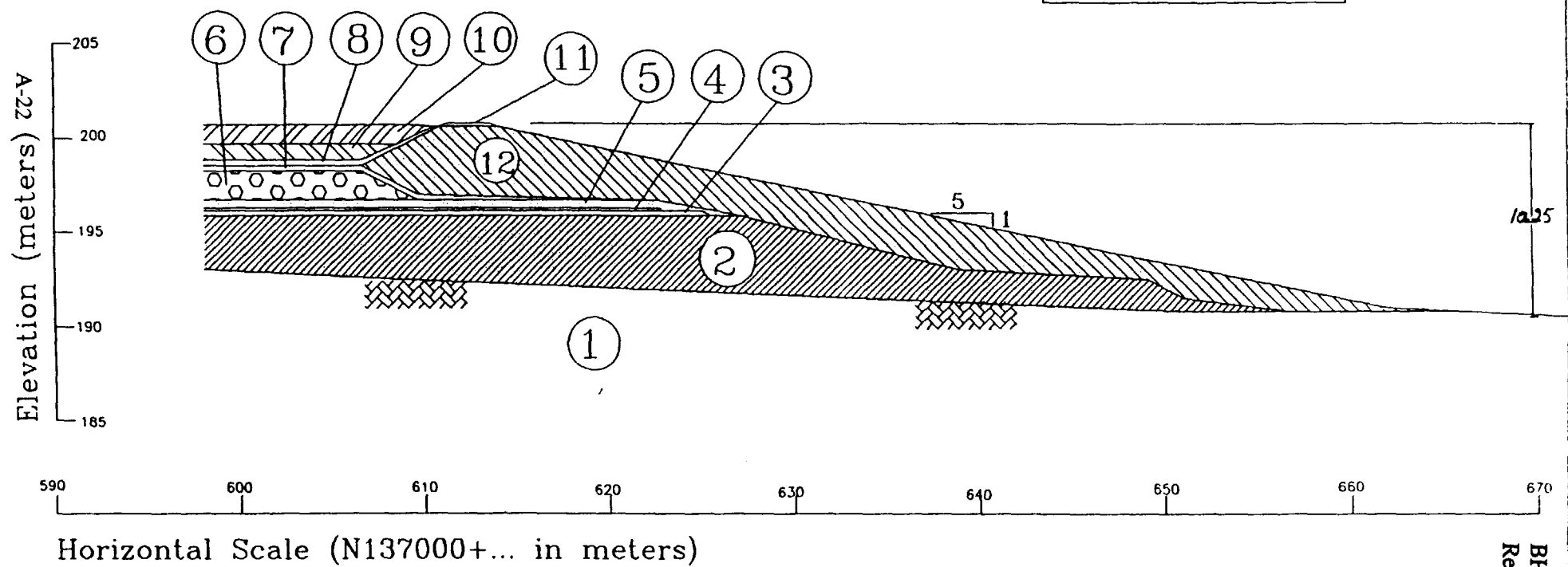


Figure 5

BHI-00145
Rev. 00

SECTION W1

(N137598.1)

A-23

Note: see Table 1 for material properties.

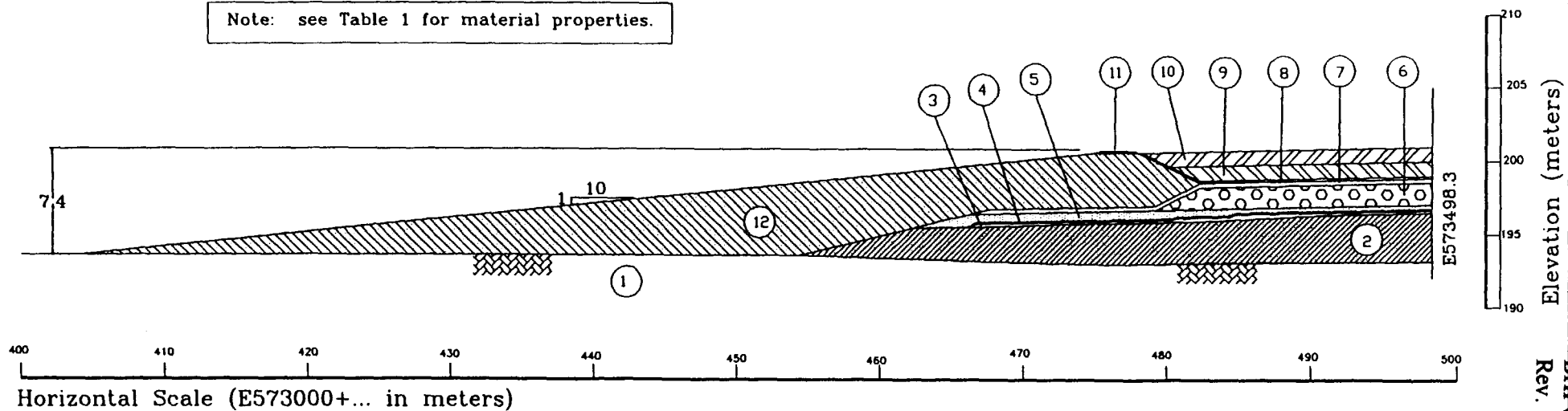


Figure 6

BH-00145
Rev. 00

Minimum Factor of Safety- Section E1

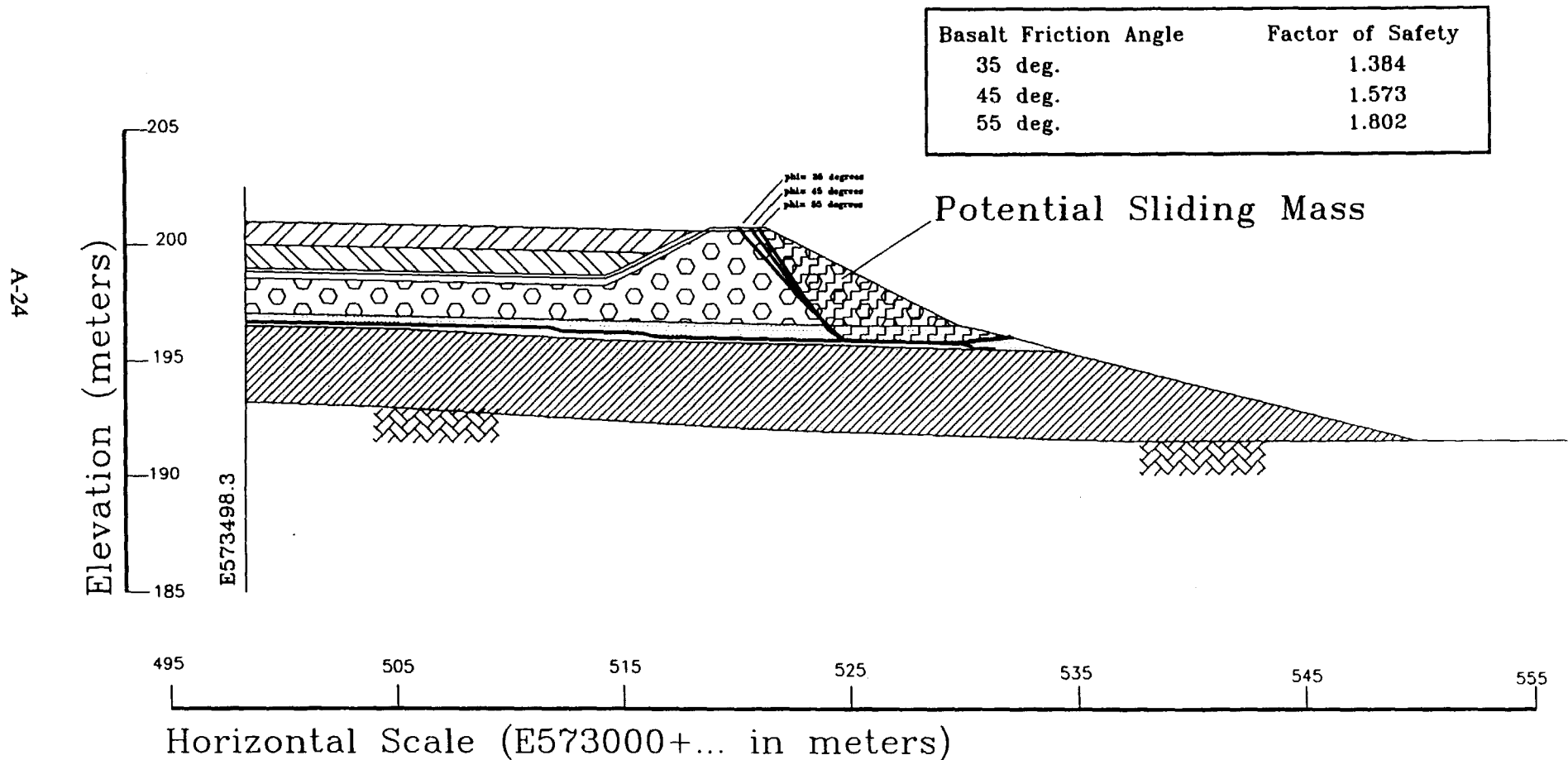


Figure 7

Minimum Factor of Safety- Section N1

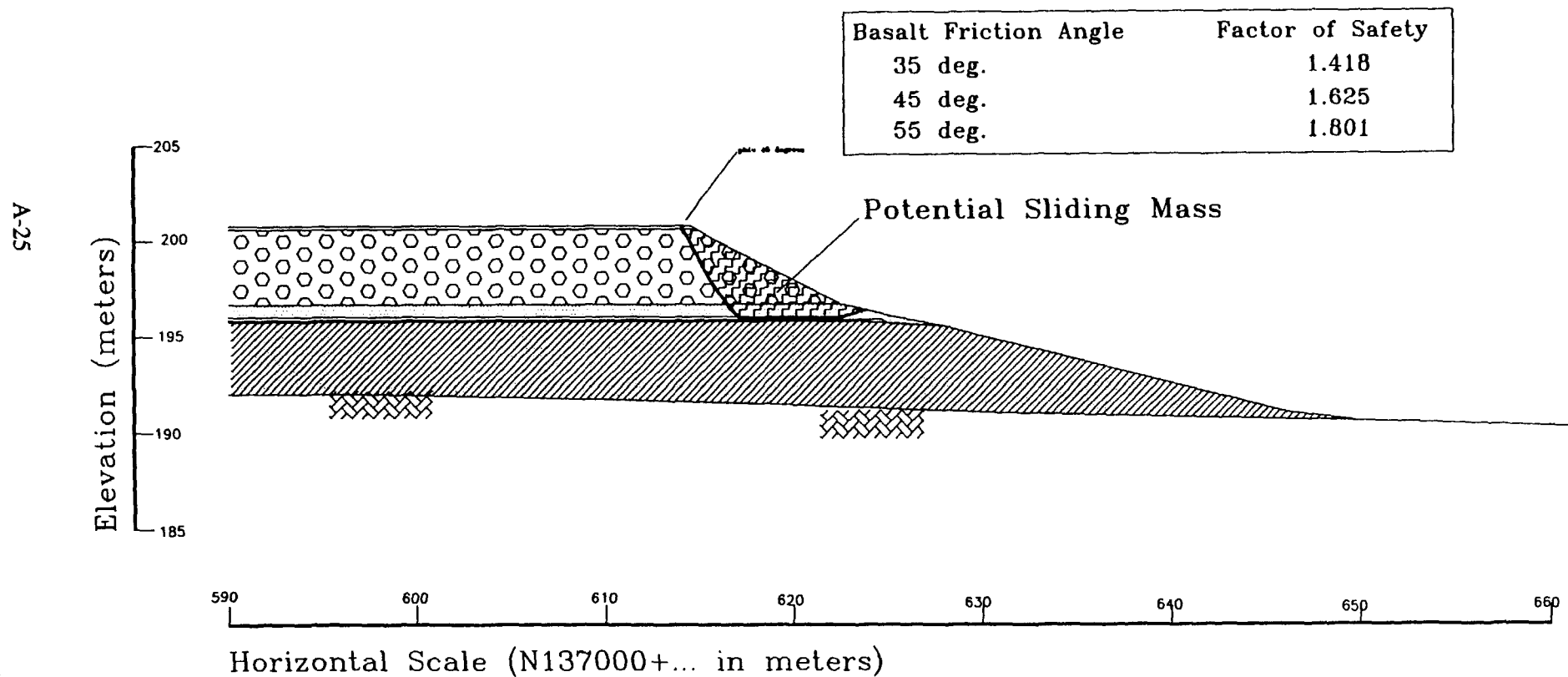
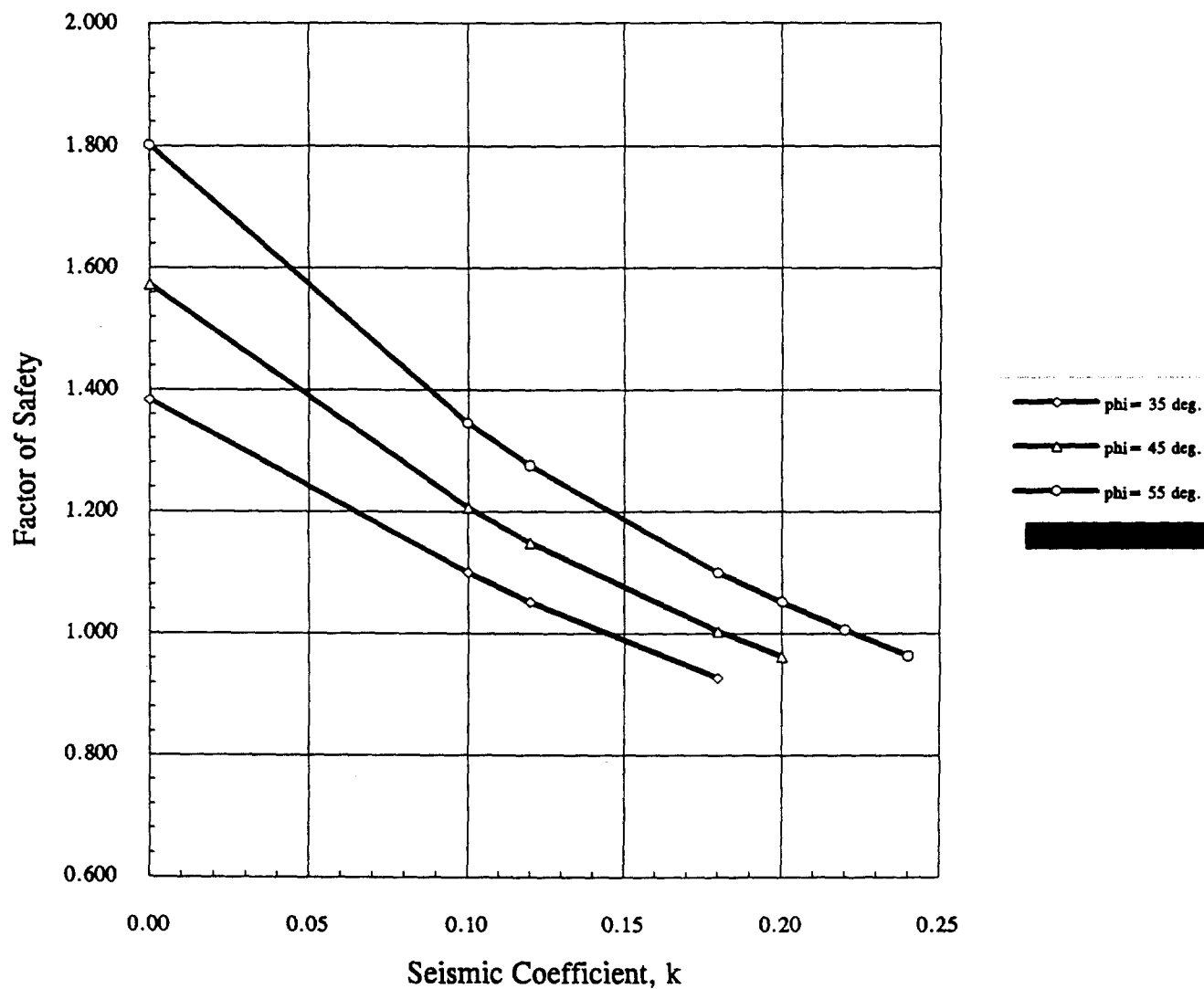


Figure 8

**FIGURE 9 - Factor of Safety versus Seismic Coefficient
Section E1**

BHI-00145
Rev. 00

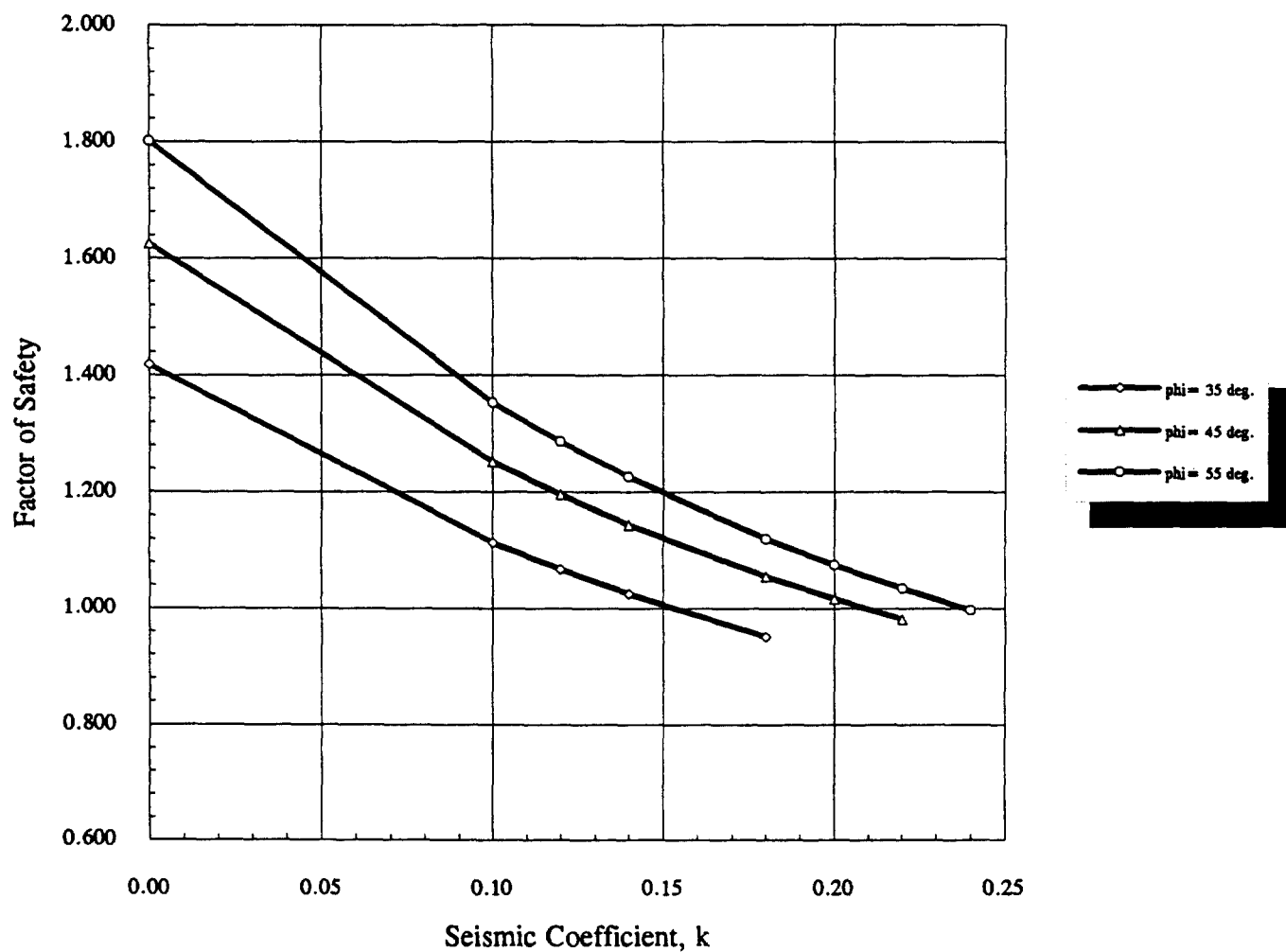


Friction Angle (deg.)	Seismic Coefficient, k						
	0.00	0.10	0.12	0.18	0.20	0.22	0.24
35	1.384	1.100	1.051	0.928			
45	1.573	1.207	1.149	1.004	0.963		
55	1.802	1.345	1.275	1.100	1.051	1.006	0.964

Yield Seismic Coef. (Ky)
0.145
0.180
0.220

**FIGURE 10 - Factor of Safety versus Seismic Coefficient
Section N1**

BHI-00145
Rev. 00

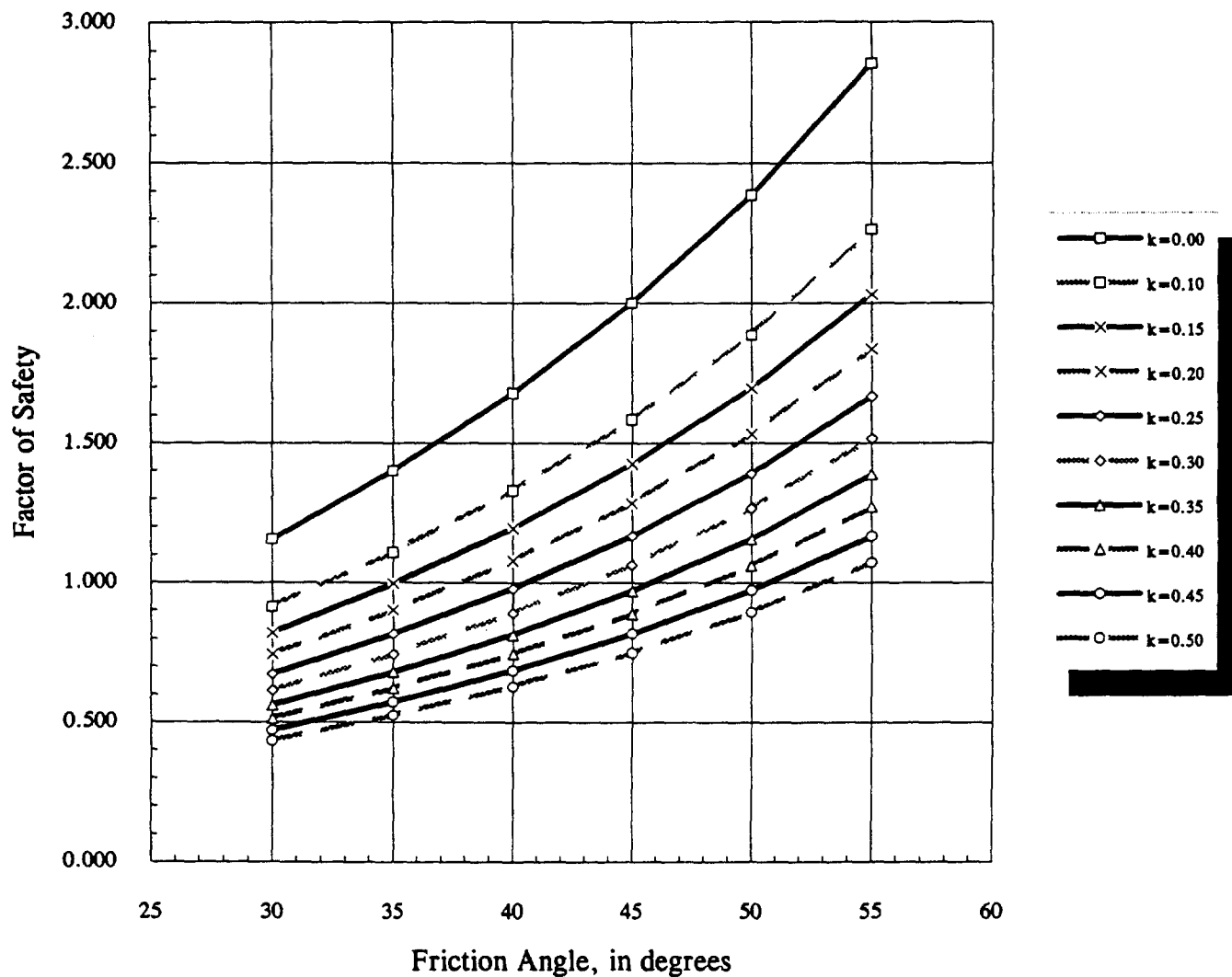


Friction Angle (deg.)	Seismic Coefficient, k							
	0.00	0.10	0.12	0.14	0.18	0.20	0.22	0.24
35	1.418	1.113	1.067	1.025	0.951			
45	1.625	1.252	1.196	1.144	1.055	1.016	0.981	
55	1.801	1.353	1.286	1.226	1.120	1.075	1.034	0.996

Yield Seismic Coef. (Ky)
0.152
0.210
0.240

**FIGURE 11- Factor of Safety for Infinite Slope
w/ Seismic Force 2 to 1 Slope**

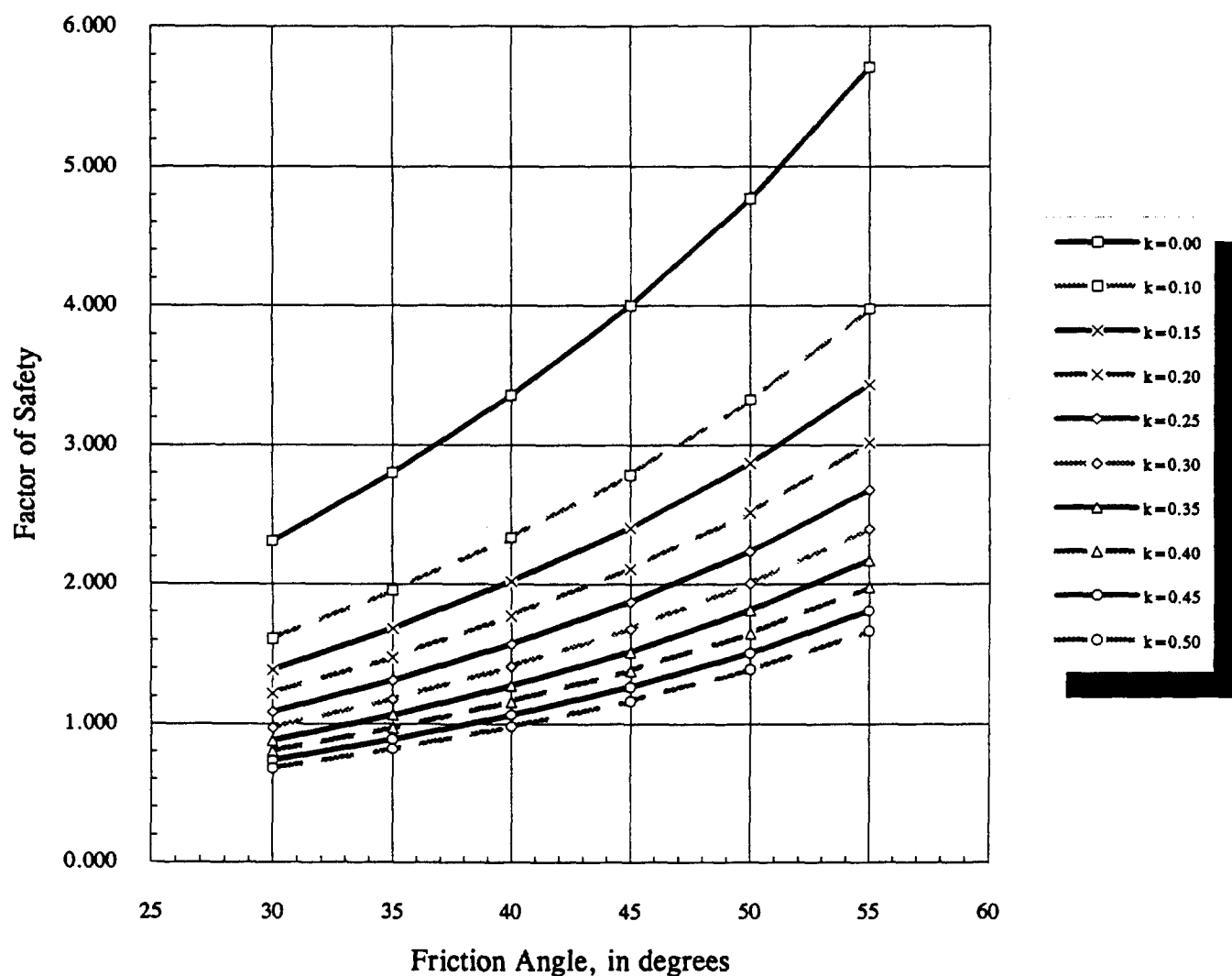
BHI-00145
Rev. 00



Friction Angle (deg.)	Seismic Coefficient, k									
	0.00	0.10	0.15	0.20	0.25	0.30	0.35	0.40	0.45	0.50
30	1.155	0.914	0.822	0.742	0.674	0.613	0.560	0.513	0.471	0.433
35	1.400	1.109	0.996	0.900	0.817	0.744	0.680	0.622	0.571	0.525
40	1.678	1.329	1.194	1.079	0.979	0.892	0.814	0.746	0.685	0.629
45	2.000	1.583	1.423	1.286	1.167	1.063	0.971	0.889	0.816	0.750
50	2.384	1.887	1.696	1.532	1.390	1.266	1.157	1.059	0.972	0.894
55	2.856	2.261	2.032	1.836	1.666	1.517	1.386	1.269	1.165	1.071

**FIGURE 12- Factor of Safety for Infinite Slope
w/ Seismic Force & 4 to 1 Slope**

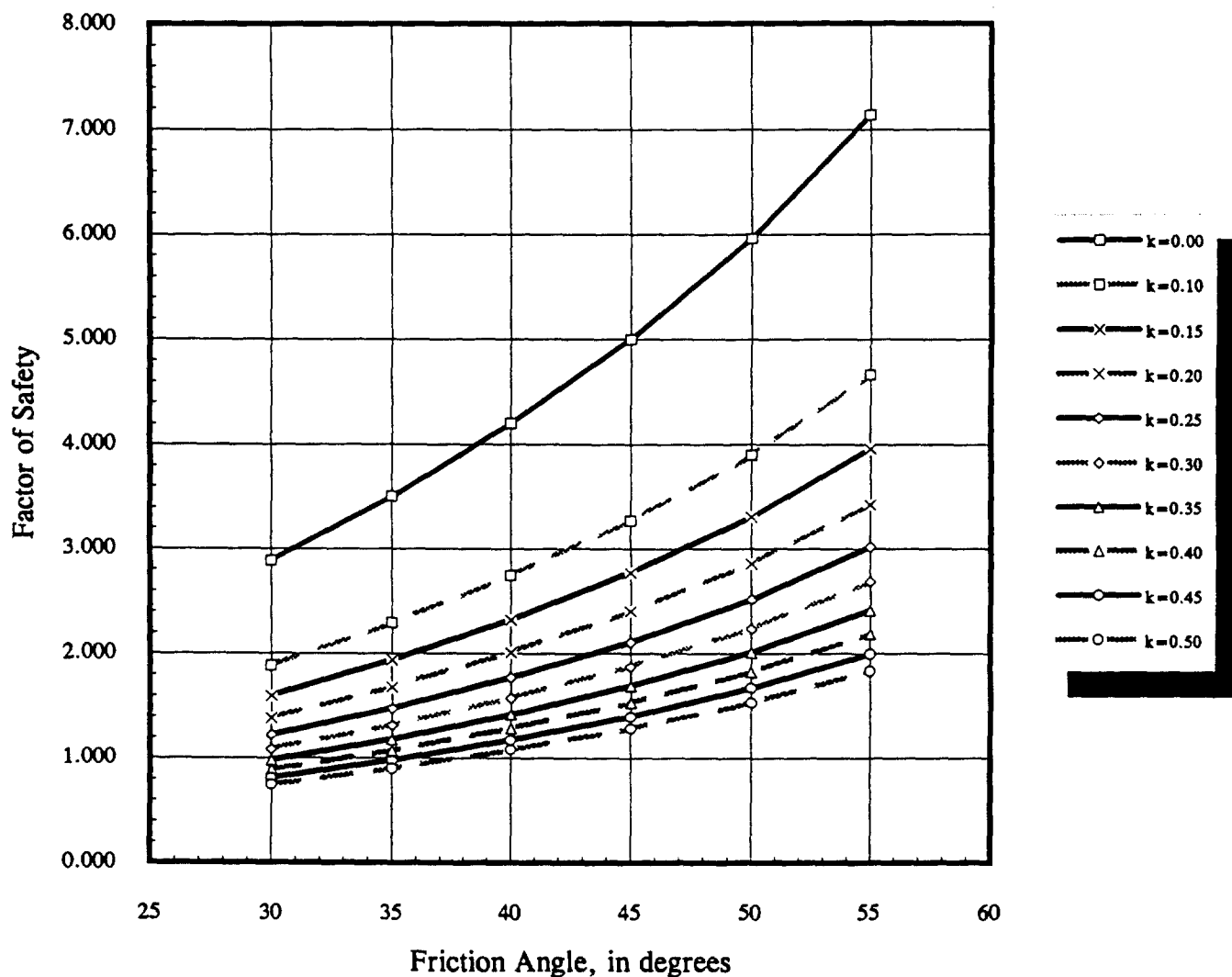
BHI-00145
Rev. 00



Friction Angle (deg.)	Seismic Coefficient, k									
	0.00	0.10	0.15	0.20	0.25	0.30	0.35	0.40	0.45	0.50
30	2.309	1.608	1.389	1.219	1.083	0.971	0.878	0.799	0.732	0.674
35	2.801	1.951	1.685	1.478	1.313	1.178	1.065	0.970	0.888	0.817
40	3.356	2.337	2.019	1.771	1.573	1.411	1.276	1.162	1.064	0.979
45	4.000	2.786	2.406	2.111	1.875	1.682	1.521	1.385	1.268	1.167
50	4.767	3.320	2.868	2.516	2.235	2.004	1.812	1.650	1.511	1.390
55	5.713	3.978	3.436	3.015	2.678	2.402	2.172	1.977	1.811	1.666

**FIGURE 13- Factor of Safety for Infinite Slope
w/ Seismic Force & 5 to 1 Slope**

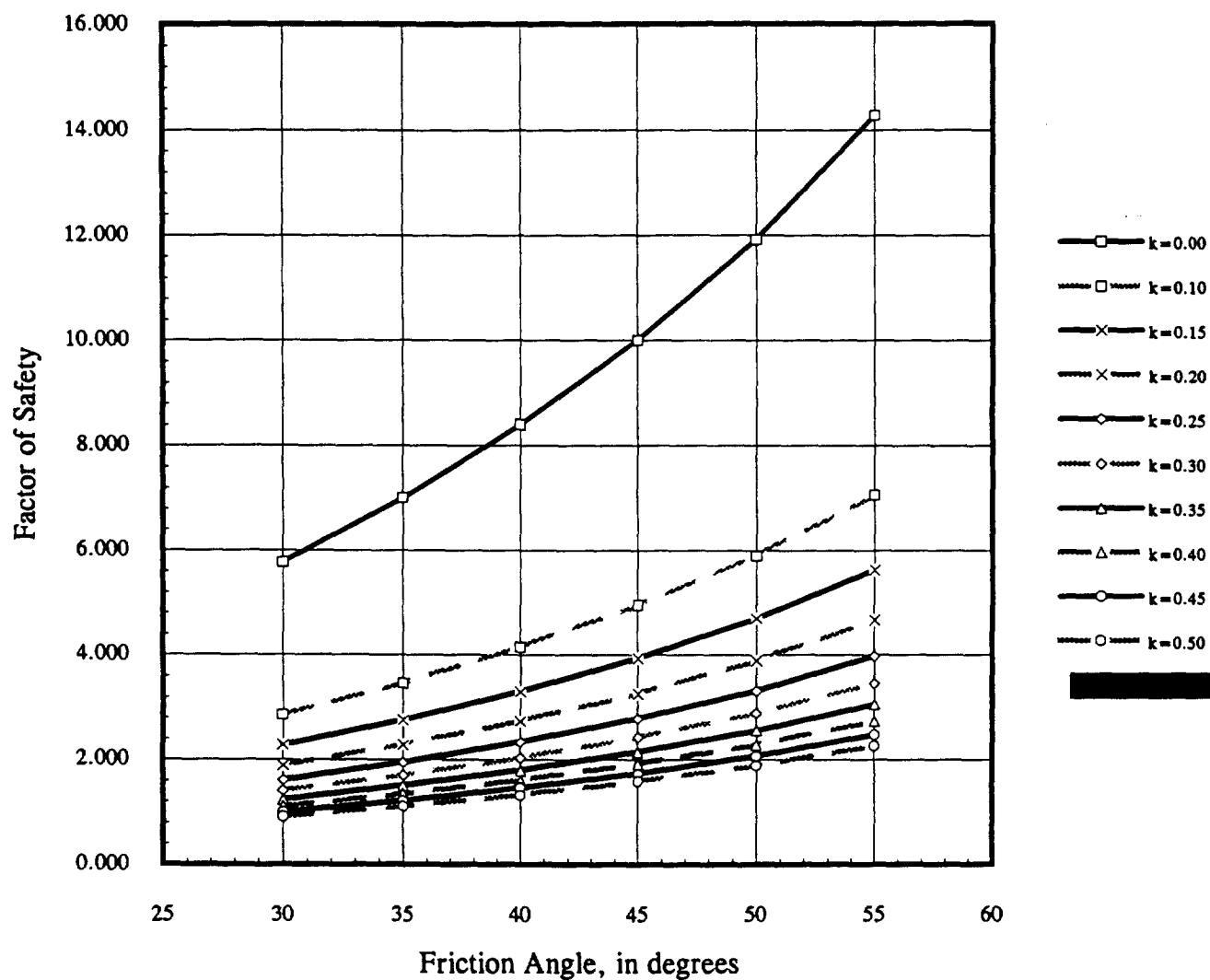
BHI-00145
Rev. 00



Friction Angle (deg.)	Seismic Coefficient, k									
	0.00	0.10	0.15	0.20	0.25	0.30	0.35	0.40	0.45	0.50
30	2.887	1.886	1.600	1.386	1.219	1.085	0.976	0.885	0.808	0.742
35	3.501	2.287	1.941	1.680	1.478	1.316	1.184	1.074	0.980	0.900
40	4.195	2.741	2.326	2.014	1.771	1.578	1.419	1.287	1.175	1.079
45	5.000	3.267	2.771	2.400	2.111	1.880	1.691	1.533	1.400	1.286
50	5.959	3.893	3.303	2.860	2.516	2.240	2.015	1.827	1.668	1.532
55	7.141	4.665	3.958	3.428	3.015	2.685	2.415	2.190	1.999	1.836

**FIGURE 14- Factor of Safety for Infinite Slope
w/ Seismic Force & 10 to 1 Slope**

BHI-00145
Rev. 00



Appendix A

Laboratory Test Results

LABORATORY SHEAR TESTS ON FLUID APPLIED ASPHALT

by J. Lai and David E. Daniel
University of Texas
Department of Civil Engineering
Austin, TX 78712

August 29, 1994

INTRODUCTION

The objective of this study was to determine the shear strength of the fluid applied asphalt (FAA), the interface between the FAA and underlying asphaltic concrete, and the interface between the FAA and overlying gravel. The shear strengths measured from this study were used for stability analysis of the surface barrier slopes.

TESTING EQUIPMENT

A Texas Double Interface Shear Device (TDISD) was used to test the fluid applied asphalt samples. The TDISD was developed by Trautwein Soil Testing Equipment Company in Houston, Texas, and was modified slightly in the University of Texas's laboratories. An overall view of the TDISD is shown in Fig. 1.

The apparatus consists of:

- an air piston assembly to apply normal stress to the samples,
- two reaction plates to provide confinement for the samples,
- a loading press (the same one used in a triaxial test) to apply shear stress to the sample,
- a load cell and dial gage to measure shear force and shear displacement.

For tests on the fluid applied asphalt, 4-inch square samples were used trimmed from a larger sample of the material provided by Westinghouse Hanford Company. The samples were placed between base pedestals of the air piston assembly and the reaction plates (Fig. 2). Four emery clothes (#80 grade) were glued to the surfaces of base pedestals and reaction plates. The objective of this operation was to prevent relative movement between the FAA samples and the metal surfaces.

For tests on gravel-asphalt interface, 4-inches diameter circular samples were used. Two aluminum boxes were machined to contain the gravel. The fluid applied asphalt samples were placed between the gravel and asphaltic concrete (Fig. 3). Two emery clothes were used to prevent relative movement between the asphaltic concrete samples and the reaction plates.

Westinghouse also provided a limited a sample containing fluid applied asphalt in contact with asphaltic concrete. The FAA-asphaltic concrete interface was tested in the TDISD, and it was obvious that the internal strength of the FAA was lower than the interface (the FAA bonded with the asphaltic concrete). Further tests therefore focused on the FAA itself and the gravel-FAA interface.

TESTING PROCEDURES

A large (roughly 1 m by 1 m) piece of fluid applied asphalt, which had been shipped to the University of Texas for testing, was cut into 4-inch-square or 4-inch-diameter samples with a sharp knife. After placing the TDISD on the Wykeham Farrance loading press, the loading rod was inserted into the loading rod housing and the entire air piston assembly was supported by the load cell. The fluid applied asphalt samples were then placed between the base pedestals and the reaction plates. The desired normal stress was applied to the samples by adjusting the air pressures supplied to the air piston. Two to three hours were allowed for the samples to reach equilibrium under the selected normal stress. A deformation rate of 0.01 in/min was used to shear the samples until they reached failure.

During the shearing stage, the readings of load cell and dial gage were taken in every minutes so that a proper shear stress-shear deformation curve can be defined.

TEST RESULTS

Initially, the loading rod housing was not available and thus the weight of the air piston assembly could not be counterbalanced. We set up three tests with fluid applied asphalt samples at normal stresses of 10, 20, and 30 psi. All three samples failed by the weight (10.7 lb) of the air piston assembly at room temperature (72° F). The corresponding shear stress was about 0.4 psi. We also set up one sample at a temperature of 53° F. With 20 psi of normal stress, the sample also failed by the weight of the air piston assembly.

After the loading rod housing was available to hold the air piston (and start as a shearing load of zero, rather than 10.7 lb), we performed two series of tests to investigate the shear strength of fluid applied asphalt and gravel-asphalt interface. Since the weight of the air piston assembly was counterbalanced, the shear stress-shear displacement relationship could therefore be measured. Three different normal stresses were used for each series of tests. Results of these tests are shown in Table 1.

Table 1 Results of Double Interface Shear Tests on Fluid Applied Asphalt and Gravel-Asphalt Interface

Test ID	Material Tested	Normal Stress (psi)	Shear Stress (psi)
1	Fluid Applied Asphalt	8.8	0.15
2	Fluid Applied Asphalt	18.3	0.27
3	Fluid Applied Asphalt	28.3	0.38
4	Gravel-Asphalt Interface	10.0	2.57
5	Gravel-Asphalt Interface	10.0	1.85
6	Gravel-Asphalt Interface	20.8	4.42
7	Gravel-Asphalt Interface	20.8	4.84
8	Gravel-Asphalt Interface	29.8	1.16
9	Gravel-Asphalt Interface	29.8	5.19
10	Gravel-Asphalt Interface	29.8	5.94

The shear stress-shear displacement curves are shown in Fig. 4 for tests on fluid applied asphalt and in Fig. 5 for tests on gravel-asphalt interface. For tests on fluid applied asphalt, the samples failed at a shear displacement of about 0.12 inch. For tests on gravel-asphalt interface, the samples failed at a shear displacement of about 0.25 inch.

The failure envelopes of the two series of tests are shown in Fig. 6. For tests on samples of fluid applied asphalt, failures all occurred within the fluid applied asphalt. The three data points fell nicely on a straight line. Curve fitting through these data yielded a cohesion intercept "c" of 0.1 psi and angle of internal friction " ϕ " of about 0.7 degree.

For tests on gravel-asphalt interface, failures also occurred within the fluid applied asphalt. The data appeared to be a little more scattered. One sample (Test #8) failed at a significantly lower shear stress than the other samples, as shown in Fig. 6. Test #8 appeared to be an outlier and was not used in curve fitting. The rest of the data yielded shear strength parameters: $c = 0.7$ psi and $\phi = 10$ degrees.

The gravel penetrated into the fluid applied asphalt when the gravel was subjected to normal stresses. The penetration of the gravel into the FAA was evidently responsible for the increase the shear strength of fluid applied asphalt. The degree of penetration would logically depend on the intensity of normal stresses and the characteristics of individual gravel particles. For the seven tests that we performed, only in one test (normal stress = 30 psi) did a gravel penetrated all the way through the fluid applied asphalt.

SUMMARY AND CONCLUSION

Two series of double interface shear tests were performed to investigate the shear strength of fluid applied asphalt and gravel-asphalt interface. Tests on samples of fluid applied asphalt yielded a cohesion intercept "c" of 0.1 psi and a angle of friction " ϕ " of 0.7 degree. For the gravel-asphalt interface, the shear strength parameters were $c = 0.7$ psi and $\phi = 10$ degrees, although failure actually occurred within the fluid applied asphalt rather than the "interface."

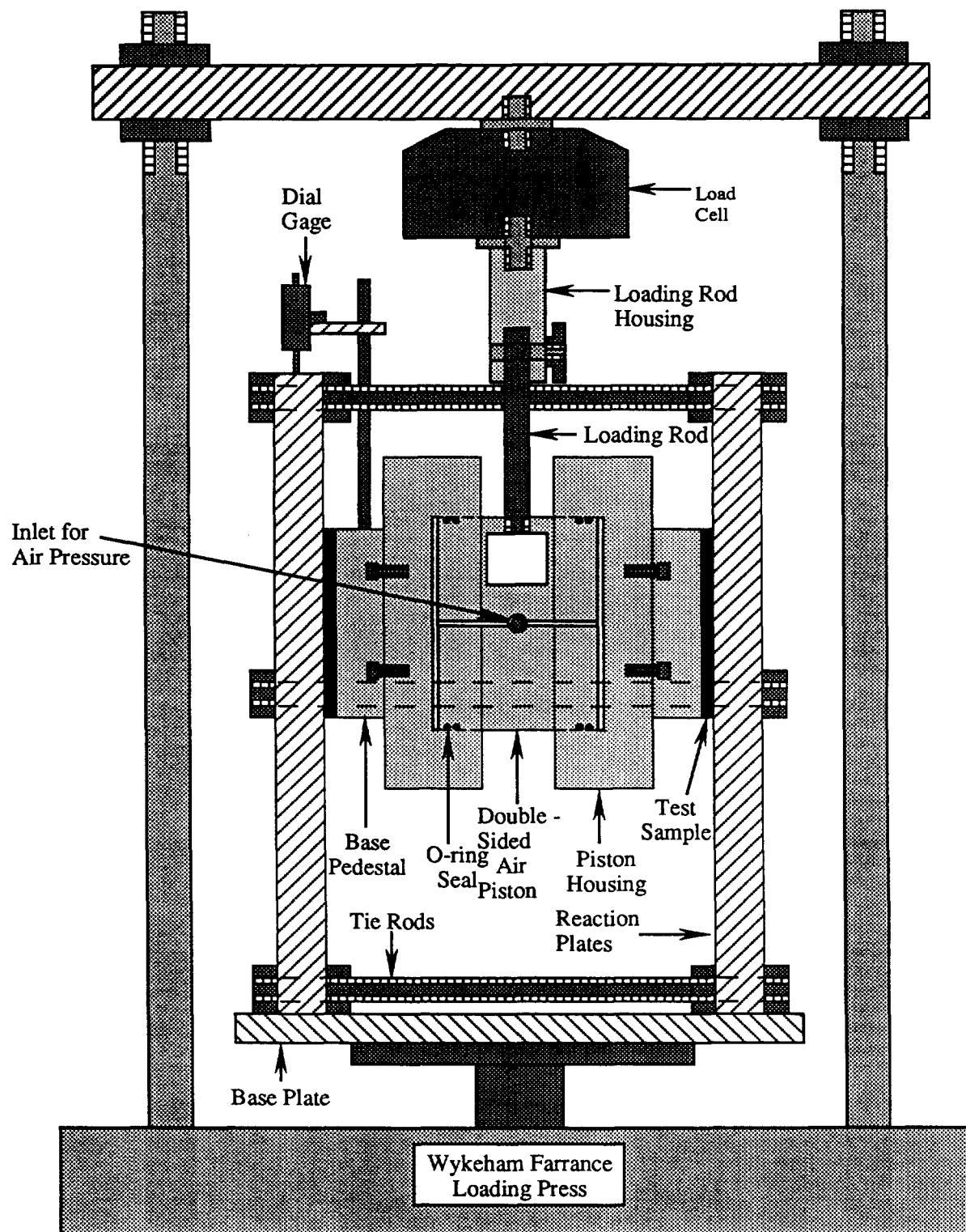


Figure 1 Schematic Drawing of Trautwein's Texas Double Interface Shear Device

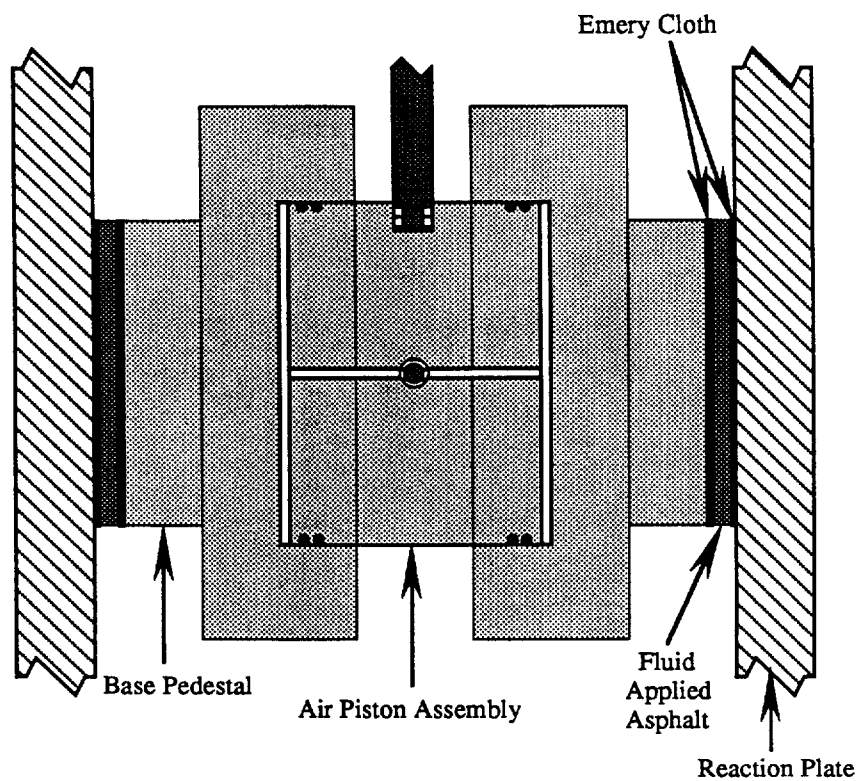


Figure 2 TDISD Setup for Tests on Fluid Applied Asphalt Samples

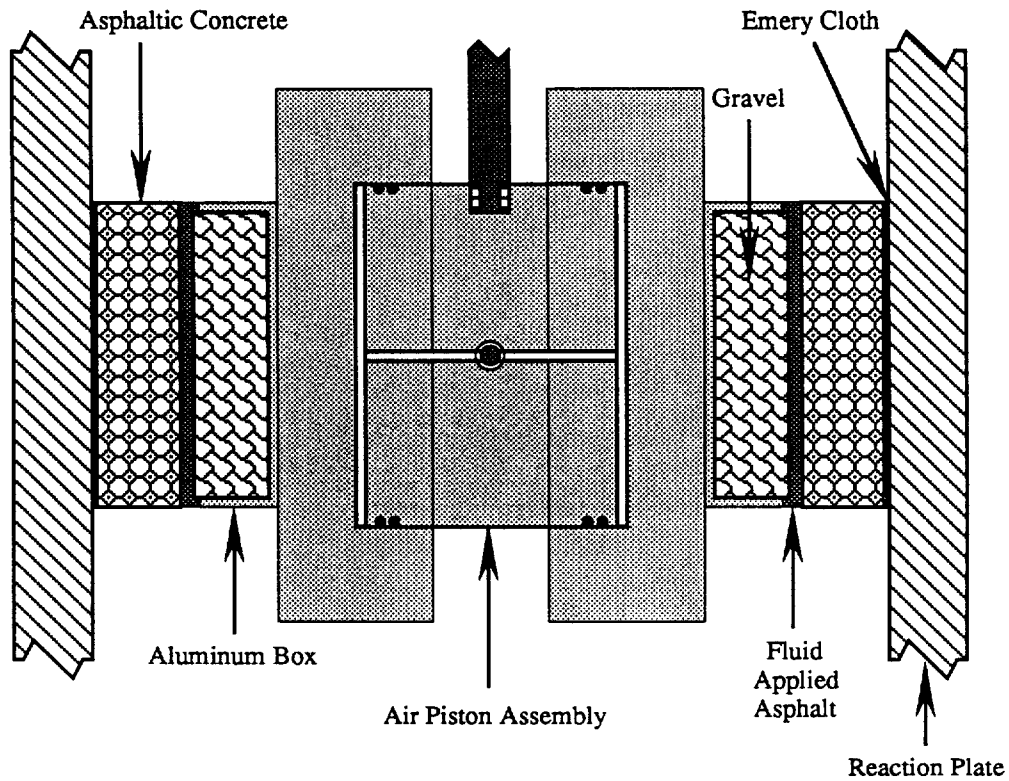


Figure 3 TDISD Setup for Tests on Gravel-Asphalt Interface

Appendix B

References

References

- Dames & Moore (1988). "Geotechnical and Corrosion Investigation, Grout Vaults, Hanford, Washington" for Kaiser Engineers, Hanford, Washington, Report No. 10805-282-016, October 10.
- Dames & Moore (1989). "Geotechnical Investigation, Proposed Hanford Waste Vittrification Plant, Hanford, Washington" for Kaiser Engineers, Job No. 10805-383-016, November 15.
- Kaiser Engineers Hanford Company (1993). "Construction Specifications for Prototype Surface Barrier at 200-BP-1 Operable Unit" for U. S. Department of Energy, Contract DE-AC06-87RL10900, June 15.
- Makdisi, F. I. and H. B. Seed (1977). "A Simplified Procedure for Estimating Earthquake-Induced Deformations in Dams and Embankments", UCB/EERC-77/19, August.
- Seed, H. B., C. Ugas, and J. Lysmer (1974). "Site Dependent Spectra for Earthquake Resistant Design", EERC 74-12, Berkeley, California.
- Seed, H. B. and I. M. Idriss (1982). "Ground Motions and Soil Liquefaction During Earthquakes", EERI, Berkeley, California, 134 pp.
- Shanon & Wilson, Inc. (1994). "Geotechnical Investigation KEH W-236A, Multi Function Waste Tank Facility, Hanford Site, Richland Washington" for SCM Consultants, Inc., Kennwick Washington, Volume 1, January.
- Westinghouse Hanford Company (1993). "Permanent Isolation Surface Barrier: Functional Performance" for U. S. Department of Energy, Contract DE-AC06-87RL10930, October.
- Wiegel, R. L. (1970). "Earthquake Engineering" (Chapter 15 by H. B. Seed), Prentice-Hall Inc., Englewood Cliffs, N.J.
- Wright, S. G., (1991), "UTEXAS3" (A Computer Program for Slope Stability Calculations) Austin, Texas, September 1991.

DISTRIBUTION

Number of Copies

ONSITE

16	M. A. Buckmaster (BHI)	H6-01
	F. M. Corpuz (BHI)	H4-85
	T. E. Curran (ITC)	H6-01
	G. W. Gee (PNL)	K9-33
	K. J. Koegler (BHI)	H6-02
	K. L. Petersen (PNL)	K6-75
	W. A. Skelly (WHC)	L4-69
	A. M. Tallman (WHC)	H6-30
	BHI Document Control (3)	H4-79
	BHI Project File (3)	H4-79
	Environmental Resource Center	H6-07
	Hanford Technical Library	P8-55
	RL Public Reading Room	A1-65